Droplet-Based Microfluidic Platform Employing Sorting and Downstream Merging for Single-Cell Analysis

By

Meng Ting Chung

A dissertation submitted in partial fulfillment
of the requirements for the degree of
Doctor of Philosophy
(Mechanical Engineering)
in the University of Michigan
2019

Doctoral Committee:

Professor Katsuo Kurabayashi, Chair
Assistant Professor Dawen Cai
Associate Professor Jianping Fu
Associate Professor Allen Po-Chih Liu

Meng Ting Chung

mengting@umich.edu

ORCID iD: 0000-0001-7539-5893

Table of Contents

List of Figures

List of Tables

List of Appendices

Abstract

Single-cell analysis techniques have emerged to overcome the limitation of bulk analysis in which the heterogeneous gene expression information from individual cells is lost. Droplet-based techniques appear to be one of the most promising approaches as they compartmentalize single cells in an immiscible two-phase flow and enable high-throughput analysis while preserving the characteristics of each cell in a small-volume droplet. One of the challenges in droplet microfluidics is the manipulation of droplets usually requires the sequential use of many custom-made microfluidic devices, and one device can only address one specific task. This makes it challenging to generate robust experimental pipelines for complicated tasks. This thesis introduces our new working pipeline for droplet-based microfluidics and its applications in transcriptomic analysis.

In the first part of this thesis, we present a droplet-based microfluidic platform (Sort-N-Merge) integrating several droplet operational units to achieve fully on-chip processing. This is the first droplet-based workflow that enables reconfigurable droplet sorting and downstream merging. With this platform, single-cells can be encapsulated, fluorescence-activated sorted, and one-to-one merge with other-sorted droplets containing necessary cells, reagents, or microparticles. Such an operational procedure is similar to using traditional pipettes and microtiter plates, making it adaptable to many well-developed biological assays with smaller reaction volume and higher throughput.

In the second part, we demonstrate the use of this system for profiling transcriptomes of rare neuron stem cells from single Drosophila's brain. The conventional droplet-based single-cell mRNA-sequencing approach by pairing a single barcoded primer-associated bead and a single cell in a droplet based on the stochastic Poisson process only allows less than 10% of cells in the sample to be effectively sequenced. Rare cells could be lost not only during harsh FACS sorting but also such inefficient sequencing processes. Our Sort-N-Merge workflow deterministically sorts target cells and barcoded beads into single droplets, thus making mRNA-sequencing of rare cells from a large population possible.

In the last part, single-cell mRNA detection using reverse-transcription loop-mediated isothermal-amplification (RT-LAMP) was demonstrated by our system. By sequentially adding lysis buffer and reactant mixtures to nanoliter-sized reactors, human hydroxymethylbilane synthase (HMBS) gene expressions from hundreds of cells were detected within one hour. The fully on-chip workflow including cell isolation, sorting, lysing, and RNA detection provides a robust experimental pipeline for a wide variety of physiological studies.

The demonstrated applications prove our microfluidic work flow could be adapted to a wide variety of single-cell assays. Furthermore, the fully on-chip processing gets rid of laborious hands-on operations and potentially leads to automation of the whole process in the future.

Chapter I

Introduction

1. Introduction and Research Background

Cells are the most basic unit of life. It is a scientists' dream to understand the function of each cell and how they coordinate their activities. Advances in biotechnologies in 2017, such as launch of the "Human Cell Atlas Project", which aims to collect information on all cell types in the human body[1], have pushed the study of biology from the tissue level into single-cell resolution. The information revealed by such high-resolution maps has also changed our understanding of biology[2]. Moreover, single-cell studies have been carried out in fundamental research fields, such as protein engineering, synthetic biology, disease diagnosis, and cell theory[3]–[6]. Compared to modern bulk cellular assays with well-established gold-standard approaches, single-cell analysis is still in its early stage. The experimental approaches for single-cell studies have evolved quickly, but none are considered mature techniques[7]. The success of single-cell experiments relies on the development of new techniques from several fields. For example, sensitive and highly specific biosensors are needed to quantify the small number of analytes in a single cell[8]. A tool for efficient and parallel handling of small

fluidic volumes is needed to scale up the number of cells studied at a reasonable cost[9]. In addition, a new data mining algorithm is needed to decrypt such big data from millions of cells[10]. This thesis provides a novel solution to address the current limitations in droplet-based single-cell analysis approaches. A new droplet manipulation workflow is developed to improve the inefficiency in the processes of capturing cells/microbeads and adding reagents for multi-step biochemistry protocols. The following sections will discuss the backgrounds and aim of this thesis..

1.1.1 The Rationale of a Single-cell Analysis

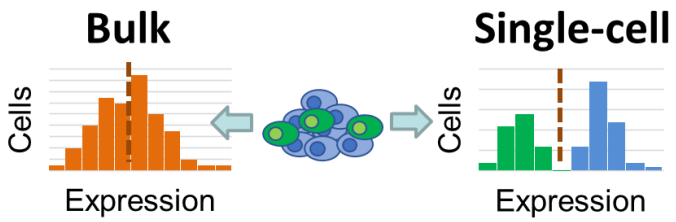

Figure 1.1 The difference between Bulk and Single-cell analysis: The cell expression result is averaged in bulk analysis. While single-cell analysis reveals the heterogeneity of cells.

Every cell is unique. Although researchers have discovered more than 200 types of cells in the human body, there could be more subpopulations or rare cell types among them[11]. Such rare cell types could be limited in number but play a significant role in the body. Even within the same type of cell, the status of each cell can be affected by the local environment as well as signaling factors from surrounding cells. Traditional bulk cell assays in which a group of cells is analyzed produce an averaged result (Figure 1.1). The distribution of analytes within a group of cells can only be considered a random event. Thus, bulk assays fail to reveal the hidden heterogeneity of responses or characteristics between cells. In general, there are two significant motivations to perform single-cell analysis in research: The first is to study the

networks within groups of cells, and the second is to discover a rare cell population in the sample.

Single-cell assays represent a fundamentally different approach than bulk assays. The usage of single-cell technologies has already yielded a significant impact on almost every aspect of biology. Some examples are discussed as follows.

Cancer. Single-cell analysis plays a significant role in understanding the hidden mechanisms of cancer formation and development leading to a potential therapeutic solution[12], [13]. Tumors originate from a single clone of driver mutations but consist of heterogeneous subclones after they grow. The cell types can differ in the same disease, the same patient, and even within the same tumor[14]. Moreover, polyclonal tumors have different responses to the same treatment[15]. Without a deep understanding of cancer biology at the single-cell level, previous cancer therapy does not have a specific molecular or cellular level target. Recent single-cell research has discovered the existence of cancer stem cells, which are critical players in tumor progression and metastases[16]. The discovery of cancer-specific biomarkers from those cells has facilitated the development of molecular, gene, and cell therapy.

Microbiology

Microorganisms are the largest and most diverse group on earth[17]. Thousands of different species coexist in a local microbial community or so-called microbiome. The microbiome can adapt to changes in the local environment or stimuli quickly, but the hidden mechanism is usually missing with the bulk analysis approach[3]. By analyzing individual microbial cells rather than a group of cells, the functionality of a single cell can be examined, and the result is decoupled from the influences of cell-cell interactions. Moreover, many

microorganisms are not culturable[17]. Single-cell analysis enables us to discover the inside world of microbiology.

High-throughput screening

In nature, it is difficult to identify a wild-type protein that has the desired properties. Directed evolution is the process of developing useful enzymes with high specificity to the desired targets by screening a huge mutant library of genes[18]. In addition, the production of monoclonal antibodies also requires screening hybridomas as a fusion of B cells and cancer cells[19]. Both require high-throughput screening at the single-cell level to pick up the cells expressing the desired proteins.

Developmental biology

In developmental biology, researchers focus on how a small number of early stage cells, such as stem cells, differentiate into different functional cell types. This process is highly temporal and spatially dynamic. Therefore, adjacent or the same cells could have different characteristics at different stages. Single-cell resolution is necessary to capture such dynamic profiles[20], [21]. This has led to many breakthroughs, such as an understanding of differentiation of neural lineages and the immune system network.

1.1.2 Types of Single Cell Studies

Single-cell analysis shares the same strategy of analytical techniques as traditional bulk analysis, but it requires more sensitive techniques to detect a small number of analytes from a tiny cell (normal human cell contains about only 6 pg DNA and 10–30 pg RNA [114]). Following the central dogma of biology, study targets can be categorized as genomic, epigenomic, transcriptomic, proteomic, metabolomic, and other phenotypic analyses.

Genomics. Genomic studies using the bulk approach provide genotypic fingerprints of many different species. Single-cell DNA sequencing further identifies the unicellular species in the complex microbial world. It also measures the somatic mutations and copy number variations at the cellular level[22]. This provides a new perspective of understanding genetic changes in normal tissues and in certain diseases. For example, the study of genetic mutations between tumors and normal tissues could improve diagnosis in personalized medicine[23]. A genetic analysis of subclones in tumors could provide a precision guide for selecting effective drugs and therapies[15]. As there is only a single copy of the genome in one cell, it is critical to perform efficient whole genome amplification for sequencing. Other than the standard pure-PCR based approach, many new approaches, such as multiple displacement amplification or multiple annealing and looping-based amplification cycles have been developed to improve the coverage, uniformity, and accuracy of amplification[24].

Epigenomics. Epigenetic processes are a series of chemical modifications of DNA (e.g., methylation) and histones that can result in changes in gene function or expression. Unlike the genome which is usually static within the same individual, the epigenome varies between different cell types. Even within the same cell type, it could be affected by changes in local environmental conditions. Therefore, the epigenome provides the first signature of mapping of the genotype to the phenotype[25]. The conventional analytical techniques involved in epigenomics include chromatin immunoprecipitation sequencing and whole genome bisulfite sequencing[26]. Compared to genomics or transcriptomics, the study of epigenomics is still in its early stage, but it is becoming more and more critical in developmental biology and cancer biology.

Transcriptomics. The single-cell transcriptome provides the complete set of genes expressed at the mRNA level, which is an intermediary molecule. Therefore, studies of the cell transcriptome are one step closer than epigenomics to the cell phenotype. In a single-cell transcriptomic analysis, RNA is converted to complementary DNA (cDNA) and amplified for detection or sequencing. The early technology using microarray had poor sensitivity and insufficient quantitative data[27]. It also required a knowledge of the RNA sequence to design the capturing probes. In 2009, the first single-cell mRNA-sequencing (sc-mRNA-seq) assay was reported, which significantly enhanced coverage of the whole genome compared to the microarray method and was used to discover some previously unknown sequences[28]. Thereafter, mRNA-sequencing methods developed quickly. New protocols such as Smart-seq or the use of unique molecular identifiers further improved the coverage of genes and the accuracy of molecular counting[27]. However, RNA is not as stable as DNA, and the number of initial templates is so small in a single cell[29]. Intrinsic and technical noise can be introduced into the sequencing data during processing[9]. Optimizing the efficiency and accuracy of sc-mRNA-seq is still a pressing and ongoing issue.

Proteomics. Proteins are directly involved in numerous functions within cells. Unlike DNA or RNA can be decoded by the high-throughput sequencing approach, proteins are distinguished by its spatial structures. This makes the design of capture probes (antibodies or aptamers) and multiplexing more difficult. Flow cytometry and mass spectroscopy with a time-of-flight analysis are the current gold standard for high-throughput single-cell proteomics studies, allowing detection of 1-38 target proteins and about 1,000 cells/sec[30]. However, these approaches can only be used to study intracellular or membrane proteins. Spatial confinement of single cells or external biosensors are required to study secreted proteins. Several sensing

technologies, such as enzyme-linked immunosorbent assay, western blot, or proximity ligation assay have been developed and coupled with microfluidic devices to study the single-cell secretome[31]–[33]. The study of secretomes is particularly crucial in immunology in which cytokines act as signaling factors between immune cells, reflecting the status of the immune system[34].

Metabolomics. Metabolites refer to the downstream substrates or by-products of enzymatic reactions, so they are directly associated with the cell phenotype under a given condition. However, similar to the proteome, there are hundreds of different metabolites from even one cell type, but they are small molecules. It is technically difficult to measure the whole spectrum of a metabolome[35]. Conventional reagent kits can only detect some general analytes, such as ATP, Calcium ions, and reactive oxygen species, which participate in common physiological processes using fluorescent indicators. Mass spectroscopy and capillary electrophoresis have wider coverage of the metabolome, but their sensitivity is insufficient for smaller cells, such as bacteria or yeasts[35]. Further improvement of coverage, sensitivity, and throughput are needed.

1.1.3. Technological Platform for single-cell Analysis

The ability to isolate and observe individual cells is necessary for the first step in a single-cell analysis. The invention of microscopy in the 17th century enabled researchers to observe the morphology of single cells, which can be marked as the beginning of single-cell study. As biological samples typically show little inherent contrast, the development of various histological stains, such as Gram stain, Periodic acid–Schiff stain, and others further enhanced the contrast between different cell types or subcellular components. In the late 20th century, many essential molecular biology techniques were invented, such as monoclonal antibodies,

green fluorescent protein, transfection, PCR, and DNA sequencing, which enable detection at the single molecule level. Therefore, studies of single cells were no longer limited in morphology but can be "omic" studies. Every single cell has to be collected into individual reactors for desired assays[36].

Traditional tools for single-cell collections include manual picking, laser capture microdissection (LCM), and fluorescence-activated cell sorting (FACS)[36]. Manual picking is the most straightforward approach that can be easily performed in any laboratory with micromanipulation instruments. The cells of interest are first visually identified under a microscope. Then, the target cells are captured with a glass pipette and transferred to separate tubes for downstream processing. However, because of the laborious operation and low-throughput, the manual picking approach may only be suitable for processing a small number of cells, such as embryonic cells or pre-sorted circulating tumor cells.

LCM uses a high power laser pulse to melt the thermoplastic film above the target cell from fixed solid tissue[37]. The melted region of the thermoplastic film fuses with the underlying cell of interest. When removing the thermoplastic film, the target cell stick to the film, so it can be removed from the tissue and transferred to a separate container. Unlike other methods that require dissociating solid tissues into a single-cell suspension, LCM directly captures single cells from solid tissues. Avoiding additional dissociation processes reduces the intrinsic noise in the end-point measurement. It also reduces the chance of cell damage while dissociating some challenging samples. Moreover, the feature of *in situ* capture preserves the spatial information, which is some of the most critical data in developmental biology. However, the throughput of the LCM method is as slow as manual picking, so its applications remain limited.

FACS analyzes the optical properties, such as the fluorescence and scattering signals, from single cells. Single-cell suspensions are squeezed into a small nozzle (diameter ~50–150 μm) by sheath flow using pressure-driven pumps and passed through an optical interrogation zone. The fluorescence signal came from labeling proteins of interest is excited by a focused laser beam and collected by photomultiplier tubes. Multiple excitations and emission bands of different wavelengths can be applied for multi-parameter measurements. Eighteen proteins from single cells were quantified using an advanced fluorescence dye featured by narrow excitation/emission wavelength [38]. The coupling of flow-cytometry and mass spectrometry, called mass cytometry, can extend the multiplexity to 38 proteins[38]. Moreover, the on-the-fly analysis provides the highest throughput among all other methods. Single cells can be screened at a rate of 1–100,000 cells/sec[38]. Such a high throughput analysis is critical to overcome the technical and intrinsic noise from each single data point. Therefore, flow cytometry has been successfully employed in single-cell analyses for a long time, and it is still the gold-standard for proteomics assays. However, there are also some disadvantages when applying FACS for a single-cell analysis. First, a large number of initial cells (>10,000) and sample volume (> 500 μL) are required for each experiment, which may limit its applications on rare cell populations (https://medicine.uiowa.edu/flowcytometry/protocolssample-prep/sample-preparation-analysis). Second, both the strong shear force caused by sheath flow in the small nozzle and charged droplets under the high electric field can damage the cells. This reduces the retention rate after the sorting process. Moreover, the fluorescence tag biomarkers are limited to the membrane surface or the cytoplasm. If the analytes are expressed outside the cells or the assays involve a lysis process, such as gene amplification or sequencing, single cells must be sorted into individual wells in microtiter plates for downstream reactions.

In these cases, the fluidic handling of bulky microtiter plates becomes the limiting factor for high-throughput single-cell analysis.

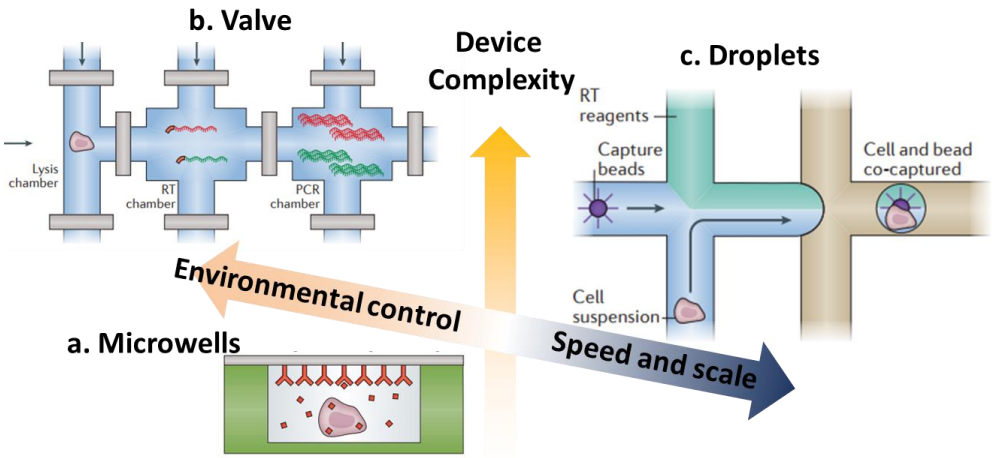

Figure 1.2 Three types of microfluidic tools for single-cell analysis: valve, microwells, and droplets. Valve-based microfluidics has best environment control; The microwells devices are easily fabricated and operated; Droplet-based microfluidics has the highest throughput and scalability. [9]

To address these issues, modern tools have used a strategy called "scaling by shrinking" with microfluidic systems[9]. The scale of the microfluidic approach is usually around a few micrometers to hundreds of micrometers. Single-cell experiments can be conducted in many micro-reactors in parallel to achieve a high-throughput analysis[39]. Shrinking the reactor size also reduces the consumption of reagents by several orders of magnitude. In addition, the analytes from a single-cell are confined to a small volume; thus, increasing the density of the analytes in the reaction. Moreover, the fluids become laminar in microscale. The Reynold's number (Re) is typically < 10 for a microfluidic system. This makes the flow pattern and diffusion of small molecules predictable, providing a well-defined microenvironment for individual biochemical reactions. Although the concept of microfluidics was proposed in the late 20th century and some conceptual microfluidic devices have been successfully made with silicon, the lack of micro-fabrication techniques using transparent materials has limited the progress of the microfluidic approach. In 1998, Duffy et al. demonstrated easy prototyping of

a microfluidic device using PDMS, so research on microfluidics became accessible to common laboratories[40]. This provided a significant boost to advances in microfluidic technology. After two decades of development, microfluidic devices for single-cell research can be categorized into microwells-, valve-, and droplet-based microfluidics (Figure 1.2).

The microwells-based microfluidic device consists of a large array of microwell patterns on PDMS. Cells are randomly seeded into microwells by gravity. The open wells are sealed with a glass slide, plastic film, or a liquid oil so single cells can be physically isolated in individual wells. The top of the microwell also provides solid support for biomolecules, such as antibodies, aptamers, or ssDNA, for the desired study[41]. The significant advantages of the microwell-based approach are its simple fabrication and operation. It can be performed in general biological labs by researchers without a robust microfluidic background. The throughput of the microwell-based approach is scalable with the size of the microwell array from a few to hundreds of thousands of cells, making it suitable for various types of samples. However, the lack of precise control of the microenvironment limits its application in some multi-step assays requiring multiple washing or buffer exchange steps.

Valve-based microfluidics provide the most precise and comprehensive control of the microenvironment among all of the other approaches[42]. Valves are used to control the flow pattern in the microfluidic channel, to capture the cells in the desired chambers, to seal the chambers, and to exchange the buffers and reagents at given time points. Due to their versatility, valve-based microfluidics are usually compatible with a wide variety of cellular assays already optimized for the bench-top, enabling us to easily convert a traditional bulk assay into a single-cell format. The valve-based microfluidic platform usually consists of an elastomer membrane between an air channel and a fluidic channel. The air channels are connected to a pressure

source so the pressure deflects the elastomer membrane to change the geometry of the fluidic channel or block fluidic flow. Fluids can be handled automatically by coupling integrated fluidic circuits with a programmable pressure controller. Although the valve-based method is convenient and powerful from the users' perspective, manufacturing the device is relatively complicated. It involves assembling three layers (fluid, air, and membrane) of PDMS and connecting many inlets/outlets [126]. It also requires a large unit area to accommodate each valve and chamber, so scalability of the system is limited. Therefore, throughput is relatively lower than other microfluidic approaches. This makes the system only suitable for applications in which precision is the first consideration. The last category, droplet-based microfluidics, features the highest throughput among all other methods, and will be discussed in the next section.

1.1.4. Droplet Microfluidics

Droplet microfluidics enables the formation and manipulation of a large number of discrete liquid droplets in an immiscible continuous phase[43], [44]. Unlike other approaches in which liquids are compartmentalized by solid walls and the number of compartments is limited by physical space in a two-dimensional area, aqueous droplets are isolated by the oil or air phase and can be generated and analyzed continuously at a frequency of thousands of Hz. Therefore, speed and scalability become unique features when applied to single-cell research. Single-cell containing droplets can be used in droplet-based single-cell assays, so researchers can generate a comprehensive data set mapping to the tissues or organs of interest. However, controlling the droplets requires a sophisticated microfluidic chip design and high-end instruments. It is also difficult to precisely manipulate a small number of droplets.

Therefore, droplet microfluidics is suitable only when a large number of samples require analysis.

1.2 Motivation of the Research

Although microdroplet-based techniques enable various high throughput single-cell assays, their workflow is not compatible with traditional tools such as a flow cytometer, micropipettes, centrifuge tubes, or microtiter plates. The traditional single-cell workflow starts with sorting or picking cells into the individual wells of a microtiter plate and adding the reagents into each well for downstream reactions. In contrast, the droplet-based workflow prohibits directly adding reagents or releasing contents from droplets because the droplets are typically immersed in an oil phase. As a result, it requires the sequential use of a custom-made microfluidic device to address those specific tasks for a complete single-cell workflow[45]. Moreover, most molecular biology protocols contain multi-step reactions with off-chip incubations as a middle step. The transition of droplets between the microfluidic channel and the external space requires good hands-on skills from a well-trained microfluidic technician, such as carefully fine-tuning the flow rate, minimizing the loss of droplets, and preventing the introduction of air bubbles. This makes it difficult to generate a robust workflow for a wider range of users.

Researchers have attempted to build an integrated droplet microfluidic platform so the whole assay process can be done automatically by one device[44]. Most of the platforms use the strategy of sequentially connecting all functions in a continuous flow manner[46]–[49]. The advantage of the continuous-flow approach is that it can generate, process, and detect the

droplets at high throughput (>1 kHz). The system can efficiently process a massive number of droplets (>10^7) in several hours by continuously running. However, for those multi-step protocols employing droplet fusion or pico-injection, it usually requires several minutes to reach a stable state at the beginning. A substantial number of droplets could be lost during this initial phase. In addition, continuous-flow strategies do not support protocols with long incubation times or that require pre-enrichment of cells/bio-particles[44], which sets limitations on many applications.

In contrast, multi-step protocols can be quickly completed by other stationary microfluidic platforms[45]. However, as mentioned above, their throughput is typically too low for single-cell analyses. Therefore, we developed a new droplet-based platform that combined the advantages of continuous and stationary droplet microfluidics for more versatile applications in single-cell analysis.

1.3 Scopes of the Thesis

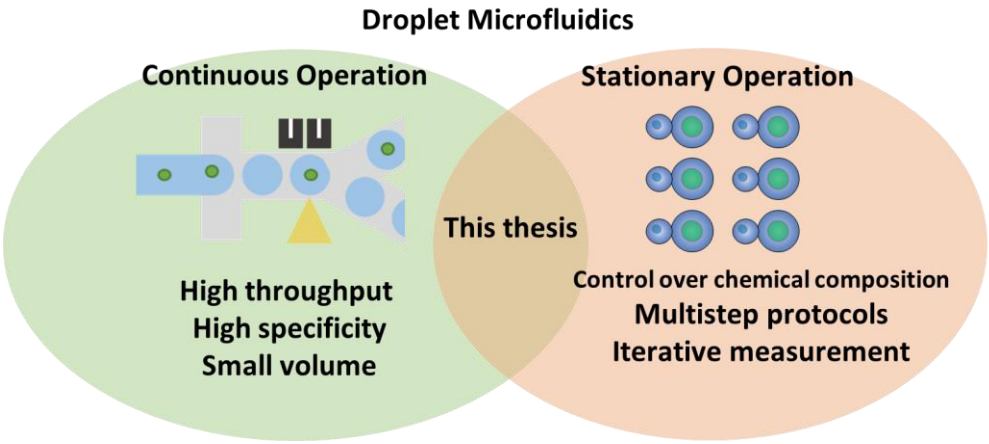

Figure 1.3 The concept of our hybrid droplet microfluidic system combining the advantages from continuous operation and stationary operation.

This thesis presents an integrated droplet-based workflow, enabling full on-chip single-cell analysis[50], [51]. We mimicked traditional single-cell assays that use FADS

(Fluorescence activated droplet sorting) [52]to sort single cells containing droplets into a static array of wells, use pipettes to add reagents, perform desired reactions in the wells, and use an image-based approach for detection. Therefore, our approach shrink the reactor size and increased the assay throughput. The key innovation in our platform is coupling continuous droplet microfluidics upstream and stationary droplet microfluidics downstream (Figure 1.3). Therefore, high-throughput droplet sorting and precise merging of droplets can be achieved in our system to generate an array of droplets containing the desired cells, bio-particles, or reagents. In addition, both the incubation and detection of the droplets are performed *in situ*, and it is compatible with a multi-round process by iterating droplet sorting and merging.

To demonstrate the utility of this platform, we applied our system to address a current challenge in single-cell transcriptomic analysis. First, we improved the efficiency of the existing droplet-based single-cell mRNA-seq method, or the so-called "Drop-seq" proposed by EZ Macosko in 2015 [53]. In Drop-seq, single-cells and bar-coded beads are one-to-one paired in the droplets for mRNA capture and barcoding. However, the current techniques assembles cells and beads by randomly co-encapsulating two objects. Due to the two independent Poisson distributions, most of the droplets are empty or contain either one bead or one cell, resulting in reduced efficiency. To overcome this issue, our approach actively selects single-cells or single-beads containing droplets and deterministically assembles them. Therefore, efficiency improves significantly, enabling wider applications such as rare cell studies. Next, we demonstrated the capability of multi-step reactions using a newly developed single-cell reverse transcription loop-mediated isothermal amplification (RT-LAMP) assay. Cell lysis, mRNA amplification, and fluorescence detection were accomplished in a static array series of droplets. This overcomes the drawbacks mentioned above in continuous-flow

microfluidics due to instability of the droplets. Moreover, our platform is not limited to transcriptomic analyses, as it is aimed to provide a robust droplet-based workflow for various types of single-cell assays.

1.4 Thesis Outline

Based on the research scope discussed above, this thesis consists of five subsequent Chapters:

Chapter II - Literature Review: We review the studies relevant to this thesis. The first part discusses current advances in droplet-based microfluidic systems and the second part discusses how researchers integrate those functions to create different types of single-cell assays. The limitations of the current approach are summarized at the end of the chapter to provide a rationale for developing our new droplet manipulation platform.

Chapter III - A Droplet Sorting and Downstream Merging (Sort 'N Merge) Platform: This chapter discusses the development of our new droplet workflow that integrates several droplet manipulation techniques, such as generating, sorting, pairing, and merging of droplets in one platform[50], [51]. We seamlessly coupled continuous and stationary droplet manipulating approaches together so the advantages from both schemes are preserved. We characterized the performance of our platform by co-encapsulating two or more microparticles of different sizes and fluorescent colors. Two different single-cell assays require co-encapsulation of two objects or multi-step reaction are demonstrated in the following chapters.

Chapter IV - Application I: Single-cell mRNA Sequencing

In this chapter, we present a high efficiency single-cell mRNA-sequencing platform by adapting the current Drop-seq protocol into our new workflow. In Drop-seq, single-cells and solid-state synthesized barcoded primer microbeads are co-encapsulated in microdroplets by a stochastic Poisson process resulting in a very poor yield. In our platform, single-cell and microbeads containing droplets are enriched separately and then merged. Therefore, the efficiency of the co-encapsulation process is significantly improved and no longer limited by a Poisson distribution. We benchmarked the performance of our system against the conventional Drop-seq method by validating it in a species-mixed experiment. Last, to demonstrate the capability for rare cells studies, we performed the sc-mRNA-seq experiment with a rare cell type from the central neural system of a single Drosophila.

Chapter V - Application II: Single-cell mRNA Detection by RT-LAMP

mRNA-seq provides a complete spectrum of the transcriptome, but the shallow coverage of total mRNA is a limitation. Amplification of specific mRNA sequences provides a sensitive way to validate gene expression. In this chapter, we demonstrate detection of single-cell mRNA using the RT-LAMP assay by sequentially adding lysis buffer and reactant mixtures to picoliter-sized reactors. Expression of the HMBS gene was evaluated among different cell lines within 1 hour. The entirely on-chip workflow and sample-in-answer-out capability provide a robust experimental pipeline for a wide variety of biology and clinical applications.

Chapter VI - Conclusions and Future Work: The final chapter summarizes the impact of our Sort N' Merge platform and discusses its potential applications in other single-cell assays. In the last section, several ongoing future studies are mentioned, including improving

the recovery efficiency of mRNA sequencing, new cell barcoding strategies, and blueprints to make the Sort N' merge platform a robotically automated turn-key system.

Chapter II

Literature Review

This chapter provides a review of previous studies related to this thesis work. First, it reviews the common operational units of droplet microfluidics, including droplet generating and manipulation. The role of each operational unit in single-cell assays is explained as well. This is followed by a review of the current advancement of droplet-based platforms for various single-cell analyses. Finally, the chapter will discuss the achievement and limitations of the existing droplet-based platform and discuss our proposed solution in this thesis work.

2.1 Droplet microfluidics

2.1.1 Droplet generation

Droplet generation is the process of partitioning a bulk sample into many nano- to picoliter droplet reactors, which is the first step for droplet-based assays. The process generates two-phase droplets containing reactants in water forming a dispersed phase surrounded by oil (continuous phase), and the surfactant at the interface is used to stabilize the droplets. The history of using a small emulsion for the parallel chemical reaction dates back to 1920, when

people produced synthetic rubber microparticles through emulsion polymerization reaction[54]. However, the poly-dispersed size of the emulsion limits its reproducibility and accuracy for biochemical assays. In the late 20th century, the use of microfluidic techniques provided well-controlled conditions for droplet generation. Three different microfluidic structures have been commonly used: co-flow, T-junction, and flow-focusing[43]. Although different in geometry, the principle of droplet generating is the same. Two-phase liquids flow into different microfluidic channels individually with a stable flow rate in a laminar flow condition. When two liquid phases meet, the competition between inertial force, viscous stress, and surface tension makes one of the phases break up from the other, forming segments of liquid or droplets. The capillary number ($Ca = \frac{\mu U}{\gamma}$, where μ is viscosity, U is characteristic velocity, and γ is surface tension), which represents the relative importance of viscosity forces with respect to interfacial tension, is one of the most critical non-dimensional quantities relevant to the formation of droplets[55]. When the *Ca* number is small, the interfacial tension force dominated the process of droplet pinch-off (squeezing regime). With the increase of Ca, droplet breakup is dominated by the shear stress and the size decreases (dripping regime). At a large Ca number, droplet breakup is dominated by the viscosity force and the size uniformity is reduced due to Rayleigh–Plateau instabilities (jetting). In general, the flow-focusing design is the most popular design nowadays since it can be stably operated in a squeezing or dripping regime and generate droplets with a wide range of size.

Cell encapsulation is conducted along with droplet generation. Single-cell suspensions, buffers, or reagents are first co-flowed into the microfluidic channel. The encapsulation process occurs when the suspended cells flow through the breakup zone of the aqueous flow. Since the cells are freely distributed in the solution, the encapsulation process is random and

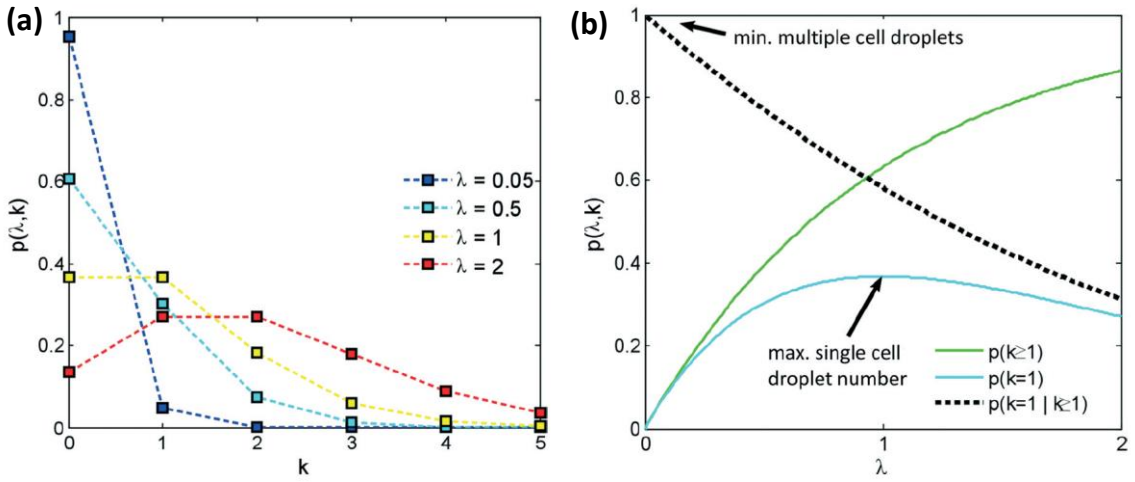

Figure. 2.1. (a) Poisson distribution at different event number λ (average cell number per droplet). (b) Effect of cell concentrations for the proportion of droplets containing single cell (p(k ≥ 1)), multiple cells (p(k = 1)), or droplets containing cells that contain exactly one cell (p(k = 1 | k ≥ 1)). [56]

the probability of observing *k* cells occupying a droplet follows a discrete *Poisson* distribution (Figure 2.1a): $P_\lambda\left(k, _{poission}\right) = \frac{\lambda^k \exp(-\lambda)}{k!}$, where λ is the average number of cells per droplet[56]. Here, λ is defined as $\lambda = \frac{c}{V_{drop}}$, where *c* is the concentration of the cell suspension and V_{drop} is the volume of each droplet. To avoid errors caused by encapsulating more than a single cell in each droplet (k>1), one must flow cells at a low concentration (λ<<1) such that $P_\lambda\left(k > 1, _{poission}\right) \ll 1$ (Figure 2.1b). As a result, most of the droplets emerge empty, which reduces the overall throughput and wastes reagents. This issue becomes more pronounced in some cases when a high percentage of single-cell-containing droplets is required. For example, in a cell-co-culturing experiment [57] or single-cell mRNA-Seq experiment [53], droplets must contain both types of cells or microparticles. In this case, the co-encapsulation rate follows two independent *Poisson* distributions and causes a poor result[58].

Several studies have demonstrated the passive control of single cells or particles that overcome the Poisson distributions by using a hydrodynamic effect to control the spatial

distribution of cells/particles in the microfluidic channel[58]–[60]. A >77% encapsulation rate can be achieved, but this requires specific loading conditions[60]. Other than passive methods, single-cell-containing droplets can be generated on-demand by actively directing cells to the droplet generating region with mechanical or acoustic force[61][62]. Alternatively, even if the number of single-cell-containing droplets is low, it can be enriched by a downstream droplet-sorting module[52], [63]. More details of droplet sorting will be provided in the next section.

2.2.2 Droplet manipulation

One of the remarkable features in droplet microfluidics is that each operation step can be modular and integrated for a complete workflow [64](Figure 2.2a). The details of each operational unit are provided in this section.

Droplet trapping. Since droplets are always generated in a continuous-flow manner, a process to immobilize droplets in a specific region is required for incubation or detection in many biochemical assays. Many operational units can also be performed with the static droplets, such as merging and sorting (releasing) in a stationary manner[65], [66]. Droplets in the microfluidic channel can be trapped by either passive or active approaches. Passive trapping involves the use of buoyancy force [67], hydrodynamic force [68], or surface energy wells[65] that can trap a large number of droplets at a time. On the other hand, active trapping provides more controllability of specific droplets and is usually reversible. However, it can only deal with a relatively small number of droplets and requires additional setup to generate the trapping force, such as acoustic waves [69], pneumatically actuated valves [70], or electrodes [71].

Droplet incubation. An incubation step is necessary for almost all kinds of biochemical reactions. Once cells and desired reactants are introduced into droplets, they can be incubated

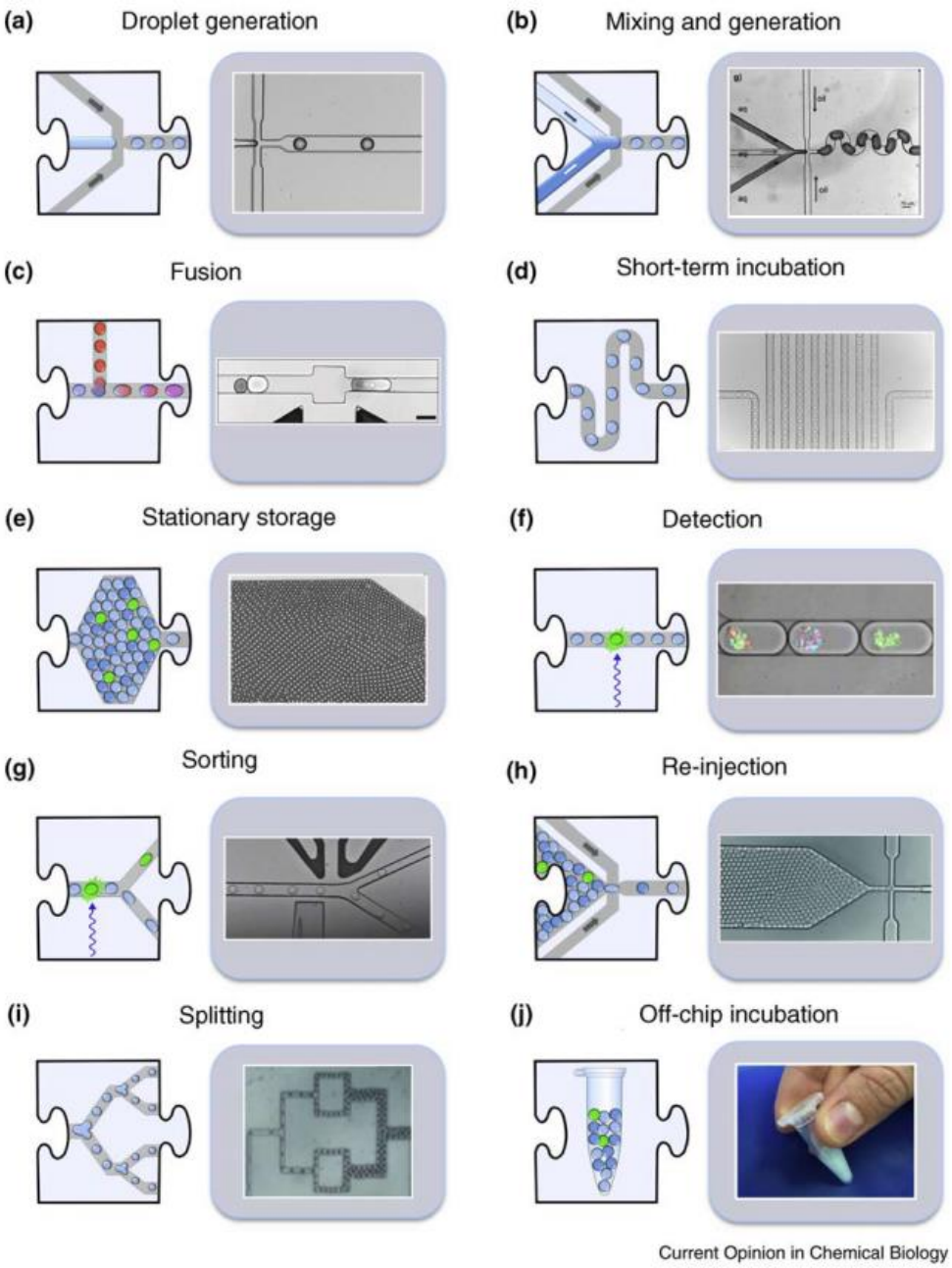

Figure. 2.2 Schematics show a summary of different droplet operational units. Each unit can be used independently or integrated together as a complete workflow for biology assays. [64]

on-chip or off-chip. For short incubation (a few seconds/minutes), droplets can be incubated in a simple delay line between other operational units [72]. For longer incubation, a reservoir or an array of droplet traps can be used to store the droplets[67], [68]. Off-chip incubation is suitable for a large number of droplets, and the applications require long incubation

(hours/days), such as growing microorganisms. For a reaction that requires thermal cycling, such as PCR, off-chip incubation can also take advantage from a commercialized benchtop instrument. Once the reaction step is finished, the droplets can be reinjected into a microfluidic chip for downstream manipulations or detection.

Droplet reinjection. Droplet reinjection is necessary for assays requiring additional processes or analysis after off-chip incubation. Although the operation of droplet injection is similar to the injection of other solutions, one must be very careful during the reinjection process because droplets are very delicate. Tiny dust or shear stress can easily destabilize the thin interface between two droplets, causing experiment failure. In addition, for off-chip fluid handling, a minimum volume of a few micro-liters is needed, which is equivalent to a very large number of pico- or nanoliter-sized droplets (For example, ~15,000 50um droplets is only equal to 1ul in volume). This restricts its application if the number of droplets is small.

Droplet pairing and merging. Droplet merging is one of the most important operation units since many molecular biology protocols require multi-step reactions. New reagents are added to the droplets to start/stop the reaction or dilute the sample. The procedure of droplet merging involves two steps. Two droplets are first brought close together to form physical contact. Then, the thin interface is destabilized by an external force, so the droplets are merged by interfacial tension. Droplets can be paired in either a continuous flow[73] or a stationary trap[66]. In the continuous-flow manner, two types of droplets flow from two separated channels into the single channel. If two types of droplets enter the channel at the same frequency, an ordered array of two types of droplets can be formed in one channel. The hydrodynamic effect can bring two adjacent droplets close together. However, the synchronization of two droplet flows relies on the stable fluidic dynamics of discrete droplets and continuous flow[74]. Any small

perturbation of droplet size, pressure, and flow rate can cause synchronization errors. A highly precise control instrument and a high-speed camera are required to guarantee the accuracy of droplet pairing. On the other hand, stationary droplet pairing does not require precise fluidic control. One type of droplet can flow into the microfluidic traps first followed by the second type of droplet to form droplet pairs. Since the throughput of the stationary droplet-merging approach is limited to the capacity of trapping arrays and difficult to integrate with a continuous operational unit, it has not been applied to any single-cell assays yet. Once two droplets are brought into contact, droplet coalescence can be achieved by mechanical collision[74], chemicals[75], [76], electrical fields[77], optical heating[65], or surface acoustic waves[78].

Droplet splitting. Droplet splitting can be easily achieved by bifurcating junctions in microfluidic channels. The channel wall at bifurcating junctions can create a strong shear force on droplets. When the shear force overcomes the surface tension, the droplets split into two or multiple daughter droplets. The splitting result, such as the number and size ratio of the daughter droplets, is determined by the design of channel geometries[79]. Droplet splitting is usually coupled with droplet merging to control the size of droplets or concentration of the chemicals inside the droplets[46], [48]. In addition, if a protocol requires multiple reactions with a single droplet, one droplet can be split into multiple droplets so that multiple reactions can be performed in its daughter droplets.

Droplet sorting. High-throughput droplet sorting might be the most powerful and unique feature of droplet microfluidics among all the other techniques[44], [80]. By coupling with the droplet detection unit, droplets containing desired cells or analytes in a continuous flow can be detected and sorted for downstream manipulation or analysis[19]. The common microfluidic design of droplet sorting involves an asymmetric Y junction connected to two outlets. The

droplets are biased to the channel with lower fluidic resistance when there is no external actuation. Only the desired droplets are deflected into a higher-resistance channel by external actuation. Many different actuation mechanisms have been reported, such as electric [52], acoustic [81], pneumatic [82], thermal [83], and magnetic control [84]. Among all the methods, dielectrophoretic (DEP) actuation appears to be the most popular due to its high sorting rate, high response time, and ease of integration [52]. The mechanism of DEP sorting is using a pair of electrodes with close proximity to generate a non-uniform electric field in a small region. When the droplets travel through this region, the strong electric field gradient and the dielectric difference between the droplet interfaces result in a strong attraction force that pulls the droplet toward the electrodes. A droplet-sorting rate of 30Khz by DEP actuation has been reported, which could be accelerated further by increasing the bandwidth of the electric circuit [85].

Droplet breaking. Droplet breaking is the last step if the contents of droplets require downstream analysis, such as DNA sequencing. The mechanism of droplet breaking is similar to droplet merging that can be chemically, electrically, or mechanically triggered, but it does not require precise pairing or control. Therefore, in most cases, droplets can be simply broken by chemical and mechanical coalescence outside microfluidic chips.

2.2 Droplet-based single-cell assays

In this section, we will discuss how the droplet operational units described above are integrated and translated into single-cell research. Four major droplet-based workflows and their applications are introduced in the following.

2.2.1 High-throughput screening of single cell

In 2009, Baret and his colleagues developed a fluorescence-activated droplet-sorting platform (FADS) by coupling fluorescent droplet detection and DEP droplet sorting [52]. This method has the feature of traditional fluorescence-activated cell sorting (FACS) in that single-cell can be analyzed at a high throughput. Moreover, unlike cells being pooled together after FACS sorting, in FADS, sorted cells are still in individual droplets and thus can be analyzed in a single-cell format. The workflow of single-cell high-throughput screening usually involves three steps (Figure 2.3a): First, single cells are encapsulated with desired reagents, such as lysis buffer or fluorogenic substrates, into droplets. Second, the droplets are incubated off-chip or in a microfluidic delay line. Third, droplets are screened using the FADS module and the sorted droplets are broken for downstream analysis.

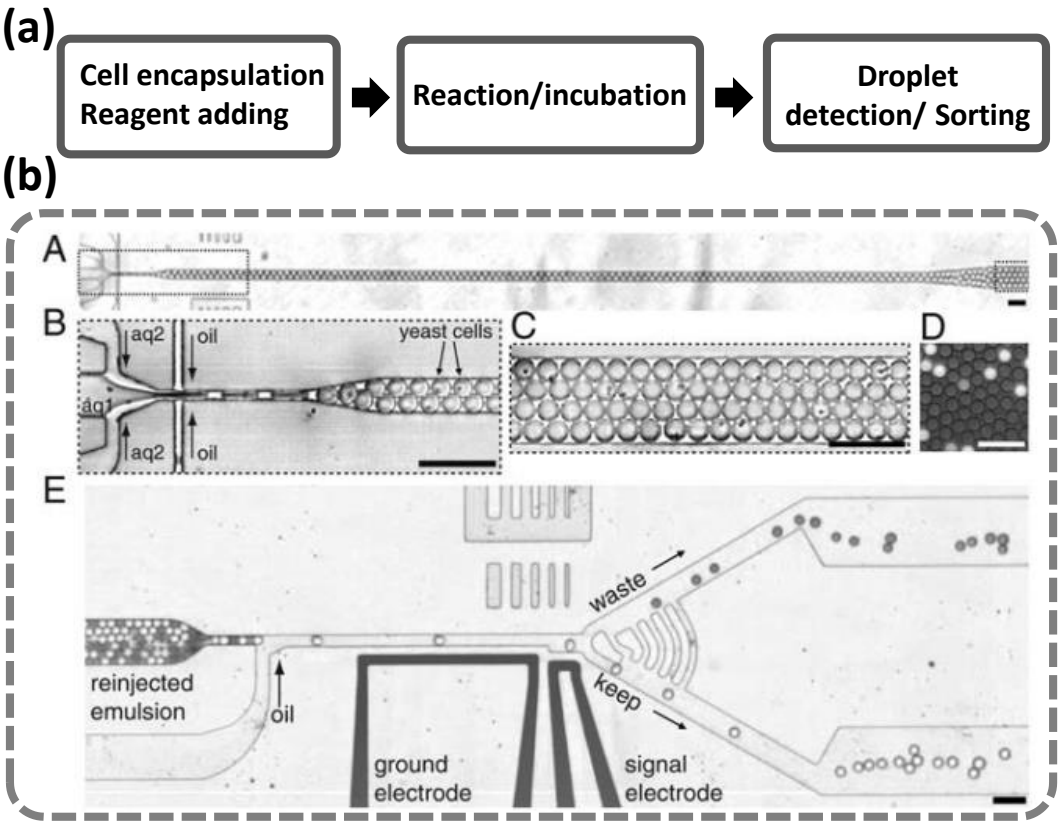

Figure. 2.3 (a) Typical workflow for high-throughput single-cell screening. (b) Microscope images show the droplet microfluidic modules for enzyme-directed evolution. <A>: Droplet-generating module with zoomed-in images <B-D>. <E>: FADS module [86].

Many biological applications require high-throughput screening at a single-cell level. For example, in enzyme-directed evolution, huge random mutagenesis libraries of the target enzyme are created and then screened for desired properties. The success of enzyme-directed evolution relies heavily on the efficiency and accuracy of the screening method used. In 2019, Agresti *et al*. first employed droplet microfluidics in enzyme-directed evolution (Figure 2.3b) [86]. An approximately 10^8 mutant library was screened in 10 hours, and enzymes exhibiting catalytic rates more than 10 times faster than their parent were obtained. This increased the throughput 1000-fold and reduced the cost a million-fold compared with the traditional screening method using microtiter plates. Other than bacteria, droplet-based screening has also been applied to functional studies of mammalian cells for drug screening [87] or hybridoma screening [88].

2.2.2 Single-cell nucleic amplification

Nucleic acid amplification techniques, such as PCR, have been commonly applied in molecular biology protocols. This technique is so sensitive that even a single copy of the initial

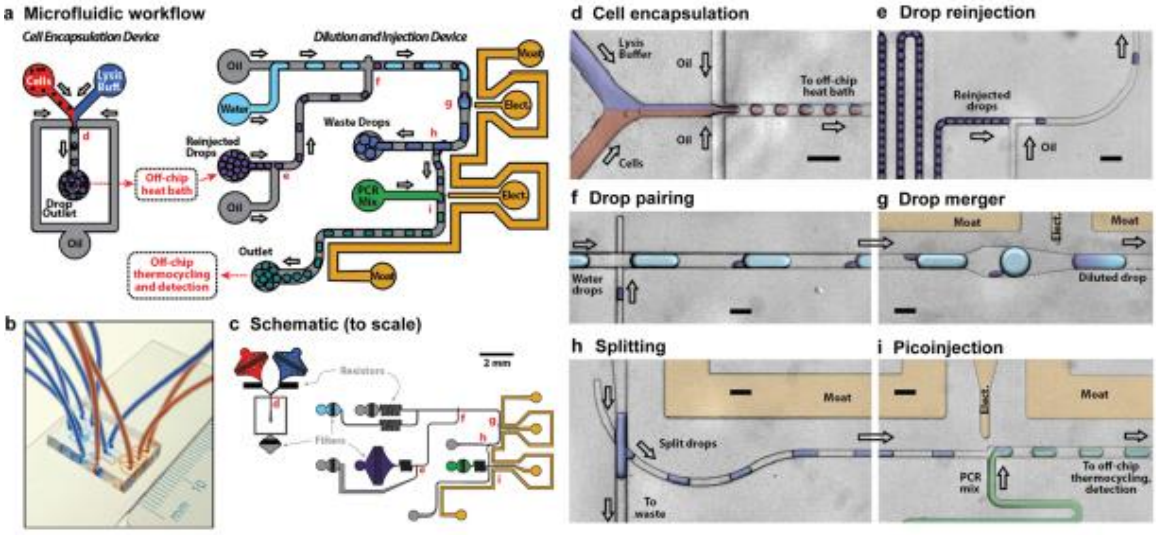

Figure. 2.4 Schematics of microfluidic workflow for single-cell RT-PCR and images of microfluidic devices. [46]

template can be amplified and detected. Thus, it is suitable for detecting a small number of analytes from a single cell. By coupling droplet microfluidics with single-cell nucleic amplification, it is possible to study cellular heterogeneity transcriptionally in a rapid manner[46], [89], [90]. Since there are two reaction steps (cell lysis and nucleic amplification) and new reagents added between them are required, the workflow becomes more complicated. In 2013, Eastburn *et al*. first presented a droplet-based single-cell RT-PCR platform for high-throughput single-cell gene expression analysis[46] (Figure 2.4). Three separated devices were used in the whole workflow, and approximately 50,000 cells could be analyzed per experiment. Recent developments in single-cell nucleic amplification attempt to make the workflow more robust by reducing the complexity of devices. For example, Kim et al. modified lysis chemistry to shorten the lysis time. Therefore, the whole workflow could be integrated into one device[89]. Guo et al. employed a non-enzymatic isothermal amplification technique for miRNA detection[91]. Therefore, it eliminated both the droplet-merging step and the thermal cycling step, thus further reducing the operation difficulty.

2.2.3 Single-cell -omics barcoding

Recently, combining genetic barcoding and next-generating sequencing (NGS) techniques for droplet-based single-cell -omics studies has become popular. The ability to access thousands of gene expression variables from thousands of cells in one run has fundamentally revolutionized the ways we study the type or status of a cell. In this type of assay, the workflow can be as simple as a one-step reaction (Figure 2.5a): Barcode sequences and single cells are co-encapsulated in a droplet so the analytes, such as DNA or RNA, are labeled with DNA barcodes. The droplets are then broken and pooled for downstream library

preparation and NGS. The sequencing data can be reconstructed *in silico* based on a reference genome and genetic barcodes.

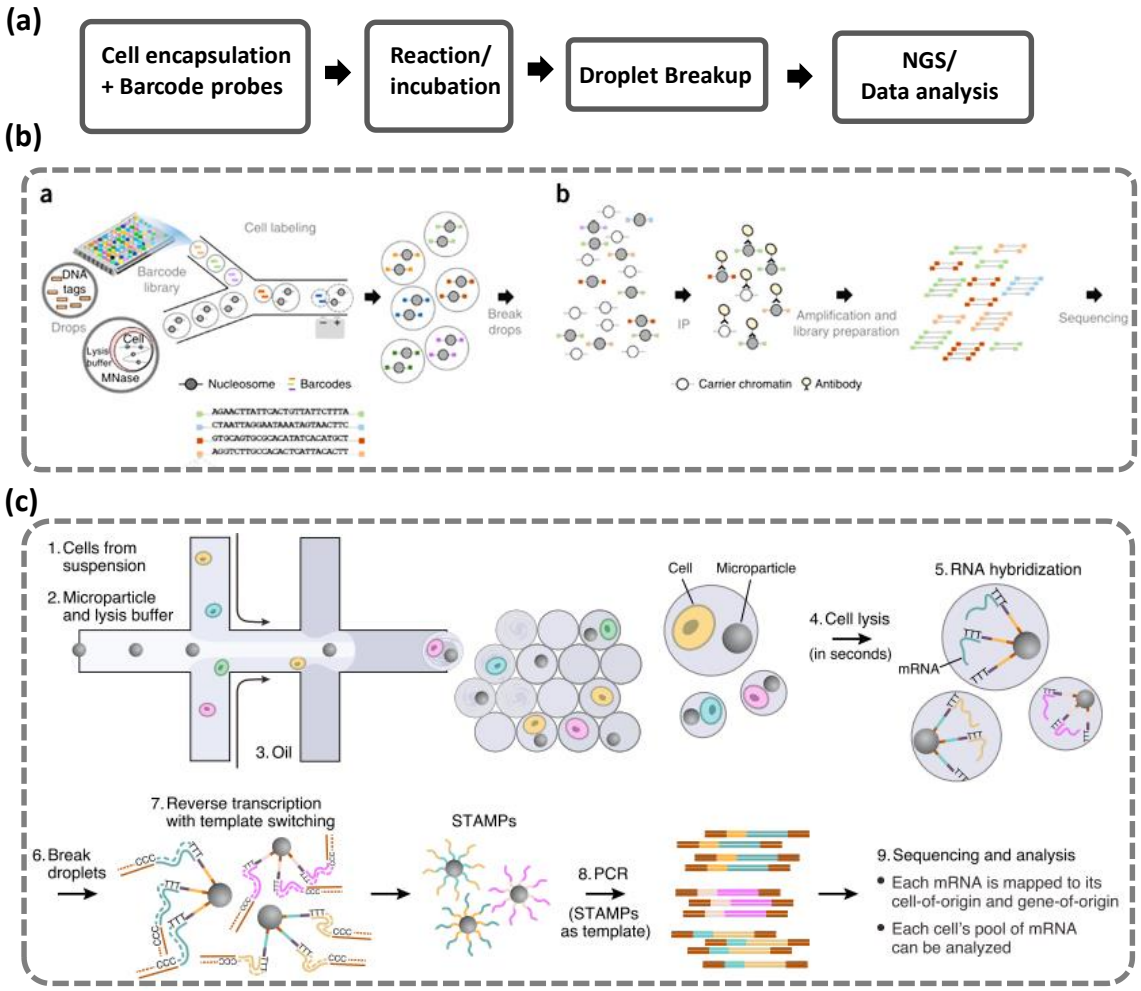

Figure. 2.5 (a) Schematics of single-cell barcoding workflow. (b) Schematics of drop-based ChIP-Seq workflow [92]. (c) Schematics of Drop-Seq workflow [53].

In 2015, Rotem *et al.* presented the first droplet-based chromatin immunoprecipitation sequencing (ChIP-Seq) for single-cell epigenetic study (Figure 2.5b) [92]. A pool of droplets containing 1,152 different DNA barcodes was first synthesized in several 384-well plates and mixed. Next, the cells were encapsulated in droplets with lysis buffer so the chromatin was released. The single-cell chromatin-containing droplets were merged with the droplets

containing DNA barcodes and DNA ligase solution. In this step, nucleosomal DNA fragments were linked with barcode sequences, thus annotating the chromatin fragments with their corresponding cells. After that, the droplets were pooled together and broken for antibody immunoprecipitation, library preparations, and NGS. Subpopulations from a mixture containing thousands of mouse embryonic stem cells were identified by differences in chromatin signatures.

Additionally, in 2015, Macosko *et al.* reported another barcode strategy and applied single-cell mRNA sequencing called Drop-Seq (Figure 2.5c) [53]. In Drop-Seq, DNA barcodes are synthesized on microparticles using a "split-and-pool" strategy. A pool of microparticles is first split at random into four different DNA bases (A, G, C, or T). Then, all microparticles are mixed and re-split again at random into another four DNA bases. After 12 split-and-pool cycles, 4^{12}= 16,777,216 possible 12-bp barcodes are synthesized on microparticles called cell barcodes. The cell barcode is identical on the same particle but different between different beads. Next, random barcodes can be introduced on each primer through the degenerate oligonucleotide synthesis approach as unique molecule identifiers. By co-encapsulating a single barcoded microparticle with single cells into droplets, this strategy enables a much larger capacity of barcoding droplets than previous methods. mRNA transcripts from thousands of individual cells can be simultaneously analyzed and mapped to their organs or tissues of origin. Since transcriptomic analysis has become one of the most popular single-cell assays recently, many new droplet-based sc-mRNA-Seq platforms have been reported with advanced features[59], [93], [94]. For example, Zilionis *et al.* used hydrogels as the material for barcoded microparticles (InDrop)[94]. Therefore, co-encapsulation efficiency is significantly improved with the close-packed hydrogel particles in the microfluidic channel. The high loading

efficiency also enables the use of an expensive RT enzyme for in-droplet cDNA synthesis. In 2016, 10x Genomics Inc. developed the first commercialized platform, "Chromium," for sc-mRNA-Seq based on droplet microfluidic technologies[93]. This makes the sc-mRNA-Seq technique widely available to biology communities.

Recently, droplet barcoding techniques have been coupled with a multi-step workflow for more versatile single-cell analysis. For example, in 2017, Shahi *et al.* presented a highly integrated droplet microfluidic workflow for single-cell protein profiling (Figure 2.6) [48]. By combining DNA-tagged antibodies with droplet-based barcoding and sequencing techniques, there are many potential advantages beyond the traditional approach using ELISA for protein profiling, including single-molecule sensitivity, quantitative results, high throughput, and unl imited multiplexing in one run.

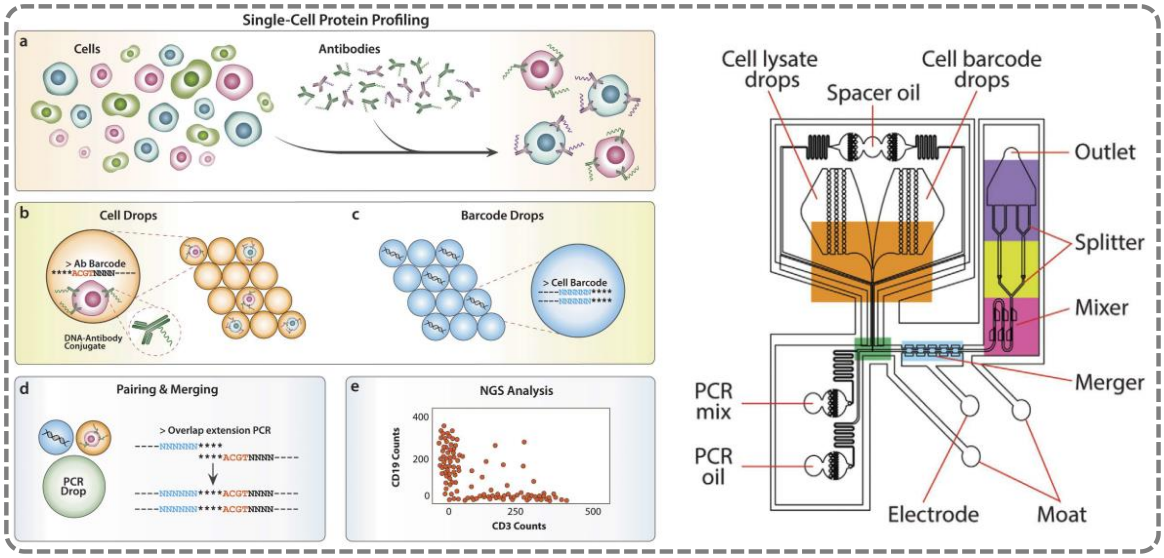

Figure. 2.6 Left: schematics of single-cell protein-profiling workflow (AbSeq). Right: Schematics of microfluidic devices for AbSeq. Three types of droplets undergo multiple incubation and splitting processes and are finally merged together for in-droplet PCR and downstream processes.[48]

2.2.4 Live single-cell functional assay using stationary droplet microfluidics

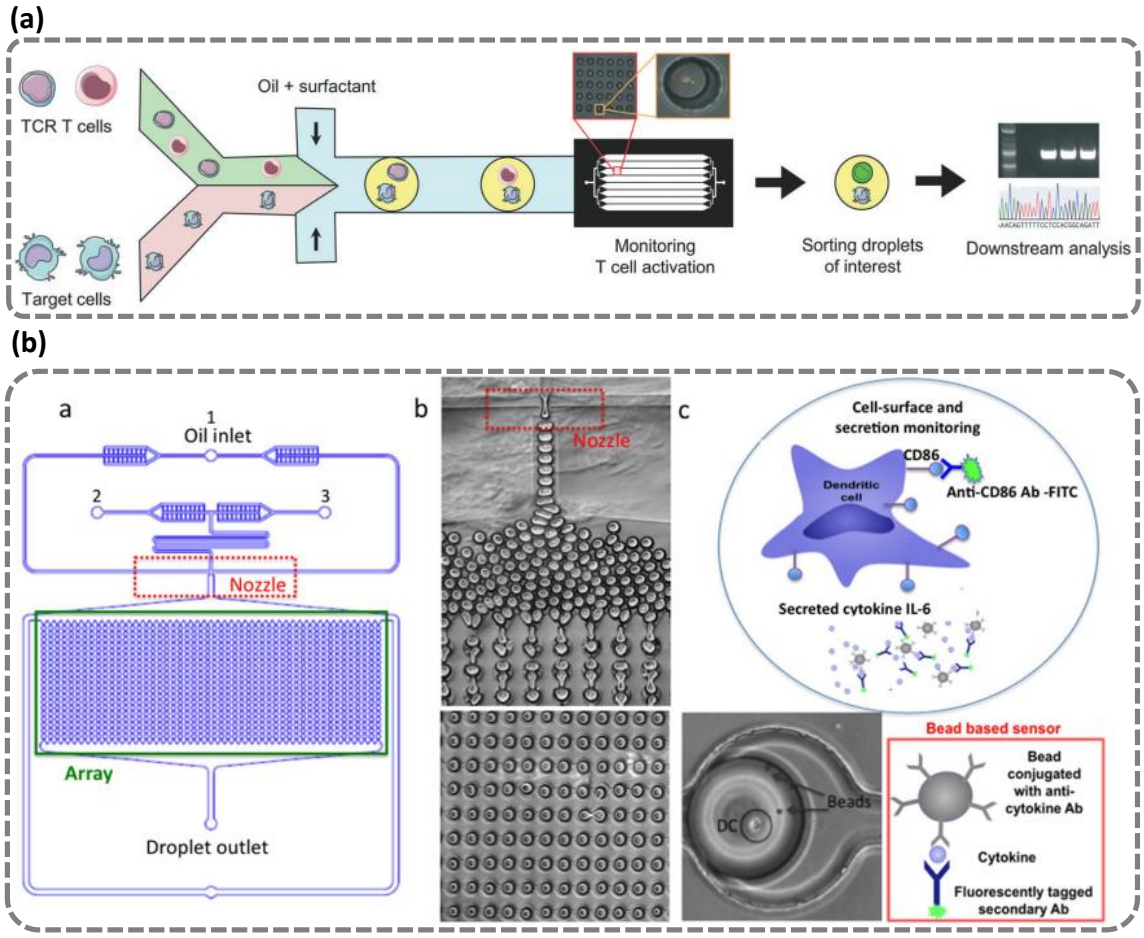

Figure. 2.7 (a) Schematics of droplet-based functional TCR T-cell-screening platform. Non-specific TCR T cells and specific TCR T cells are co-encapsulated with target cells for screening. Only droplets containing activated T cells were sorted for downstream molecular analysis. [95] (b) A microfluidic platform for simultaneous monitoring of surface markers and secreted proteins from dendritic cells. [96]

In the above sections, we discussed several single-cell studies using continuous-flow droplet microfluidics. However, the continuous-flow scheme only allows us to capture a glimpse of the current status of cells. In some cases, people are interested in the long-term monitoring of the single-cell functional status in a confined space, such as studies on cell–cell communication or protein secretion[95]–[98]. Since there is no way to track hundreds or thousands of droplets dynamically so far, droplets must be immobilized in an array format for long-term monitoring. The static droplet scheme is expected to have a simpler workflow than the continuous droplet microfluidic scheme described above. However, only a few proof-of-

concept experiments been undertaken to demonstrate the static scheme. For example, S.Sarkar et al. integrated a droplet generator with a droplet capturing array for screening functional TCR T-cell (Figure 2.7a) [98] and phenotyping dendritic cell function (Figure 2.7b) [99]. Their droplet capturing array provides a static environment for long-term monitoring of the cell status which is necessary for such phenotypic studies. However, the lack of other integrations and control mechanisms in static droplets limits further operations. After on-chip measurement, the captured droplets can only be released from the microfluidic traps into microtubes individually and analyzed with traditional benchtop setup. Many high-throughput analysis techniques described in the sections above are prohibited in the stationary droplet workflow. Even though the stationary droplet microfluidics does not have competitive scalability and speed than continuous droplet microfluids, its unique advantages such as time-course monitoring, image-based measurement, high stability, and ease of operation, remain attractive. Therefore, in this thesis, we will present a hybrid platform that combines both advantages from the continuous-flow scheme and stationary scheme for a more versatile single-cell analysis.

Chapter III

A Droplet Sorting and Downstream Merging (Sort 'N Merge) Platform.

3.1 Introduction to the Study

Merging multiple aqueous droplets containing different reactants is a fundamental process for biochemical reactions. For microdroplets-based single-cell assays, droplets containing single cells, aqueous reagents, and solid particles are generated and manipulated to form desired combinations and results. In many droplet-based single-cell assays, co-encapsulation of a cell-particle or cell-cell pair is a critical process [53], [94], [95], [99]–[101] (Table 1). For example, co-encapsulating cells in a droplet with surface modified

Table 3.1. Examples of single-cell assays that require pairing two or more particles inside a microreactor.

Particle		**Buffer**	**Applications**	**Ref.**
A	**B**			
Cell	Primer coated bead	Lysis and RT buffer	Single-cell RNA-seq	[53][94]
	Antibody coated bead	Fluorescent antibody	Single cell secretion	[95][99][100]
	Cell(s)	Culture medium	Cell-cell interaction	[98][101

microparticles that provide solid support to various biomolecular probes enables transcriptomic or proteomic assays [53],[94]; Co-culturing two or more cells in a confined environment enables the study of how distinct cells interact with one another[98]. The ability to precisely control the contents of such microdroplets is essential for an accurate result. In most cases, the assay process strictly requires one-to-one pairing of either a cell and a microbead or two cells to obtain unambiguous single cell study results. The conventional approach to pairing two distinct particles by a co-flowing scheme suffers from low pairing efficiency that results from multiplying the low-probability *Poisson* statistics of two rare events[56], which require the two distinct particles to be trapped exactly in the same droplet (Fig. 3.1.a). As a result, co-encapsulation assays turn out to generate mostly negative droplets, including those with a single particle or a doublet of particles of the same type, thus yielding significant sample loss and error in downstream analysis. Such sample loss is particularly intolerable if biological particles are rare and precious cells[102], [103]. Moreover, the probability of gaining droplets with a desired combination of particles decreases exponentially

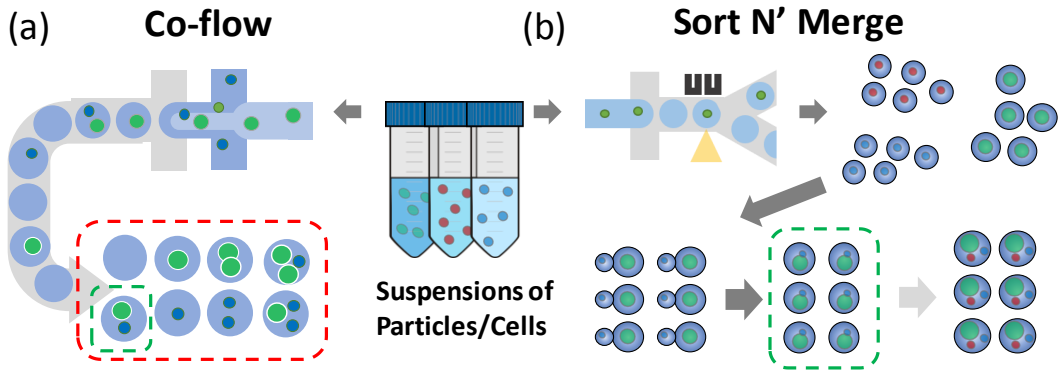

Figure 3.1 (a) Conventional co-flow scheme for encapsulation of two distinct particles. Due to two independent Poisson events, the population of droplets encapsulating a pair of two distinct particles constitutes a small fraction. (b) Our new approach to particle co-encapsulation in droplets. This approach first involves sorting of single-particle encapsulating droplets, which is followed by paring and merging of two sorted droplets, each encapsulating a different particle. As a result, nearly 100% of the sorted droplets contains only one particle. Then, the merged droplets turn out to contain exactly two distinct particles. By iterating this process, it is possible to co-encapsulate even three or more particles.

with the number of particles in each droplet, making it impossible for co-encapsulating more than two objects. This prevents the wider use of droplet technology in biological study.

To overcome the *Poisson* statistics limitation, a few studies have explored alternative encapsulation approaches. For example, Edd *et al.* [58] created self-ordered trains of cell particles by a hydrodynamic effect so that each particle is lined up with the same interval before its encapsulation in a droplet. Such ordered cell particle trains can be synchronized with the formation of droplets at the same frequency, thus resulting in high single-cell occupancy of the droplets. Later, Lagus *et al*. demonstrated co-encapsulation of cell-cell pairs by co-flowing two distinct cell types based on a similar synchronization mechanism to the one above[104]. This approach has limited application because forming a cell train requires a high density of cells that are homogeneous in size. Moreover, owing to the enormous time needed to adjust the balance between the aqueous and oil inflows, it is still challenging for this approach to obtain a high co-encapsulation yield with minimized sample loss. Alternatively, Abate *et al.* used mechanically deformable particles which can be closely packed in a channel to achieve ordered encapsulation to increase paring efficiency and accuracy[105]. This method has been further applied to co-encapsulation of cell-bead pairs during inDrop single-cell mRNA sequencing[94]. However, only particles made from soft materials, such as hydrogels, are capable of being closely-packed in a channel to achieve ordered encapsulation. Given these limitations, we sought to develop a more robust method that permits one-to-one encapsulation of desired objects.

Here, we demonstrate a novel microfluidic droplet-based platform (Sort ‘N Merge) resulting in highly efficient co-encapsulation of two distinct particles with significantly low loss (Fig. 3.1.b). Our approach first generates two different types of droplets, for example,

encapsulating either a single cell or a single bead individually and eliminates empty droplets by photo-activated droplet sorting. Next, the two different types of droplets are paired on a one-to-one basis and merged to generate droplets that contain exactly two different objects. Traditionally, efficient post-sorting droplet merging has been perceived as unfeasible for samples of low abundance because it requires highly challenging off-chip handling of a tiny total volume of sorted droplets (for example, 1,000 of 50um droplets are only 65nl in total volume) and precise one-to-one pairing. Droplet pairing and merging are performed based on either a serial or parallel coalescence approach. A serial approach pairs two types of droplets after sequentially injecting them into a flow channel and forming a flow of their equidistant pairs[74]. Although the approach appears to work well with a large number of droplets available, its overall recovery rate would be low when handling a small number of droplets. This method wastes a significant number of droplets at the initial stage of the droplet injection process before the system operation reaches stability. Therefore, a serial approach is unlikely to serve well for rare sample applications. In contrast, a parallel approach first forms multiple static droplet pairs in a storage array and later merges them all together in a massively parallel manner[66], [76], [106]. This approach provides a basis for our method here and may handle a small number of droplets better with appropriate microfluidic design. Our study seamlessly integrates droplet generation, sorting, capturing, pairing, and merging in one system to reduce the complexity of the assay. The desired particles are actively selected and one-to-one paired precisely inside the droplets, therefore, overcomes sample loss due to *Poisson* statistics. The ability of our system to generate and sort droplets encapsulating particles with distinct sizes and photo properties permits its versatile implementation in a wide spectrum of single cells- or microbeads-based assays.

3.2 Materials and Methods

3.2.1 Microfluidic system

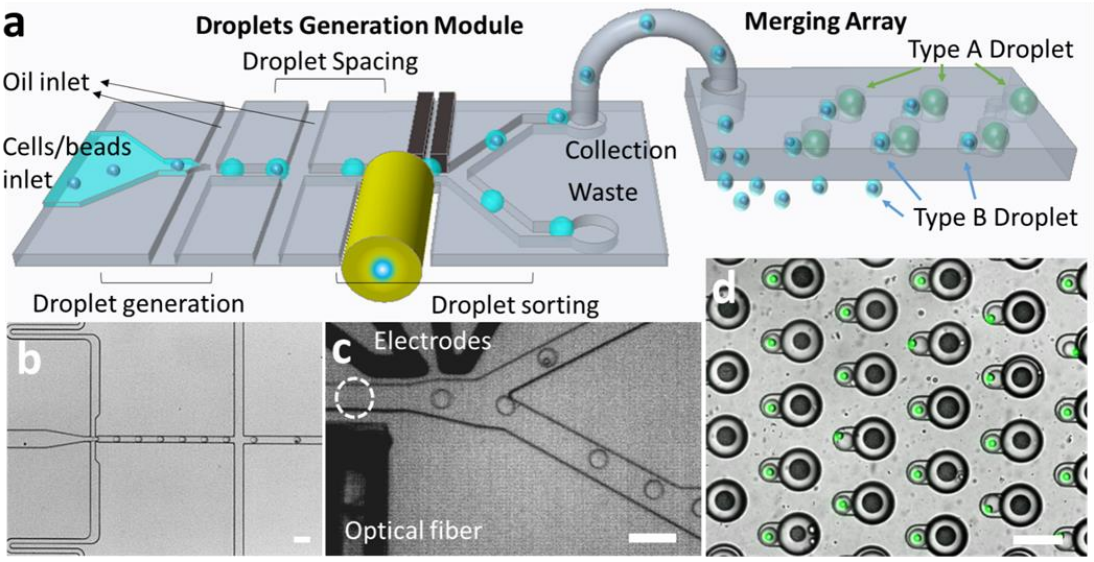

Figure 3.2 (a) Schematic of microfluidic system composed of droplet generating/sorting and droplet merging devices. (b) Droplet generation process. Water-in-oil droplets, each encapsulating a single particle, are generated at the flow-focusing structure. (c) Droplet sorting process. The droplets generated in (b) are sorted to the upper outlet channel connected to the downstream droplet merging device by photo-activated sorting. The white dashed circle indicates the position of the interrogation zone next to the embedded optical fiber illuminating laser light and collecting a droplet optical signal. The merging device is composited of 1152 trapping sites where droplets of two different sizes are captured and paired. (d) Image of 40um-diameter fluorescent bead-encapsulating droplets paired with 80um-diameter non-fluorescent bead-encapsulating droplets at the merging device. Some of the fluorescent beads stay at the water-oil interface due to the hydrophobicity of their constituent material, polystyrene. The water absorption by the PDMS material results in droplet shrinkage within the merging device, leading to a droplet size variance < 10% after 100 min. Scale bar:100μm.

Our microfluidic system consists of two sub-component devices: a droplet generating device with a built-in fluorescence-activated sorting function (Fig. 3.2a-c) and a droplet merging device (Fig. 3.2a, d). The outlet of the former device is connected via a microbore tubing to the inlet of the latter one. Both devices are made of Polydimethylsiloxane (PDMS) by the standard soft lithography method (Appendix A). In brief, SU-8 molds fabricated on a 4-inch silicon wafer were constructed by multiple spin-coating, baking, exposure, and developing processes for different layer thicknesses. SU8-2050 and 2100 were used to create

molds of the microchannel and optical fiber grove features with heights ranging from 45-120µm. Afterward, the Poly-dimethylsiloxane (Dow Corning, Sylgard 184) and curing agent were mixed at 10:1 ratio, poured onto an SU-8 mold, and baked at 65 °C overnight to replicate the SU-8 features into a cured PDMS layer. The PDMS layer was subsequently punched with a 0.75mm-diameter puncher to form inlets/outlets and bonded to a glass slide after the PDMS surface was activated by oxygen plasma (Femto Scientific Inc.). Then, an optical fiber (F-MCB-T-1FC, Newport Corp.) was polished using a polishing paper (Thorlabs) and manually embedded into a fiber grove formed in the PDMS layer. Microelectrodes were created on the glass substrate by injecting low melting alloy (247solder) into the electrode channels in the PDMS layer at 150˚C. To make the fluidic channel hydrophobic, the channels in the PDMS layer were treated with Trichloro (1H,1H,2H,2H-perfluorooctyl)–silane (Sigma-Aldrich) at a concentration of 2% (v/v) in Novec7500 (3M Corporation) prior to use.

3.2.2 Droplet generating/sorting setup

Fig 3.3 shows the CAD layout of our droplet generating/sorting device. We use two nozzles of different sizes for the device's flow-focusing zone structure to generate different

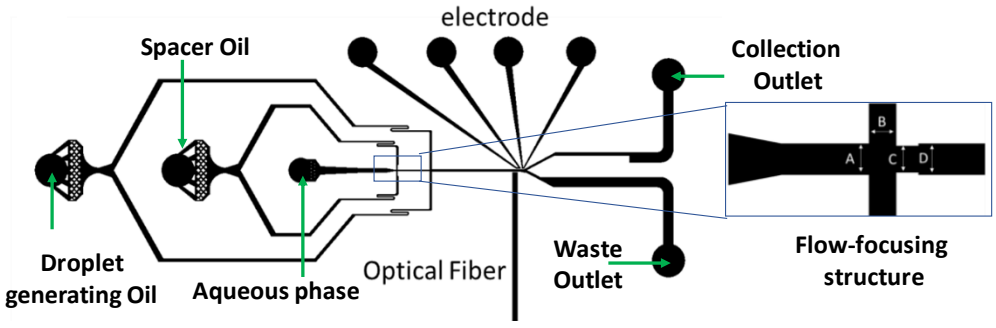

Figure 3.3. CAD layout of droplet generating/sorting device (top view). Right: Dimensions of flow-focusing zone. For generating larger (80 µm) droplets: B=C=60 µm, A=D=70 µm, channel height=70 µm. For smaller (40 µm) droplets: A=B

sizes of droplets. Right after the generating of droplets, it incorporates an active droplet sorting function by which only desired droplets are selected and guided to its collection channel.

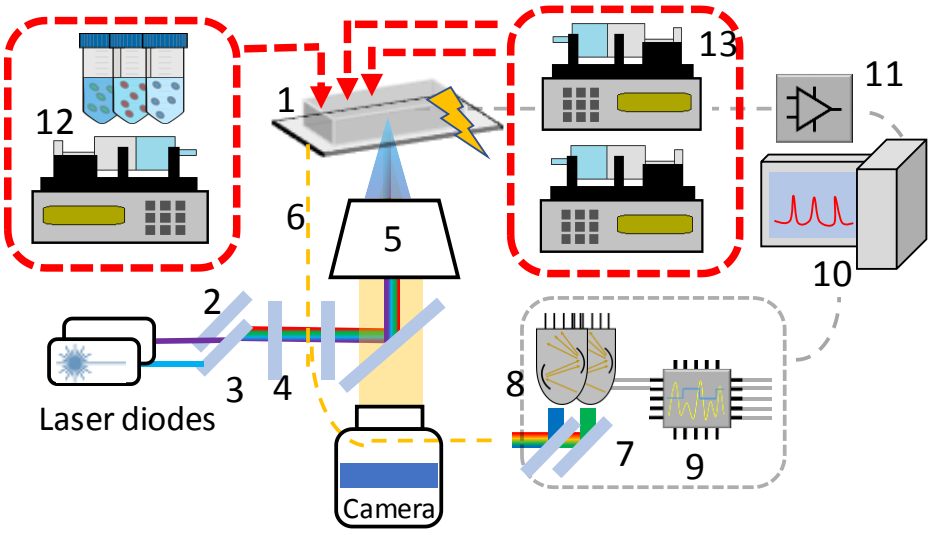

Figure 3.4. Schematic of the experimental setup of the DMDS platform. The detection/sorting device (1) is placed on an inverted microscope (TS-100, Nikon) for observation using a high-speed camera (phantom Miro eX4). Two lasers (2) (λ=405 nm, 50 mW and λ=450 nm, 50 mW) are aligned into single beam by dichromic mirrors (4). The laser beam passed through shaping lens (4) and guided into objective lens (5) to excite fluorescent objects in the microfluidic channel. The detection system incorporates two photomultiplier tubes (8) (Hamamatsu H9306-03) that receive emission signals passing through optical fibers (6) and optical band pass filters (450 nm and 525 nm CWL). Two dichroic mirrors (7) (LP425nm and LP505nm) are used to combine and separate different excitation wavelengths. Optical emission signals are detected and converted to voltage signals by the PMTs, and are recorded by a DAQ card (PCI-6111, National Instrument). The control module is composed of a customized signal processing circuit and a micro controller board (9) (Uno32, Chipkit) to generate TTL signals. The TTL signals trigger a function generator (10) (33220A, Agilent) to generate square wave pulses which are subsequently amplified through a voltage amplifier (11) (AV-110B-PS-D, Avtech) and sent to the microelectrodes of the detection and sorting device. The aqueous phase and oil phase (pure Novec7500) are pumped into the flow channel from syringes (12,13) using syringe pumps (KDS-200, KD scientific) to generate droplets. Only droplets emitting signals detected above a threshold readout are deflected to the collection outlet and the rest of the droplets flow to the waste outlet.

Figure 3.4 shows the experimental setup of the droplet sorting platform. We inject the aqueous phase and oil phase (HFE 7500, 3M) into a flow-focusing channel by syringe pumps to generate water-in-oil droplets. The droplets are stabilized with 2% EA-surfactant (RAN biotech.) in the oil phase. While passing by the interrogation zone in front of an embedded optical fiber (F-MCB-T, Newport), the droplets are excited by a laser beam focused with an objective lens. The fluorescent and scattering light are collected by an optical fiber and detected

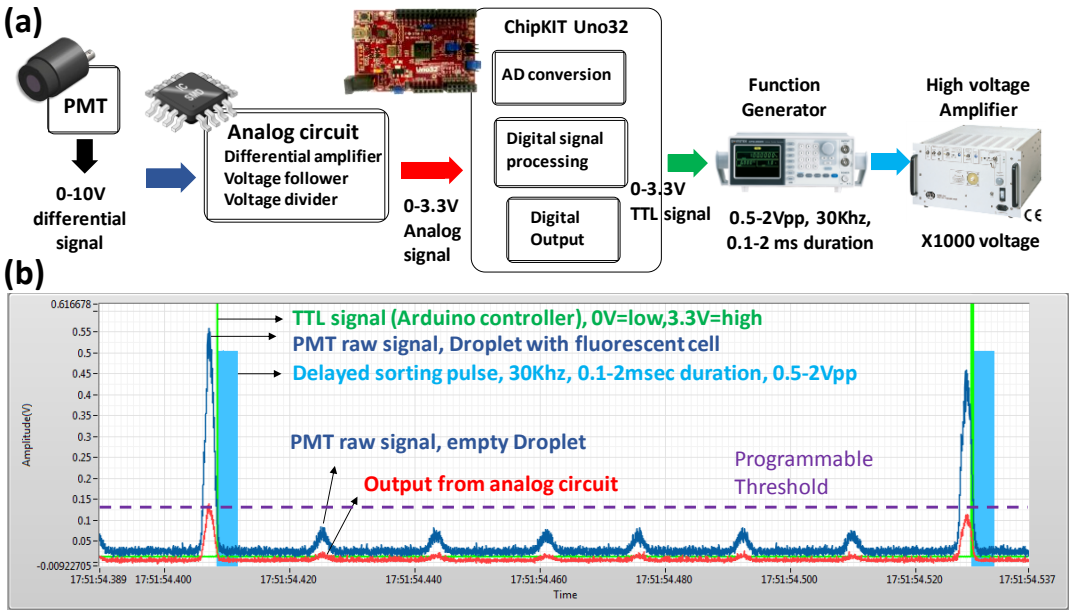

Figure 3.5. (a) Processing flow of our home-made control module for generating feedback sorting signal. (b) Snapshot of our LabVIEW program shows the time sequence of PMT raw signal (blue), processed signal (red), TTL signal (green), 30kHz electrical pulse for droplet sorting (cyan), and sorting threshold (purple). Unit of x-axis: hh:mm:ss.msec

by two photomultiplier tubes (H9306-03, Hamamatsu). A dichroic mirror (500LP) and two bandpass filters (CW450nm and 525nm) are used to separate fluorescent and scattering light. The electrical signal is then processed in real time by a customized control module (Fig. 3.5a). The signal output from PMT is a differential signal and is connected to the DAQ card for signal recording (Fig. 3.5b) and to our customized control module in parallel. Our analog pre-processing circuit includes a differential amplifier, voltage follower, and voltage divider. The differential amplifier converts the differential signal to single-end signal; The voltage divider compresses the dynamic range of the signal from 10V to 3.3V which is the operating voltage of typical microcontroller; The voltage follower has substantial input impedance and small output impedance which prevents the interference between PMT circuit and control circuit. The chipKIT Uno32 has Arduino header which accepts the analog signal up to 3.3V and has a built-in 10-bit analog-to-digital converter with its bandwidth up to 142Ksps per channel. The

microcontroller was programmed by Arduino IDE to process the input signal (Appendix B). In each computing cycle, the input analog signal is compared to a given threshold. A delayed TTL (Transistor-Transistor Logic) pulse was generated through digital output if a positive droplet is detected. The delay time ranges from 0-500 μs which is the time required for droplet traveling from interrogation zone to the the sorting zone. Each iteration of this system cost about 7 μs which is fast enough for our FADS system. The computing speed can be even faster by using an external AD converter, FPGA processor, or commercialized FPGA embedded DAQ card if a higher sorting throughput is desired. The TTL signal triggers a short AC pulse (<2Vpp, 30kHz) by a function generator. The electrical pulse is amplified 1000-fold by a high voltage amplifier and delivered to microelectrodes in microfluidic devices. The dielectrophoretic effect due to a strong AC electric field around the microelectrodes pulls signal-emitting droplets into the collection channel while empty droplets simply flow into the waste channel following lower fluidic resistance.

3.2.3 Droplet merging device

The droplet merging device incorporates a flow channel that contains a uniquely designed 1152-microwell array. The merging device captures droplets entering from the upstream collection channel of the droplet generation/sorting device by buoyancy trap. Each microwell is designed to trap exactly two droplets with deferent sizes (Fig. 3. 2d, Fig. 3.6). We first flow 80μm-diameter droplets (volume:268pL) into the merging device channel (height: 500μm) and then trap them in the microwells until all the trapping sites are filled. Similarly, we sort and trap 40μm-diameter droplets (volume:34pL) and then pair them one-to-one with the 80μm droplets in the microwells. The number of droplets flowed into the device are varied for different purposes and the relation is discussed in the result section. After flushing out the

excess of untrapped droplets, the droplet pairs are merged by either chemical or electrical induced coalescence. For chemical induced calescence, an oil containing 2%(v/v) perfluoro-butanol (PFB) is flowed into the device channel as a demulsifier to trigger merging events. Subsequently, an oil with 2% EA-surfactant is flowed into the device channel again to re-stabilize the merged droplets, which are then released from the microwells by flipping the device. For electrovalence, droplets are merged by applying a high voltage AC pulse (<1kVpp, 10kHz, 0.5sec duration) at microelectrodes beside the droplet array.

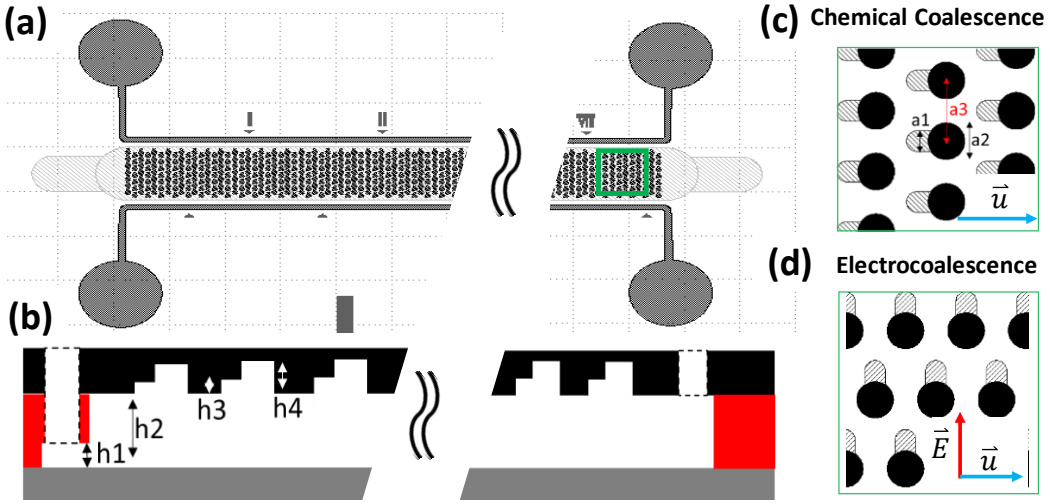

Figure. 3.6 (a) Top view of the droplet merging device. The red line represents the microfluidic channel structure and the black patterns represent the array of microwells. Two thick red lines outside microfluidic channel indicate the microelectrodes for electrocoalescence. (b) Side view of the device (the drawing is not to scale). h1=100 μm, h2=500 μm, h3=40 μm, h4=70 μm. (c-d) The lattice structure of the array. a1=45μm, a2=80μm, a3=140 μm. Two lattice orientations are used for different merging mechanism. (c): Chemical coalescence. (d): Electrocoalescence. The blue arrow and red arrow indicate the direction of the fluidic flow and the electrical field, respectively.

3.2.4 Co-encapsulation experiment

The droplet capturing and merging efficiencies of our device are characterized using two-color (red and green) dyed droplets for visualization. The co-encapsulation experiment is performed using 15μm fluorescent micro-beads (F8844, ThermoFisher Sci.) and 30μm non-fluorescent micro-beads (TOYOPEARL HW-65S). These beads are suspended in PBS

solution with 16% (v/v), OptiPrep density gradient medium (Sigma), and 0.2% TWEEN 20 to prevent their aggregation.

3.3 Results and Discussion

3.3.1 Droplet generating and sorting

Hydrodynamic trapping in a microfluidic device has been used for single-cell capturing [57]. However, the size heterogeneity of cell types often found in biological samples limits the wider use of conventional trapping methods simply assuming particles uniformly in size. Alternatively, a flow-focusing structure can be used to encapsulate single cells varied in size within monodisperse micro-droplets, which provides an ideal means to capture these

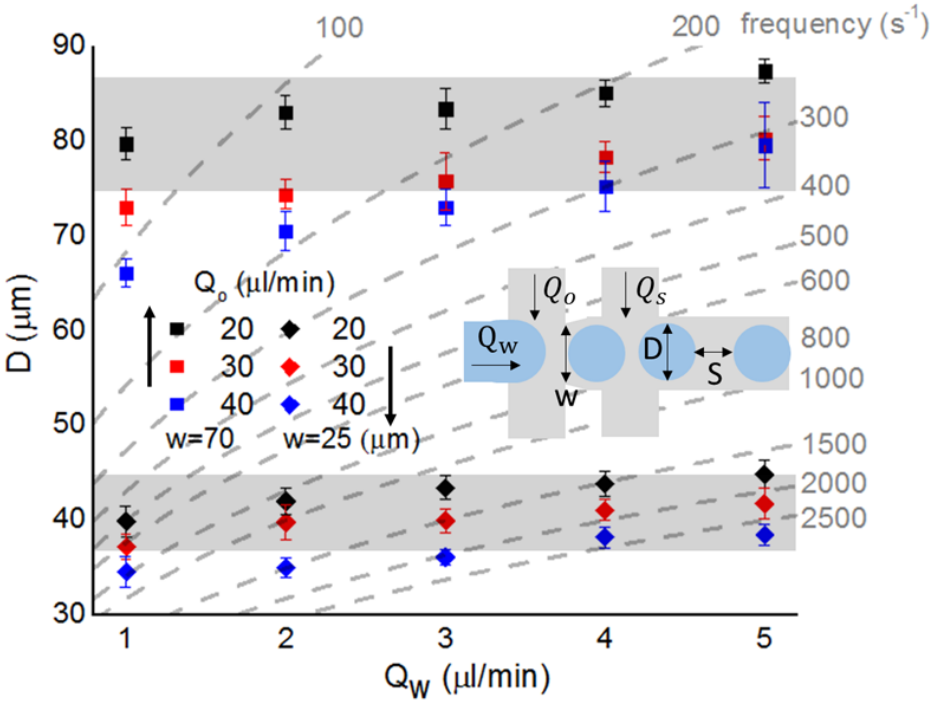

Figure 3.7 Diameter D (mm) and throughput (s^{-1}) of droplet generation (or sorting) under different original oil (Q_o) water (Q_w), and spacing oil (Q_s) flow rates (ml/min). Devices with two different orifice features (25μm×40μm and 70μm×70μm) are used to generate droplets with diameters staying within the tolerance range of 40+/- 4 μm and 80+/- 8 μm. The 10% size tolerance allows the pairing and merging process to yield reproducible results. Q_s is set to guarantee a minimum distance S~12D between two adjacent droplets. Therefore, $Q_s = (S \cdot Q_w) - Q_o$. The error bars were determined from photo images across at least 100 droplets from three repeated experiments.

heterogeneous single cells. This approach first requires generating droplets in a constant size that is large enough to encapsulate cells of any sizes and still fits the size of a downstream single-droplet capturing chamber. Although many other studies elucidated the mechanism of droplet formation, there exists no simple scaling law towards generating the desired droplet size as many dimensional and fluidic parameters need to be considered [43]. Here, we empirically determined conditions that generate 40μm- and 80μm-diameter droplets using two droplet generating/sorting devices with different orifice sizes at their flow-focusing regions. The 40μm- and 80μm-diameter droplets can encapsulate at high throughput most of the the mammalian cells and engineered microbeads (< 60μm), respectively. Fig. 3.7 shows the formation of different droplet sizes that result from different combinations of water and oil flow rates (Q_w and Q_o). By adjusting the water/oil flow rate ratio, both devices met the design specifications leading to the targeted droplet sizes (shaded zone in Fig.3). The interface of the generated droplets was stabilized during their passage through a short channel, and a spacing oil was added to provide a proper distance between adjacent droplets. The presence of a droplet itself generates additional hydraulic resistance against other droplets flowing within the channel. Thus, setting enough inter-droplet spacing is important to prevent physical interferences between droplets at the Y-shaped outlet junction. The optimal spacing distance was empirically determined by adjusting the oil-to-water flow ratio until all the droplets flowed into the collection channel (or the waste channel) at the presence (or absence) of the electric field. Here, the flow rate of spacing oil Q_s is given by $Q_s=(S\cdot Q_w)-Q_o$, where S=12 represents the droplet-to-droplet distance normalized by the droplet diameter, which is approximately equal to the disperse phase-to-continuous phase volume ratio.

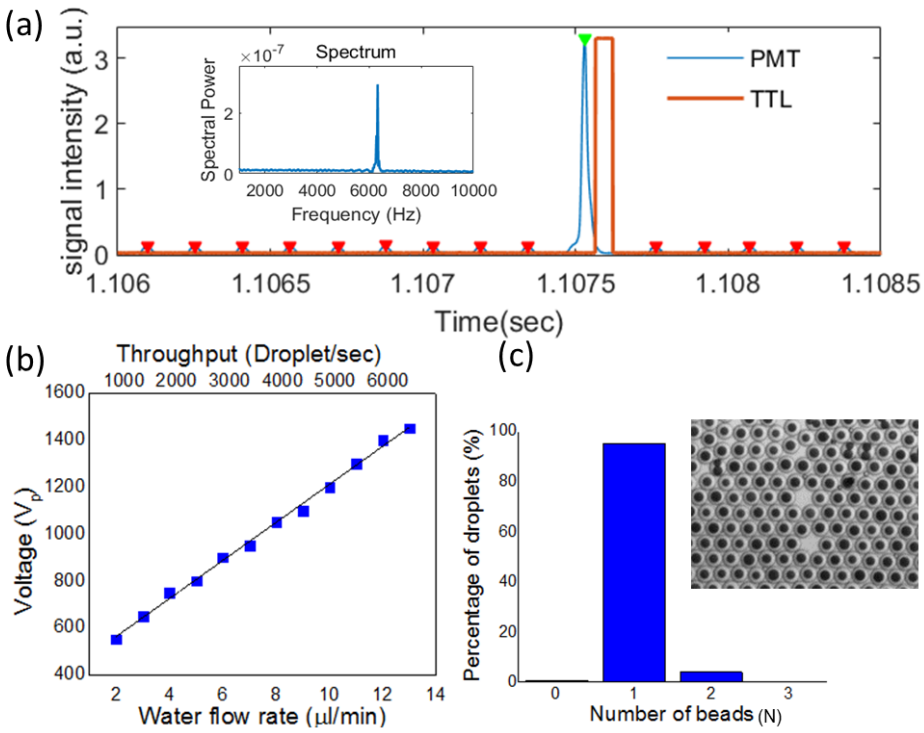

Figure 3.8 (a) Time sequence of fluorescent signals (blue line) detected from empty droplets (red dot) and from droplets containing beads (green dot). The orange line represents the logic signal processed by a microcontroller for triggering the sorting pulse. (b) Relationship of minimum voltage required to deflect droplets into collection channel for given throughput and water (cell culture medium) flow rate. The flow rate of the oil phase is fixed at 11 folds of the water flow rate. (c) The histogram shows the percentage of sorted droplets that contain N beads.

Figure 3.8a shows measured fluorescence signals from empty droplets and droplets containing microbeads. We found uniform time interval distributions across these droplets because the integration of droplet generation and sorting reduces the unstable factors during droplet reinjection. Figure 3.8b shows the linear relationship between the throughput (aqueous flow rate) and the voltage required to deflect droplets into the other channel. Although sorting droplets at a throughput up to 6000 droplets/second is possible, it requires fine tuning of the pressure difference between two outlets and the intensity of the applied voltage. We found that at a higher flow rate, there is a higher chance that the droplets could be torn up by vigorous dielectrophoretic force. This sets the practical sorting throughput at about 2000s^(-1) for 45μm droplets and 300s^(-1) for 80μm droplets, respectively.

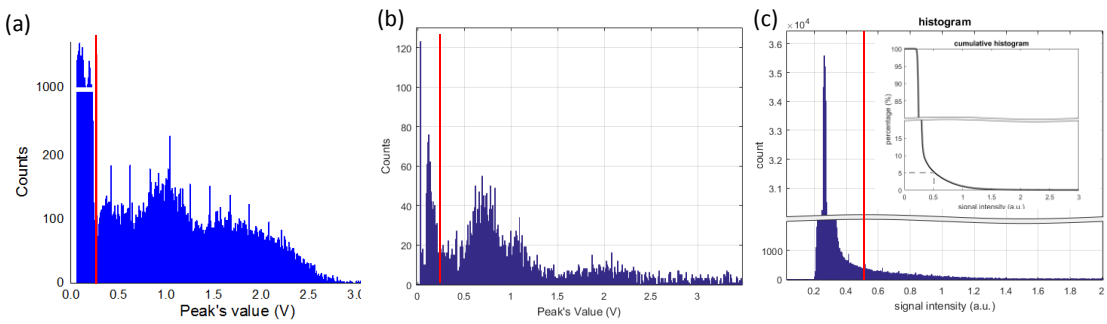

Figure 3.9 Histograms of detected peak values for type-a (a), type-b (b) beads, and Hela cell encapsulated droplets.

We next validated the accuracy of the droplet generating/sorting device performance by using both fluorescent (type-a) and non-fluorescent (type-b) microbeads. We generated 40μm-diameter droplets with a single type-a bead and 80μm-diameter droplets with a single type-b bead at a concentration of 1,500 and 200 beads/μl, respectively. These concentration values correspond to 0.05 beads per droplet ($\lambda_a = \lambda_b = 0.05$) for both droplet types. The generated droplets were subsequently sorted on the same device while empty droplets were discarded to the waste reservoir. We found more than 99.5% of the sorted droplets encapsulated at least a single bead (Fig. 3.8c). We observed that a small (<3%) population of the sorted droplets contained a doublet or clumps. Our sorting process could not easily exclude these droplets. Further sample dilution and sample pre-filtration would be necessary to eliminate the formation of these droplets and to remove the clumps. At a given signal-to-noise ratio (SNR) of our setup, the setting of the sorting gate determined the rate of the false positive output associated with the presence of an unsorted bead-encapsulating droplet. With an appropriate sorting gate being applied, we were able to suppress the false negative output rate down to < 1% (Fig. 3.9a-b). We also tested our system's capability of sorting droplets encapsulating non-fluorescent Hela cells detected by scattering light. The result was

comparable to the sorting result with the fluorescent beads above (Fig. 3.9c). The label-free sorting could bring a technological benefit to droplet assay as it simplifies the assay process.

3.3.2 Droplet capturing and pairing

The technical challenge to efficiently merge two droplets with one-to-one precision is significant. Here, we proposed a solution, in which the droplet generation/sorting process and the droplet merging process were performed serially using the two sub-unit microfluidic devices. This approach eliminated the need for the practically challenging process of synchronizing the flows of two droplets prior to their merging. The microbore tubing (0.010" ID × 0.030"OD) connecting the merging device to the droplet generating/sorting device guaranteed no-loss droplet transfer while protecting the droplets from the destruction caused by surface tension force emerging from the off-chip operation. The merging device exerted no significant back-pressure to the droplet generating/sorting device, therefore not interfering the flow speed originating from the droplet generating/sorting device. Meeting these requirements would be difficult with a conventional droplet merging technique driven by a hydrodynamic pressure gradient along the flow direction. Instead, we introduced a novel approach of utilizing buoyancy generating a vertical trapping force orthogonal to the flow direction. This feature also allowed us to do "hot-swapping" of the filled merging device without disrupting the independent sorting function.

Another challenge that we addressed was to achieve a high droplet retention rate, which is given by the ratio of the number of captured droplets to the number of input droplets. Most of the conventional droplet merging experiments require the use of abundant droplets to guarantee the filling of nearly all capturing sites. While this leads to a high occupancy rate, a large proportion of droplets are wasted, thus resulting in a significantly low retention rate. In

contrast, our post-sorting/alignment strategy could retain a very small number of droplets in the merging sites to achieve both high retention and high trapping site occupancy rates at the same time.

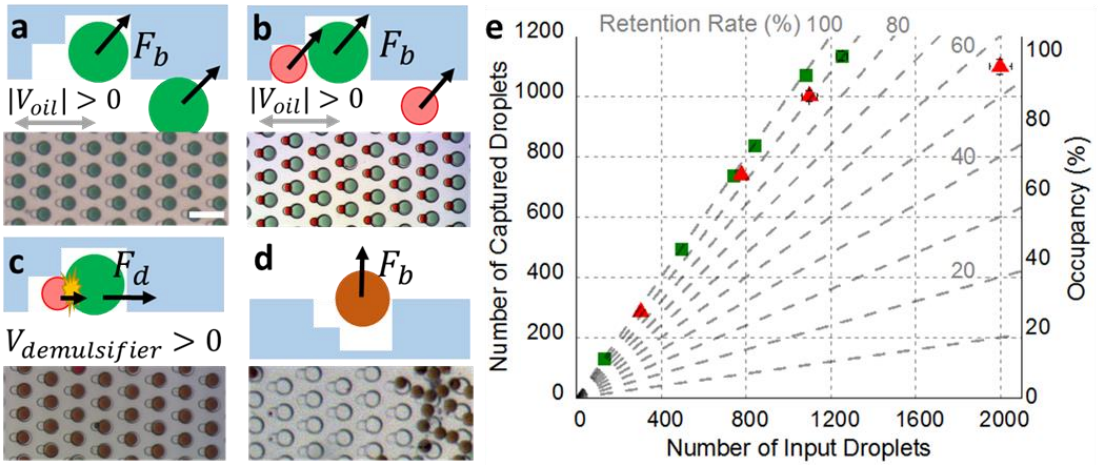

Figure 3.10 . (a-d) Sequential schematics (side-view) and images (top-view) of droplet capturing, pairing, and merging steps. The black arrow indicates the dominated force in each step. (a) 80µm-(green) droplets introduced to the droplet merging device first settle in the trapping sites by buoyance force. An external oscillated flow in the bottom channel enhances the capturing efficiency. (b) Similarly, 40µm-(red) droplets are captured and paired with the green droplets already captured in the trapping sites. (c) An external flow containing demulsifier is used to make two paired droplets in contact by drag force and merge them. (d) After re-stabilizing them, the droplets can be released by flipping the device. (e) Number of input droplets versus number of captured droplets. The green and red dots indicate 80µm (green) and 40µm (red) droplets, respectively. The retention rate (gray dash line) is defined as the number of captured droplets/the number of input droplets. The occupancy (right axis) is defined as the number of captured droplets/the number of available capturing sites. The error bars are standard deviations. Only standard deviations >20 are plotted. Centers of the squares and triangles represent the mean values of at least 2 independent repeats.

Fig 3.10a-d shows the side views of the merging device and the workflow of merging pairs of 80µm-diameter droplets dyed green and 40µm-diameter droplets dyed red. The device chip has 1,152 trapping sites, each of which consists of larger and smaller microwells to trap the 80µm- and 40µm-diameter droplets, respectively. We first flowed the larger green droplets into the device, where its large-dimension flow channel slowed down the flow speed and allowed the introduced droplets to be first stagnant and then move slowly along the top side of the channel. Once the desired number (detailed below) of the green droplets were collected,

we turned off the upstream sorting operation and disconnected the tubing from the droplet sorting device. Then, the droplets were floated into the empty trapping sites by tilting the merging device and consequently trapped inside the larger microwells. This operation was performed under an optical microscope to achieve better device tilting control and visual confirmation, which allowed all the droplets to be gradually captured in the trapping sites. In addition, we found that an externally oscillated flow in the bottom channel could further enhance the alignment between the droplets and the capturing microwells to achieve both high occupancy and retention rates. Nearly 100% retention rates could be achieved when fewer droplets were introduced to the device than the on-chip trapping sites (1,152 wells/chip) (Fig. 3.10e, green squares). A nearly 100% occupancy rate was achieved when loading droplets as few as ~1300 into the device (Fig. 3.10e, green squares). Once all the larger microwells were filled with the 80μm-diameter droplets, we introduced an external oil flow to wash out uncaptured excess droplets. The captured droplets stably remained in the capturing-sites during the washing process at an oil flow speed < 10mm/sec.

Similarly, we flowed the 40μm-diameter droplets into the merging device to fill the smaller microwells adjacent to the larger ones filled with the 80μm-diameter droplets in operation above (Fig. 3.10b). Once all the trapping sites were filled with droplet pairs, we again introduced an external oil flow to wash out the excess droplets. We could achieve retention and pairing rates close to 100% when smaller droplets fewer than 400 flowed into the device. These rates slightly dropped down to ~90% when the number of the droplets increased to 1100 (Fig. 3.10e, red triangles). It should be noted that achieving an occupancy rate of 95% required ~2000 of smaller droplets. This condition decreased the retention rate to 55% (Fig. 3.10e, red triangles). Overall, the retention rate for the 40μm-diameter droplets was lower. It is because

these droplets have fewer chances of flowing through the smaller microwells. Also, the smaller droplets experience relatively stronger drag force than buoyancy force, which decreases the trapping chances as well.

3.3.3 Droplet merging

To merge those captured droplets in the microwell array, an external oil containing 5% PFB was flowed into the device to destabilize and merge two adjacent droplets (Fig. 3.10c). The PFB molecule presenting at the interface between the two types of droplets increases the surface tension[73]. An additional pressure provided by the oil flow generates physical contact between the two droplets, which triggers the merging events. Only a very small fraction of the droplet pairs did not merge (typically < 1%) because the 40um-diameter droplets became wetted to the PDMS channel surface before contacting the 80um-diameter droplets. A PFB-free HFE oil with EA surfactant was then immediately flowed to the channel to dilute the PFB concentration once all the droplets merged. Since PFB molecules may cause permanent wetting of the droplets onto the PDMS channel surface, we limited the time for which they are exposed to PFB to a few seconds. After re-stabilized with EA surfactant (within a minute), the merged droplets were released from the capturing-sites by flipping the merging device chip. (Fig. 3.10d).

Although droplet merging with PFB added into the oil phase was convenient and easy-to-implement, this raised concerns about biocompatibility and the stability of droplets after merging. To overcome such potential drawbacks, we developed another droplet merging mechanism based on electrohydrodynamic (EHD) effect. We applied a uniform electrical field generated by a pair of parallel electrodes and triggered electrocoalescence across all the droplet pairs. This approach had less impact on the contents inside the droplets because the electrodes

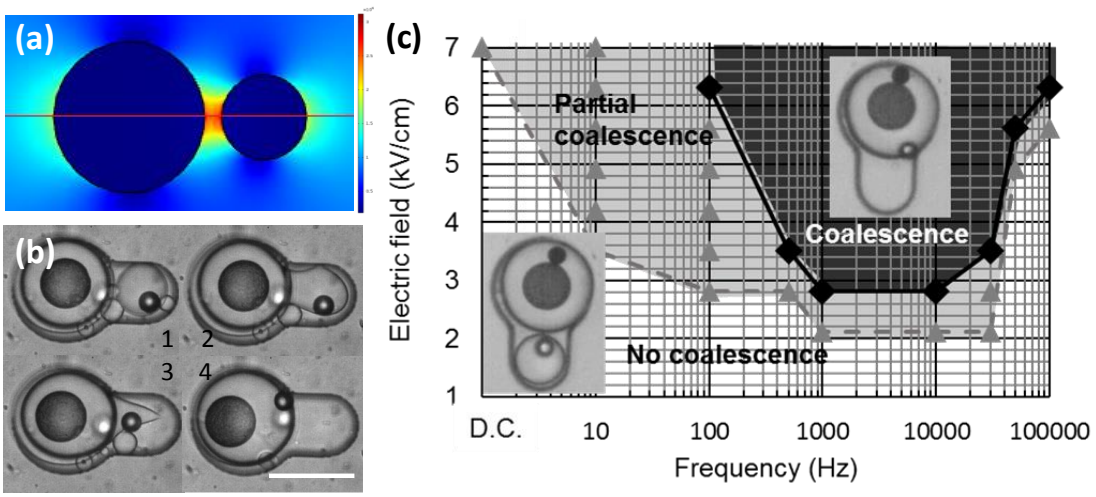

Figure 3.11 (a) COMSOL simulation shows the strength of the local electric field between two droplets under a uniform external electric field. (b) Time series images of droplet merging. Interval: 2.5 msec. (c) Observed coalescence response under different electric field strength and frequency. The dark shaded area indicates all the droplets pairs are merged. Only a fraction of droplets is merged in the light shaded area. No merging event occurred in white area. The electric field is calculated by the applied voltage V across two electrodes with a separation distance of 15mm (E=V/0.15, kV/cm).

did not directly contact the aqueous phase. Our simulation shows the electric field strength in the aqueous phase is about one order magnitude lower than that in the oil phase (Fig. 3.11a), which is in the tolerance range of living cells. The electric field near the droplet surface was non-uniform and amplified by dipole-dipole interactions between the two droplets. However, it is still technically challenging to predict the optimal coalescence condition using numerical simulation since it involves the behavior of interfacial surfactants at the molecular scale and the boundary change of two-phase fluidics at the macro scale. Thus, we empirically tested the droplet fusion efficiency by varying the strengths and frequencies of the applied electrical field (Figure 3.11b-c). We found that the merging efficiency was maximized under a 2.9 kV/cm electric field (oil phase) at 1–10 kHz. This frequency dependency can be attributed to both electrostatic and dielectric forces. The larger droplets increase their sizes as more small droplets merge into them. The fixed size of the microwells limits the maximum number of droplets that we could merge; we achieved the merging of up to four guest droplets without

observing any problems. The merged droplets could also be collected by manually flipping the device chip under gravitation.

3.3.4 Microbead co-encapsulation

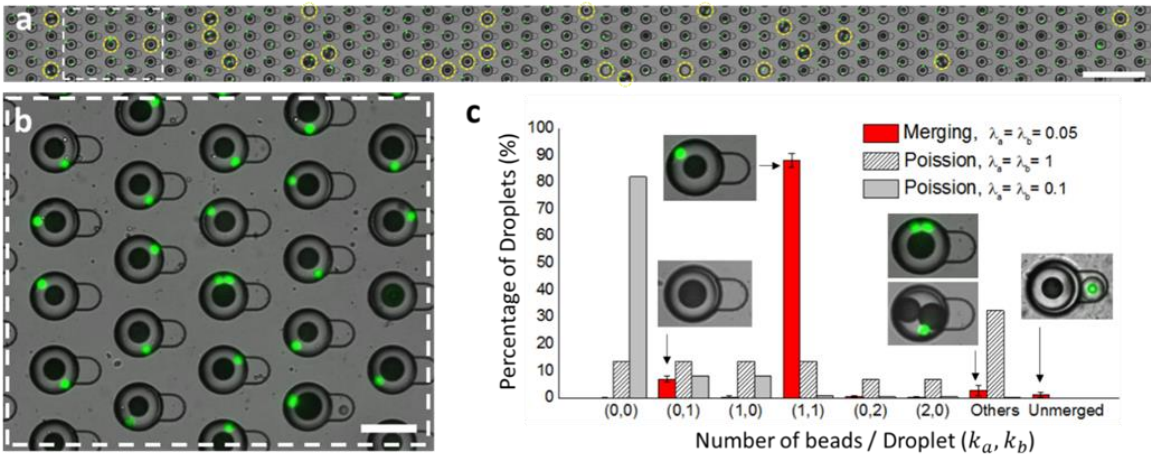

Figure 3.12 (a) Scanned image of merged droplets in the droplet merging device. Florescent/non-fluorescent microbeads are co-encapsulated one-to-one in each droplet. The yellow dash circles indicate the droplets contain undesired combinations of beads. (b) Zoom in of the droplets from (a). (c) The histogram shows the percentage of droplets that contain the numbers of fluorescent beads (k_a) and non-fluorescent beads (k_b). The estimated co-encapsulation resulting from the co-flow method is also plotted based on *Poisson* statistics with $\lambda_a = \lambda_b = 1$ *or* 0.1. Three sets of experiments were repeated with and average number of droplets for each test = 1050. The error bars are standard deviations of the means.

Using the system mentioned above, we sequentially sorted 1,300 of the 80µm-diameter droplets encapsulating a non-fluorescent bead (type-*a*) and 2,000 of the 40µm-diameter droplets encapsulating a green fluorescent bead (type-*b*) and injected them into the merging device with 1,152 trapping sites. Nearly 100% of the trapping-sites were filled with type-*a* droplets, and 95% of theses droplets were paired with subsequently trapped type-*b* droplets. After merging all the droplet pairs with chemical coalescence approach, we counted the number of beads per droplet. Fig. 3.12 shows the optical image of the merged droplets on the device (Fig. 3.12a,b) and plots the fractions of droplets encapsulating k_a of type-*a* beads and k_b of type-*b* beads across the total counted droplets of *N*=3,150 from 3 repeats with 3 devices (Fig. 3.12c). We found that 88.1+/-2.6 % of the droplets exactly encapsulated a one-to-one pair

of the type-*a* and type-*b* beads. Another 7.2+/-1.6 % of the droplets contained only a single bead (either type-*a* or type-*b*) mostly due to a failure in droplet pairing before the merging process. Another 3.5 +/-2.7 % of the droplets encapsulated undesired pairs of the beads such that (k_a, k_b) = (0, 2), (2, 0), (1, 2), (2, 1), …as a result of a doublet beads existing in some fraction of the sorted droplets. And the rest population (1.1+/- 0.9%) contained empty or unmerged droplets. In general, the probability of achieving the one-to-one paring of a single type-*a* bead and a single type-*b* bead in the merged droplet with our device is given by

$$P\left(k_a = 1 \cap k_b = 1, _{merging}\right) = \eta * P_{\lambda_a}\left(k_a = 1 \mid k_a \geq 1, _{poission}\right) * P_{\lambda_b}\left(k_b = 1 \mid k_b \geq 1, _{poission}\right) \quad (2),$$

where η is the occupancy of the 40μm-diameter droplets in the merging array, defined in Fig. 3.10e. $P_{\lambda_a}\left(k_a = 1 \mid k_a \geq 1, _{poission}\right)$ is the probability of obtaining a droplet with a single type-*a* bead after sorting and $P_{\lambda_b}\left(k_b = 1 \mid k_b \geq 1, _{poission}\right)$ is the probability of obtaining a droplet with a single type-*b* bead after sorting.

F**ig. 3.12c** also shows the co-encapsulation result expected for the conventional scheme, where the probability of obtaining a droplet with k_a of the type-*a* beads and k_b of the type-*b* beads is simply given by multiplying two independent *Poisson* statistics fractions as

$$P_{\lambda_a, \lambda_b}\left(k_a, k_b, _{poission}\right) = P_{\lambda_a}\left(k_a, _{poission}\right) * P_{\lambda_b}\left(k_b, _{poission}\right) \quad (3).$$

At a concentration leading to one bead per droplet (λ_a = λ_b = 1), the one-to-one pairing rate reaches a theoretical maximum rate such that $P_{1,1}\left(k_a = k_b = 1, _{poission}\right) = 13.5\%$. However, there is a high fraction (26.4%) of droplets that encapsulate undesired pairs (ex. : (k_a, k_b) = (1, 2), (2, 1)…). Such a population is even 2-fold larger than the desired population of droplets

with an exact pair of one cell and one bead. Minimizing the percentage of droplets encapsulating those undesired combinations is important in practical droplet-based assays. For example, Drop-seq assay strictly requires one-to-one pairng between a cell and a bead engineered with unique ssDNA barcodes[53]. If such a bead was paired with more than a single cell, it could capture mRNA molecules from multiple cells. The resulting cDNA from the different cells will be tagged with the same barcodes and recognized as the cDNA from the same cell. Therefore, the transcriptomic information extracted from this particular DNA-barcoded bead becomes incorrect and leads to a wrong data interpretation. To avoid this, the conventional Drop-seq assay uses a low concentration of cells (beads), which is equivalent to ~ one cells (beads) per 10 droplets ($\lambda_a = \lambda_b = 0.1$) or even lower[53]. Governed by the *Poission* statistics, the assay needs to dilute the sample as much as 90% of cells (beads) become wasted to reduce error (*i.e.*, the probability of incorrect cell-bead pairing down to 0.1). If we assumed the type-*a* beads to be cells, our approach would achieve cell-bead pairing at high accuracy, which results in an error as small as 0.038 ($\lambda_a = \lambda_b = 0.05$) without increasing the sample loss. Indeed, the loss remains constant with λ_a and λ_b (i.e., the original concentrations of cells and beads before encapsulation) while it is solely determined by the number of loaded droplets and the droplet merging device design, not by the *Poission* statistics. As a result, such accuracy can be further enhanced by reducing the sample concentration in our method without affecting the sample loss.

Next, we demonstrated our platform is even capable of performing multi-round droplet merging by co-encapsulating three fluorescence beads (Fig 3.13). The yield of desired beads combination is reduced to 80.1% due to the additive error, but it is still a significant improvement comparing to the co-flowing approach, in which the best scenario predicted by

three independent Poisson distributions is only 5.1%. Co-Encapsulation of 3 or more particles for practical applications is nearly impossible to achieve under such low efficiency. Moreover, the ability to precisely adding any desired content into the droplet is not only useful in controlling the cells or beads numbers but even more important for multi-step protocols for different kinds of cell assays.

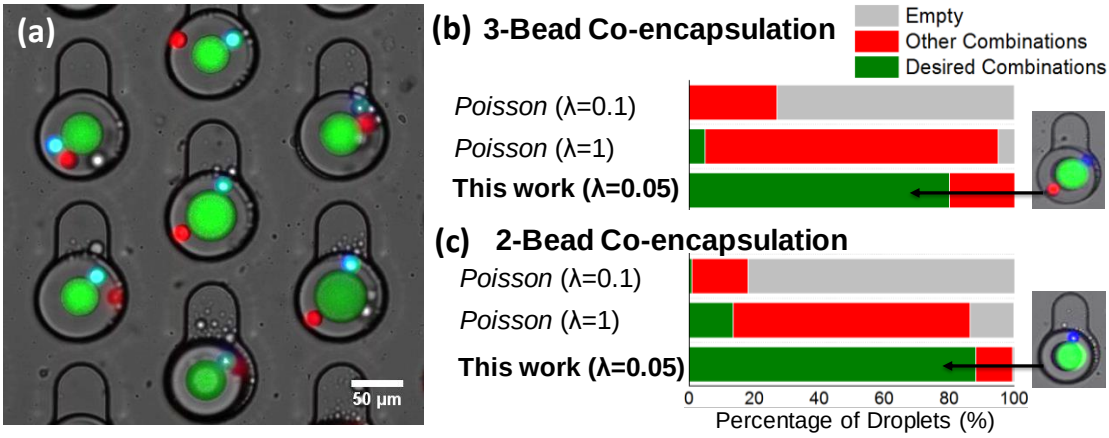

Figure. 3.13 (a) Image of merged droplets in merging device. Blue, red, and green florescent microbeads are co-encapsulated in each droplet. (b-c) The histogram shows the success rate of droplets that contain the correct numbers of blue, red, and green fluorescent beads. The data was collected from a total 1176 host droplets in a merging device with 3 repeats. Two cases were demonstrated: (b) Co-encapsulation of blue, green, and red beads and (c) blue and green beads. The estimated co-encapsulation rate resulting from the co-flow method is also plotted based on the Poisson statistics with an event rate λ=1 or 0.1.

3.4 Summary of Sort'N Merge platform

To summarize, we developed a microfluidic system that couples passive encapsulation, opto-activated sorting, stop-flow capturing, size-selective pairing, and on-demand merging in a highly-integrated platform. The multi-functional integration enabled one-to-one pairing of two distinct particles inside droplets with a very high yield. By actively capturing and pairing each particle, we achieved a two- or three-particle encapsulating efficiency of 88.1% and 80.1%, respectively, which represents a significant improvement in both pairing accuracy and yield as compared to the paring efficiency of 13.5% and 5.1% achieved by conventional *Poisson* distribution-limited co-flow systems, respectively. We found that it was the droplet

retention rate resulting from our device design, not the *Poisson* statistics, that determined the particle loss in our method. Thus, we could further prevent sample loss by improving the retention rate with the microfluidic device design optimized.

The developed platform imposes no restrictions on the physical properties (size, shape, stiffness…etc.) of particles as long as they can be optically differentiated. The system shows the ability to perform assays with a wide range of sample density. The number of microwells in the droplet merging device is also scalable from just a few to thousands of arrays due to its simple design. Furthermore, our system enables on-device examination before and after droplet merging, which allows both direct measurement of pairing quality and direct observation of post-merging regent reactions. The versatility of our system makes it suitable for a wide spectrum of assays. In the following chapters, we will describe the use of this platform for single-cell mRNA sequencing and detection.

Chapter IV

Application I: Single-cell mRNA Sequencing

4.1 Introduction to the Study

Over many years, scientists have dreamed of fully understanding the connections and functional mechanisms of brain cells to elucidate the sources of human thought and emotion. A notable number of studies indicate that the neuronal population in any animal's nervous system is highly heterogeneous and that distinct gene expression determines the functional state and activity of different neurons[107]. Also, cellular morphology and axonal/dendritic projections physically constrain the connectivity of these neurons, which makes these properties crucial to the brain function. Traditionally, neuron subtypes are identified by their physical and molecular properties. Modern genetic labeling techniques allowed labeling of subsets of neurons based on the expression pattern of one or two particular genes [108]. In the post-Human Genome Project era, transcriptomics – the study of the complete set of RNA transcripts – further elucidates the protein expression landscape of the subpopulation of neurons . For instance, a large population of genetically labeled cells can be pooled and profiled

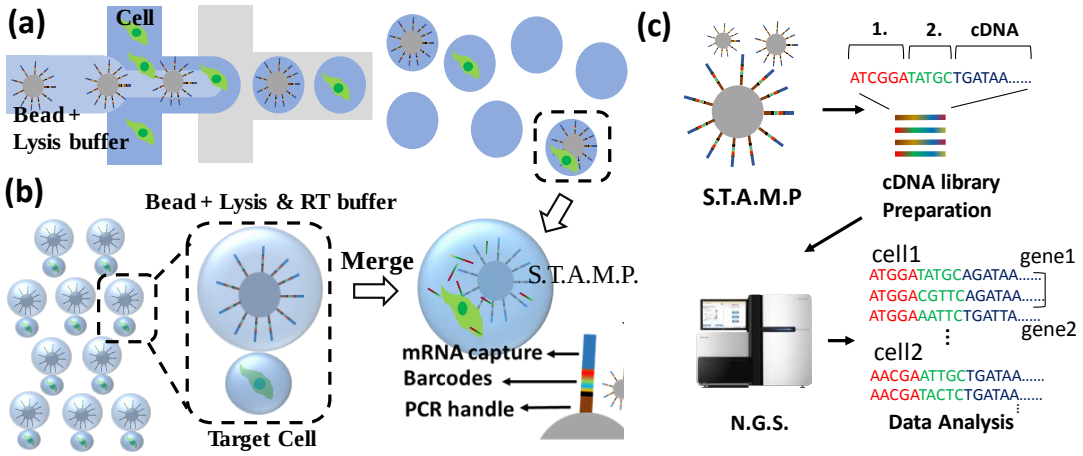

Figure. 4.1 Schematics of (a) conventional Drop-seq based on co-flowing of cells and beads. (b) our new droplet-seq system. Cells and primer-coated beads are individually encapsulated in droplet and form droplet pairs. After merging of two droplets, the cell is lysed, and the mRNA will hybridize to the bead. (c) Workflow of obtaining single-cell transcriptome from STAMPs. Each cDNA contains a sequence that is (1.) unique to each bead for cell barcoding and (2.) a random sequence that is unique for each primer as unique molecular identifier (UMI).

in a bulk analysis[53], [93]. However, such experiments only provide averaged data in which the heterogeneous gene expression information from individual cells is lost. In recent years, single-cell analysis techniques have emerged to overcome the limitation of bulk analysis to identify different cell types, including neurons, and revealed their intrinsic molecular differences from a mixed population in the tissues. Among all the single-cell analysis techniques, droplet-based sequencing techniques appear to be the most promising approach as they allow encapsulating and barcoding thousands of single cells within pico-liter volume droplets in a few minutes using microfluidics and allow partitioning sequencing results to each cell based on unique cell-barcode readouts (Fig 4.1.a,c) [53]. In Drop-Seq, solid-state synthesized barcoded primer microbeads are introduced to capture mRNA to form single-cell transcriptome attached microparticles (STAMPs). However, to avoid sequence assignment ambiguity, STAMPs must be created from droplets that contain only one bead and one cell for each. The current Drop-seq approach guarantees the single particle encapsulation based on the

stochastic Poisson process, which unfortunately shows a very poor yield that allows less than 10% of cells to form STAMPs. Moreover, the conventional cell screening and sequencing approaches have commonly employed fluorescence-activated cell soring (FACS) process in a flow cytometry setting which results in a significant loss of the extracted cells, and the high shear force may alter the gene expression. Therefore, they are not suitable for studying the extremely rare population of cells, such as quiescent stem cells or neurons in small brain nuclei. Recently, there are other approaches like InDrop[94] and 10xGenomics[93] trying to improve the capturing efficiency by replacing the rigid barcoded beads with deformable hydrogel beads. Since the hydrogel beads can be packed tightly during the encapsulation process, more than 90% of droplets can be loaded with barcoded beads. Recently, a cell retention rate of 65% has been reported with this approach. However, the passive co-encapsulation mechanism still limits its ability in processing challenging sample, such as rare cell subpopulations or cells with diverse dissociation quality. For example, Drosophila has been a standard model system for studying the development of the neural system. Each adult Drosophila brain composes about 100k neurons. Among all the neural cells, studying neuroblasts (NBs), the stem cells in the developing fly brain, has brought critical insights into cell division and differentiation. One must perform additional sorting or purification process to enrich the desired neurons, which number can have a range from few tens to thousands of cells per fly. Such rare populations could be easily lost during harsh sorting and inefficient Drop-seq process. Also, while single-cell sequencing methods provide a global survey of all subtypes, the spatial information of each cell is lost in the sample preparation process. This prevents high-throughput and high-content studies of the molecular-and-structural relationship which is essential for studying

lineage progression of neuron system. Novel approaches to solve these problems are highly desired.

In this work, we employed a new droplet workflow for single-cell mRNA-seq using our Sort N' Merge platform. We combined fluorescent activated droplet sorting (FADS) [52] for high-throughput capturing of target cells and droplets storing array for the precisely one-to-one merging of two droplets contain either a single cell or a single primer-bead. (Fig. 1B). Therefore, our new approach significantly improved the efficiency of conventional Drop-Seq method which limited by the stochastic co-encapsulation of one bead and one cell in a droplet. The ability to work with a wide range of cell concentration enables the flexibility of sample types and a faster sample processing time. Our platform not only provides an efficient and reliable single-cell mRNA-seq platform but also avoids the need of flow-cytometry based cell sorting with its active droplet sorting feature. This makes it specifically suitable for type-specific or rare cells study directly from the primary tissues. As proof of concept, we demonstrated it is possible to retrieve transcriptomic data of hundreds of genetic labeled neural stem cells from only one Drosophila's brain.

4.2 Material and Result

4.2.1 Reagents and materials

Barcoded beads coated with synthetic probes, each of which, from 5'- to 3'- end, consists of (1) a PCR handle for library amplification, (2) a sequence that is unique to each bead for cell barcoding, (3) a random sequence that is unique for each primer as unique molecular identifier (UMI) to quantify each mRNA molecule, and (4) an oligo dT sequence for mRNA capturing (*5'-Bead-Linker—TTTTTTTAAGCAGTGGTATCAACGCA GAGTACJJJJJJJJJJJJNNNNNNNNTTTTTTTTTTTTTTTTTTTTTTTTTTTT---3'*, where J

represents the cell barcode and N represents the molecular barcode) as described by Macosko et al. [53] are purchases from ChemGenes. The reaction mixture containing lysis buffers, Template Switch Oligo (TSO, *AAGCAGTGGTATCAAC GCAGAGTGAATrGrGrG*), and RT reagents are prepared as listed in table 3.4.1. The TSO is a primer that hybridizes to additional deoxycytidine at 3' end of the second strand cDNA added by the reverse transcriptase during the reverse transcription process and switches the template from RNA to DNA. TSO also adds a common 5' sequence to full length cDNA so it can be efficiently amplified in the downstream PCR step. Barcoded beads were washed twice with 0.1X TE/TW buffers, resuspended in the reaction mixture at a concentration of 250 beads/ul, and stored on ice before use. The rest reagents for exonuclease treatment, PCR, tagmentation, and purification of cDNA library are described at the standard Drop-seq protocol elsewhere (http://mccarrolllab.org/wp-content/uploads/2015/05/Drop-seq-protocol-v1.0-May-2015.pdf). The materials for microfluidic devices and dro plet manipulations have been described in chapter 3 of this thesis.

Table 4.1 Compositions of reactant mixture for barcoded beads suspensions.

Reactant mixture per 250uL			
Nuclease free water	82.8	10% NP-40	2.9
20% Ficoll-400	37.4	25mM dNTPs	11.5
5X RT buffer	57.6	RNase inhibitor [40U/ul]	7.25
1M Tris PH8	28.8	100uM TSO	7.25
Maxima H-RTase	14.5	Unit: μL	

4.2.2 Cell preparation

Drosophila single-cell suspension were prepared with following procedue: 1. Dissect eye-brain complex from 3rd instar larvae and wash once and resuspend in 80ul of 1X rinaldini's solution. 2. Add 10ul 20mg/ml papain and 10ul 20mg/ml collagenase. 3. Incubate at room

temperature (25C) for 60mins. 4. Resuspend the brain up and down with 100ul pipette 30 times or until no visible chuck.

4.2.3 Procedures for microfluidic Encapsulation and Single-cell RNA-seq

The general operation procedure of microfluidic devices has been described in chapter 3.2. Such co-encapsulation of microbeads process can be easily converted to the single-cell mRNA-sequencing experiment as described below. Bead suspension, droplet generating oil, and spacer oil were injected into the droplet generating/sorting device at a flow rate of 2.5ul/min, 10ul/min, and 15ul/min, respectively. 80um droplets containing barcoded beads were enriched based on scattering light-activated droplet sorting. The beads containing droplet can be collected into droplet merging devices at a rate of about 600 beads/min. For a merging device containing 1152 capturing sites, we overflow about 2000 beads-containing droplets into each device so an occupancy of 98-99.9% can be easily achieved. Once the droplet array was formed in the merging device, we stored the device at 4°C in a water bath to prevent droplet evaporation before the next step. Multiple devices containing droplets with barcoded beads can be prepared at a time if multiple samples are studied. Next, to generate the single-cell encapsulated droplets with a diameter of 40um, the cell suspension, droplet generating oil, and spacer oil were injected into another droplet generating/sorting device at a flow rate of 2.5ul/min, 15ul/min, and 10ul/min, respectively. Droplets were sorted into the merging device from the previous step based on their fluorescence signal at a throughput of 670 droplets/sec. Once the desired number of sorted droplets is reached, we turned off the sorting program and disconnected two microfluidic modules (merging device and sorting device). After the droplet pairing and washing process, the whole array of droplet pairs can be imaged. Therefore, the sample quality can be evaluated at this step. This feature is important for processing some

challenging sample such as Drosophila's neural cells which dissociation result shows a considerable variation from one fly to another fly. A quick snapshot before cell lysis could be helpful for downstream processes such as determining the sequencing depth or predicting the impact of multiplets during data analysis. Droplet merging was performed by chemical coalescence, so the cell in the merged droplet was lysed immediately. The released mRNA is hybridized with the primer-coated microbeads, followed by the synthesis of second strand DNA via reverse transcription (incubated in a water bath for 10 min at 25°C and 90 min at 42°C) leading to the formation of STAMPs. After the reverse transcription, the droplets are broken, and the microbeads are collected into 1.5 mL centrifuge tube with 6X SSC buffer. The beads were washed with TE-SDS buffers to terminate the enzyme activity and then washed twice with TE-TW buffers. Finally, the cDNA library is constructed from STAMPs according to the standard Drop-seq protocol (http://mccarrolllab.org/wp-content/uploads/2015/05/Drop-seq-protocol-v1.0-May-2015.pdf) for the downstream next-generation sequencing analysis.

4.2.4 Sequencing and data analysis

The DNA library was sequenced by illumina Hiseq 4000 with a sequencing depth adjusted to about 100,000 reads/cells. The data were analyzed by Dr. Danny Nunez in Prof. Dawen Cai's lab using SEURAT , which is a R toolkit for single cell genomics developed by Satija *et al.* (https://satijalab.org/seurat/).

4.3 Result and discussion

4.3.1 Assay benchmark

The fundamental difference of our approach comparing to conventional Drop-seq is the method to assemble necessary reactants into the droplet including barcoded beads, cells, lysis

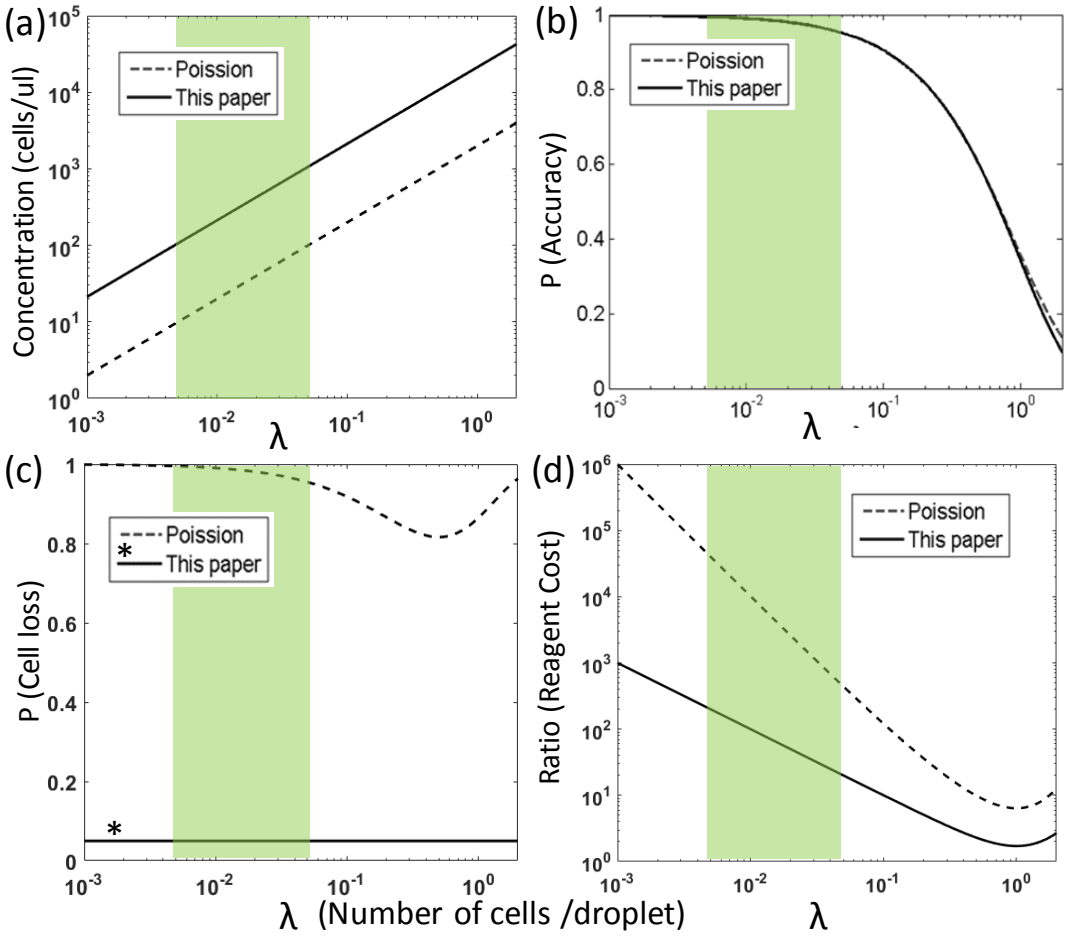

Figure 4.2 Comparisons of our method and conventional co-flowing method predicted under different event rates λ (number of cells per droplets). (a) Concentration of cells suspensions. (b) Accuracy: Probability of obtaining particle pairs that contain exactly 1 cell and 1 bead. (c) Cell loss: ratio of waste cells to total cells. *The cell loss in our method is independent with the density of cells. (d) Reagent Cost: Volume ratio of waste droplets to the droplets containing 1-1 particle pairs. The shaded green zone indicated the conventional range of the cell density.

buffer…etc. We decoupled the encapsulation of single-cell and single-bead to separated steps and performed one-to-one pairing of them. The advantage of this approach can be theoretically estimated from various aspects. First, we evaluated the accuracy between our approach and conventional co-flowing method under different event rates λ (average number of cells per droplets). The accuracy was defined as the probability of obtaining particle pairs that contain exactly one cell and one bead, and it could be predicted by Poisson distribution. The droplets contain only one type of particles or empty droplets did not take into account since no cDNA

can be synthesized from them. Fig. 4.1a shows the relation between the density of single-cell suspension and the event rate λ. Since we reduced the volume of droplets for cells encapsulation by ~10-fold, the single-cell suspensions can be partitioned more efficiently thus provides a large dynamic range of cell density. This also suggests that we can maintain the same accuracy without the need for much dilution with our approach (Fig 4.2b). Therefore, a large number of cells can be processed within a short period.

Furthermore, the features of active sorting and the deterministic pairing of droplets increased and flexibility of the experiment design and utilized the materials efficiently. In our platform, the cells were selected based on their optical properties, like the conventional fluorescence-activated cell sorting (FACS) by flow cytometry. For unbiased sc-RNA-seq, all cells can be stained with a cell-permeant tracking dye just before the experiment. Different ways of fluorescent labels such as functionality probes, immunostaining, or genetic labeling can also be used for additional proposes. For example, figure 4.3a shows the post-sorted droplets containing single Hela cells stained with Calcein AM. Since a clean single-cell suspension can be easily prepared from such cultured cell lines with a small batch-to-batch variance, a near-perfect single-cell encapsulation result can be achieved. On the other hand, for primary cells dissociated from solid tissues, the sample usually comes with many debris and dead cells due to the individual difference from animals and complicated dissociation processes. Figure 4.3b shows the encapsulation result of adipocytes staining with Calcein-AM from mouse adipose tissues before the sorting process. Many dead cell and debris can be observed from droplets containing non-fluorescent objects. In conventional Drop-seq, there is no way to evaluate the impact of those undesired dead cells or debris, which might be one of the sources resulting in batch effects between different data sets. The use of our Sort N' Merge platform with Calcein-

AM, a cell viability dye, excludes the dead cells and tissue debris (Fig 4.3c). This feature could enable further controlling of the sample quality, making a more robust sc-mRNA-seq process.

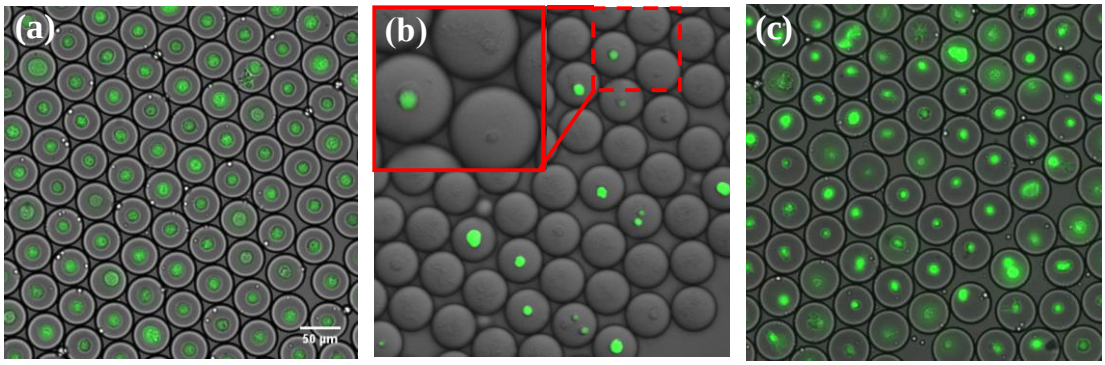

Figure 4.3 Merged white light and fluorescent images of (a) Sorted droplets containing Calcein AM stained Hela cells, (b) droplets containing Calcein AM stained adipocytes dissociated from mouse adipose tissues before sorting and, (c) after sorting. In (b), Droplets containing not only live adipocytes (green fluorescent cells), but many dead cells (non-fluorescent cells) and debris.

After the enrichment of single-cell containing droplets, about 90% sorted cells can be paired with the droplets containing a barcoded bead with an equal amount of either type of droplets. A more than 97% retention rate of sorted cells can even be achieved if we increase the ratio of bead-containing droplets to cell-containing droplets as demonstrated by color-coded droplets in Fig 3.10. Therefore, cell loss is no longer associated with Poisson distribution or the concentration of cells (Fig 4.2c). With appropriate fluorescent tags, each cell can be reliably captured for mRNA sequencing. Moreover, our approach not only preserved the cells but also reduce the waste of reagents (aqueous phase). We achieved a more than 10-fold reduction of reagent cost (Fig 4.2d) comparing to conventional Drop-Seq platform. This could enable a wider application such as the studying of rare cell type or including expensive reverse transcriptase into droplets for integrated cDNA synthesis.

4.3.2 Single-cell mRNA-seq with Sort N' Merge platform

To validate the single-cell mRNA-Seq performance of our platform, we performed a mixed- species experiment with cell suspensions and bead suspensions at a concentration of 1000 cells/μl and 250 beads/μl, respectively (both λ=0.05). The cell suspensions contained the one-to-one mixture of calcein-AM stained Hela cells and mAmetrine expressed N2A cells, and both cell lines were unbiasedly sorted based on the green fluorescent signal. One thousand cells were collected and paired with barcoded bead by our system as Fig. 4.4 shows.

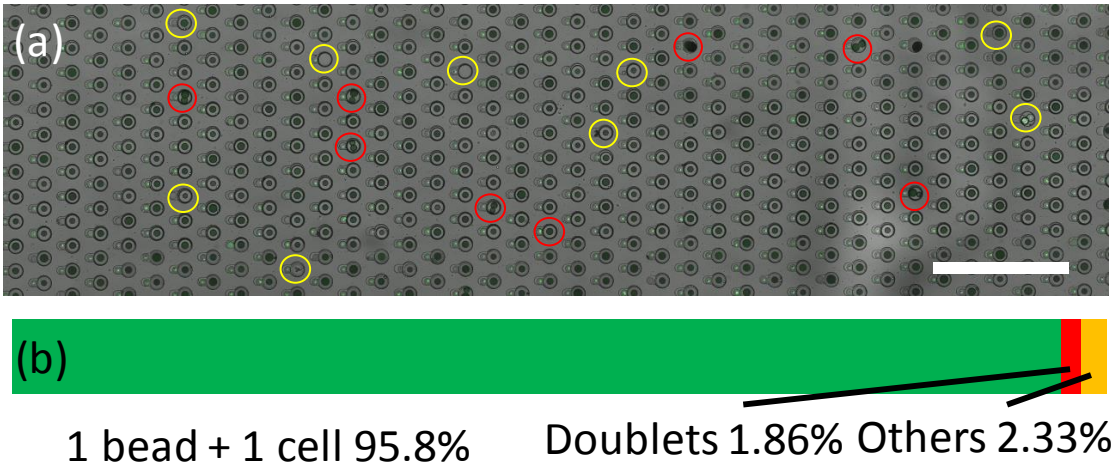

Figure 4.4 (a) Image of paired droplets in merging device. The red circles indicate the droplet pairs that contain the doublet cells or beads which lead inaccurate readouts. The yellow circles indicate other undesired combinations but have either no cell or bead. (b) The histogram shows the droplet pairs containing exactly 1 bead & 1 cell, doublet of beads / cells, or no bead / cell. Scale bar:0.5mm.

The image indicates that the pairing process achieved a 1-1 pairing accuracy as high as 95.8 %. The ability to examine the pairing accuracy before sequencing is also critical for quality control. In conventional Drop-seq, there are always a few percents of the STAMPs that have multiple cells [10]. However, the current approaches to identify those multiplets either through computational or experimental means require analyzing sequencing data. In other words, there is no way to perform quality control before cDNA library preparation and next-generation sequencing which is both time-consuming and expensive. Our approach addresses this issue thus make it suitable for processing challenging samples. Figure 4.5 shows the

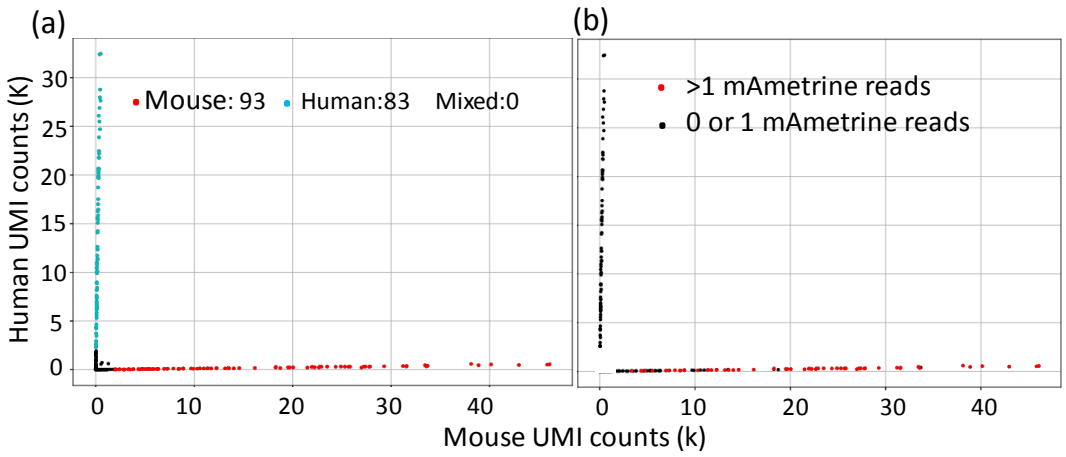

Figure 4.5 The mixture of human (Hela) and mouse (mAmetrine expressed N2A) cell lines was used to evaluate technical performance. The scatter plot shows the UMI counts from the same cell barcodes. (a)Red: 99% UMI counts are associated with mouse genes. Green: 99% UMI counts are associated with human genes. (b). Red: More than 2 mAmetrine UMI counts.

sequencing result of the mixed-species experiment. 97% single-cell purity was achieved which is comparable to other mRNA-seq methods[109]. A very low number of mixed-species STAMPs (3/500) was observed, which matched well with the theoretical prediction and was also confirmed from the microscopic images. If we setup the cut-off UMI counts by 1000, there are no mixed-species STAMPs existed from sequencing data. Indeed, the sequencing result can only reflect the multiplets from different cells. Other error sources such as the multiplets of the same type of cells or beads are hidden which could mislead the interpretation of the sequencing data. Figure 4.5.b shows the result of mAmetrine gene detection. The STAMPs with more than two mAmetrine UMI counts were labeled with red color, and the difference between non-Ametrine expressed cells (Hela) and Ametrine expressed cell (N2A) can be differentiated. 0% false positive rate and 12.1% false negative rate was observed with this experiment. This result suggests that combing fluorescent reporter with the mRNA-seq method is feasible for more flexible experiment design.

4.3.3 Single-cell mRNA-seq with rare-cell type from Drosophila

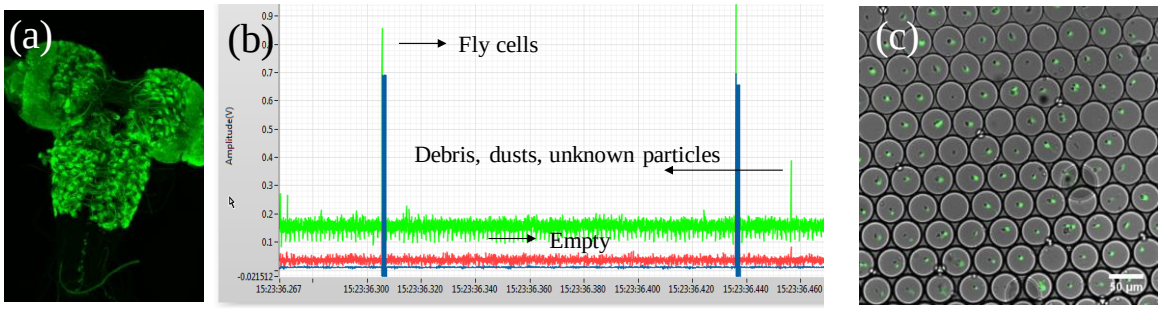

Figure 4.6 (a) Drosophila brain contains ~100,000 cells with ~1% labeled neurons (R57D02-Gal4 >> GFP) were disassociated. (b) Only fluorescence expressed cells were detected and (c) encapsulated in droplets for barcoding and sequencing.

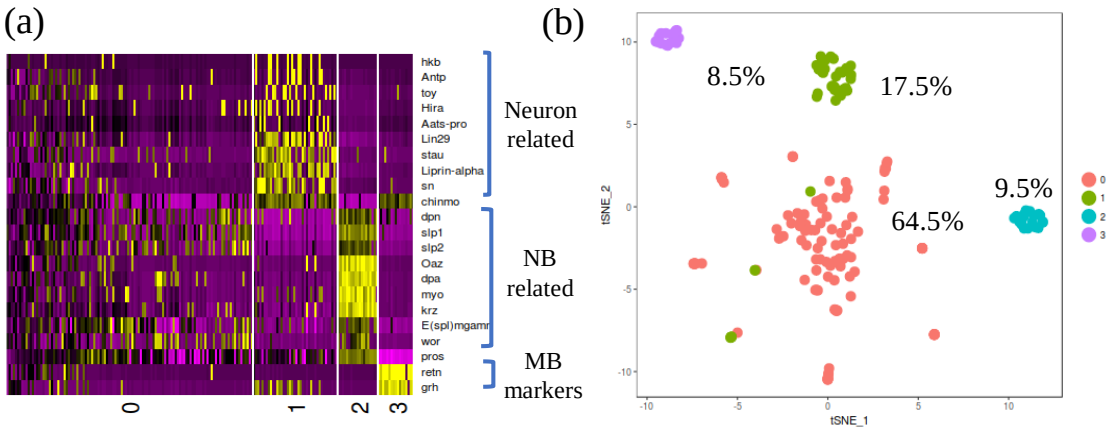

Figure 4.7 (a) The heat map shows normalized gene expressions of top variable genes from the 4 clusters: 0. intermediate stage, 1.neurons, 2. Neuroblast, and 3. Mushroom body. (b) tSNE projection of labeled neurons from single Drosophila brain. Each cell was grouped into one of 4 clusters.

To demonstrate the capability of processing challenging sample for rare cell study using our system, we perform single-cell mRNA sequencing with our platform for rare neuron stem cells from single Drosophila. To test the sorting and sequencing limit of the rare population of neurons from a single animal, we use Gal4 driver flies to label different number of neurons in a single brain [14]. These Gal4 driver lines label different neuronal subpopulations by expressing green fluorescence protein (GFP) and provide consistently different labeling density (R73A06-Gal4: ~90, R57D02-Gal4: ~1000, and R14F08-Gal4: ~4000, unit: cells/fly). Figure 4.6a shows the image of a central neuron system from an R57D02-Gal4 Drosophila line before dissociation. About 1000 GFP expressed neuron stem

cells distributed in about 100,000 neurons. After the dissociation process, single-cell suspensions are injected into our microfluidic devices to sort the GFP positive cells into individual droplet (Fig. 4.6b,c) for mRNA sequencing. Due to the small size of Drosophila cells (~5μm in diameter), the signal-to-noise ratio (SNR) is much lower than the mammalian cells, making them difficult to be differentiated from other fluorescence debris. To determine the accurate sorting threshold, flow cytometry calibration microbeads (SPHEROTECH) that contains the same size particles with different fluorescence intensities were used as a reference. The threshold of fluorescent cells can be defined by comparing the fluorescence intensity of beads and cells under fluorescence microscopy and our sorting system. With a proper threshold, the true positive of sorted droplets could achieve nearly 100%. However, comparing to the experiment using cultured cells, the sorting sensitivity (false negative rate) is relatively difficult to verify for primary cells. The number of recovered cells varies from one fly to another fly, and the number of actual GFP positive cells were difficult to measure, either. Typically, more than 500 cells can be recovered from R57D02-Gal4 fly lines and up to ~900 cells has been recovered from one fly. Such numbers of cells is enough to provide meaningful information for downstream analysis. For each sequencing result, reads with the same cell barcode will be pooled to assemble the transcriptome of that cell. The transcriptomes of individual cells will be clustered to identify neuronal subtypes. In a library prepared from a R57D02-Gal4 fly line, ~300 single cells with >300 identified genes can be clustered into four groups by tSNE analysis (Fig 4.7). The gene expression pattern in each cluster corresponds to neurons (cluster 1), lobe type-II neuroblasts (cluster 2), and mushroom body neuroblasts (cluster 3) based on the distinct gene makers reported in previous literature. For examples, Deadpan (dpn) is a gene marker that exists in all type-II neuroblasts and some intermediate neural progenitors (INPs) that are

generated through asymmetric cell divisions from type-II neuroblasts[110]. Therefore, the identities of cluster 2 can be confirmed since they are all dpn positive cells (Fig. 4.8a). The cells in cluster 0 do not show a clear signature in this analysis. This suggests that some of them could be INPs or other types of cells in a transition stage from neuroblasts to neurons. Also, datasets from single-cell mRNA-seq are in an N-dimensional space in which N equal to the number of measured gene makers. Our tSNE plot compresses data in a two-dimension space for visualization thus some information is hidden in it. There are three subpopulations in cluster 1 not shown in Fig. 4.7b. Those distinct neurons can be realized by three non-overlapped gene makers showed in Fig. 4.8b: Twin of eyeless (toy, a marker of a sub-population within type-II lineages [112]), Fig. 4.8c: huckebein (hkb, a maker shown an important role in embryonic neurodevelopment in central brain population [111]), and Fig. 4.8d: Aats-pro (a transcriptional factor for mitochodrial prolyl-tRNA synthetase [112]).

Our result suggests that our platform is capable of performing single-cell mRNA-seq from the rare sample at a very high yield. We have also successfully sorted and sequenced an even rarer subpopulation from R73A06-Gal4 fly line, in which less than 100 cells expressing GFP in one fly. However, the limiting factor for such a small number of cells is no longer the cell recovering efficiency but the mRNA recovering efficiency. The current Drop-seq protocol only allows 5-10% mRNA to be sequenced. Without a sufficient number of cells, it is challenging to perform statistical analysis with those missing mRNA information. Therefore, improving the mRNA recovering yield for rare cell study will be the next critical goal for studying those extremely rare populations.

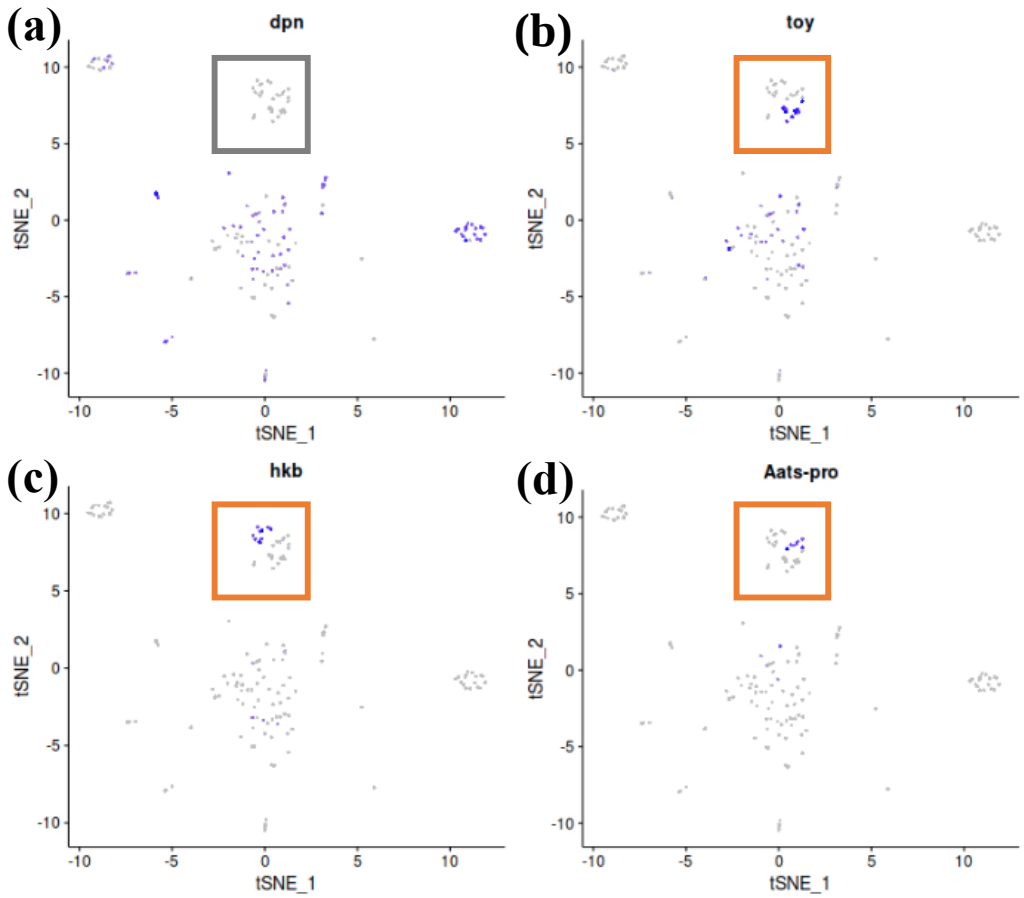

Figure 4.8 Highlighted gene makers in cluster 1 and 2. The cells with positive highlighted gene were labeled with purple color. (a) dpn positive populations. (b-d) Three distinct neuron populations containing different neuron makers (toy, hkb, and Aats-pro) marked in Cluster 1.

Chapter V

Application II: Single-cell mRNA Detection by RT-LAMP

5.1 Introduction to the Study

Single-cell profiling techniques have overcome the limitation of bulk analysis to enable discovering the heterogeneity of different cells in the same tissue[6], [9]. For example, in chapter 4, a single-cell mRNA sequencing assay (cs-mRNAseq) isolates each cell in an individual reactor, extracts its mRNA transcripts, uniquely barcodes each cell's amplified transcriptome, and finally pools the cDNA library for next-generation sequencing. Being able to reveal the transcriptomes of individual cells, cs-mRNAseq has become a powerful way to identify distinct cellular subtypes, to understand gene expression transitions between cell developmental stages, and to reveal the lineage composition of an organism[113].

Unlike DNA, mRNA is not stable in a wide range of buffer conditions and temperatures due to its susceptibility to hydrolysis at 2' hydroxyl position[114]. Extracted mRNA molecules degrade rapidly in the presence of RNase in the cell lysate or the environment. Even before cell lysis takes place, the expression of mRNA can quickly change over time when experiencing a non-physiological extracellular environment[21]. Therefore, once the cells are

dissociated from the original tissue, converting the mRNA to structurally stable cDNA in a timely manner is critical to retain and capture the transcriptomes that the cells possessed in their original tissue. Flow cytometry is commonly used to rapidly sort single cells of the desired population into each microwell of a 96- or 348-well plate to avoid the time-consuming manual cell picking process. However, this approach experiences significant sample loss due to shearing force induced cell lysis[115]. In addition, sorted cells are often landed on the side wall of each microwell when only a few μL of lysis buffer is loaded in each well to satisfy the volume requirement of a single-cell assay[116]. Nonetheless, to gain a statistically meaningful single-cell dataset, it still requires a time-consuming and labor-intensive pipetting process to assay many individual cells that are sorted by flow cytometry. Novel approaches are desired to replace flow cytometry-based assays for rapid and high-throughput single-cell processing.

Recently, droplet microfluidics has emerged as one of the most promising techniques for high-throughput single-cell analysis. Microfluidic platforms permit partitioning and manipulating of single cells in individual droplets by sequentially performing droplet generation, incubation, reinjection, merging, and detection[117]. For example, a multi-step, droplet-based workflow was proposed for single-cell reverse-transcriptase polymerase chain reaction (RT-PCR), which can process more than ten thousand cells in a single test[46]. Several studies reported on the development of droplet microfluidics-based single-cell barcoding techniques for transcriptomic or epi-genomic analysis[53], [93], [94]. However, these techniques need to perform multi-step biochemical reactions, which require users to add a new reagent into the droplet reactors at each reaction step. These multi-step reactions are processed with several separate microfluidic devices. Consequently, the assays are accompanied by time-consuming and laborious device-to-device droplet transfer processes

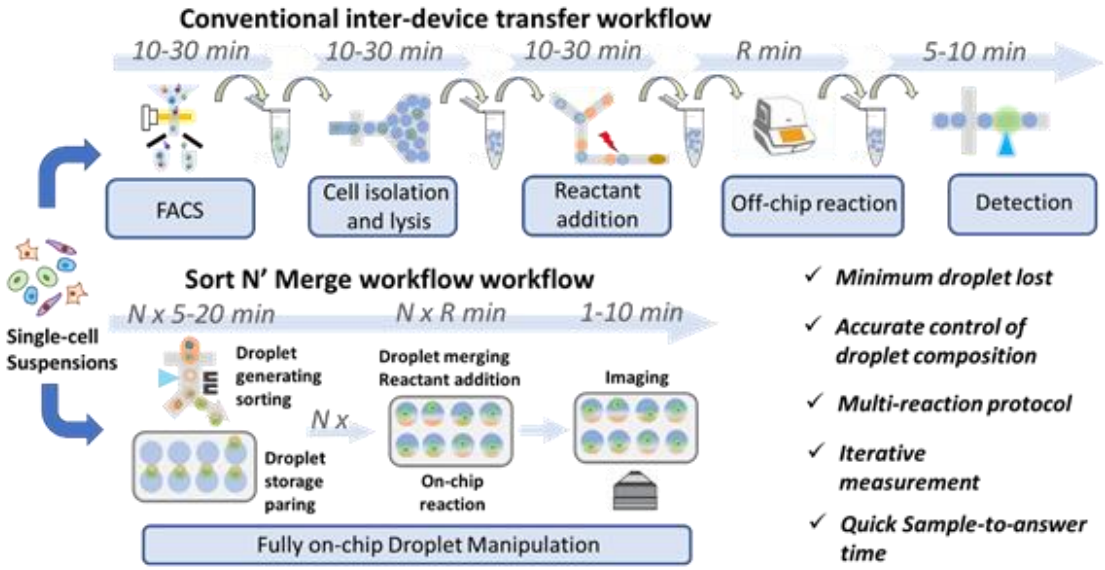

Figure 5.1 Schematic comparisons of conventional inter-device transfer workflow and our novel integrated "Sort N' Merge" workflow for single-cell mRNA detection: Upper: conventional droplet-based workflow permits high throughput processing of large number of droplets but requires off-chip transfer between each reactant addition, reaction and detection step. Lower: Our integrated Sort N' Merge system combines the advantage of continuous and stationary droplet microfluidics, enabling an efficient workflow for multi-reaction single-cell analysis.

between reaction steps, which may also result in loss of mRNA due to degradation over time or loss of cell-containing droplets due to handling error (Fig. 1 upper). Furthermore, wasteful and inefficient nature of these techniques limits their application for studying rare cell populations, such as adult stem cells and circulating tumor cells. The conventional methods involve droplet-merging assays to process multi-step reactions. These assays are carried out by synchronizing two self-ordered droplet flows, which requires a significant number of cell-containing droplets. The droplets are prone to lose before synchronized flows. For this reason, a rare cell population study requires a cell enrichment step prior to all the droplet-based assays, but this flow cytometry-based cell enrichment step makes the whole assay less attractive because it increases the chance of sample loss due to harsh cell sorting by FACS or sample transferring. Ideally, the cell sorting step should be directly coupled to downstream droplet-

merging processes. Despite notable research efforts, it is still challenging to integrate these two functions into a single microfluidic platform.

To solve the problems mentioned above, we employed our "Sort N' Merge" platform (Fig. 5.1 lower) for a novel droplet-based single-cell assay workflow. The "Sort N' Merge" platform directly couples the continuous-flow droplet-generation/sorting and stationary droplet-pairing/merging to enable precisely adding new reactants to the generated droplets without the need of inter-device transfer or droplet flow synchronization. The operation details of Sort N' Merge platform has been described elsewhere in chapter 3. In brief, it first generates a large number of "big" droplets and then enrich the desired ones by fluorescence activated droplet sorting (FADS)[52] into a pairing-and-merging chip. The sorted "big" droplets, i.e. microreactors, can spontaneously fill in the larger side of the pairing-microwell arrays due to buoyant force. To add new reagents to the microreactors, "small" droplets containing a different type of cells or reagents are generated and sorted into the same pairing-and-merging chip. The "small" droplets spontaneously fill in the smaller side of the pairing-microwell arrays and paired one-to-one with the previously occupied microreactor "big" droplets in the microwell array. Efficient merging between the paired droplets is then realized by applying high voltage electric field induced dielectric force. As the "big" droplet is at least ten times larger in volume than the "small" droplet, the merged "bigger" droplets remain in the pairing well. By repeating the "small" droplet generating-sorting-pairing-and-merging processes, it is possible to sequentially add multiple reagents to each reactor droplet, similar to how they are precisely added to a centrifuge tube or microtiter plate well using a pipette. Also, the other features of our platform, such as integrated fluorescence sorting, image-based measurement, and reconfigurable droplet merging, could provide a highly flexible and adaptable way for

performing novel droplet-based bioassays. Here, we demonstrate the unique droplet manipulation capability of our "Sort N' Merge" platform by developing a high-sensitivity scRT-LAMP assay that detects selected genes from single cells.

5.2 Methods

5.2.1 Microfluidic devices

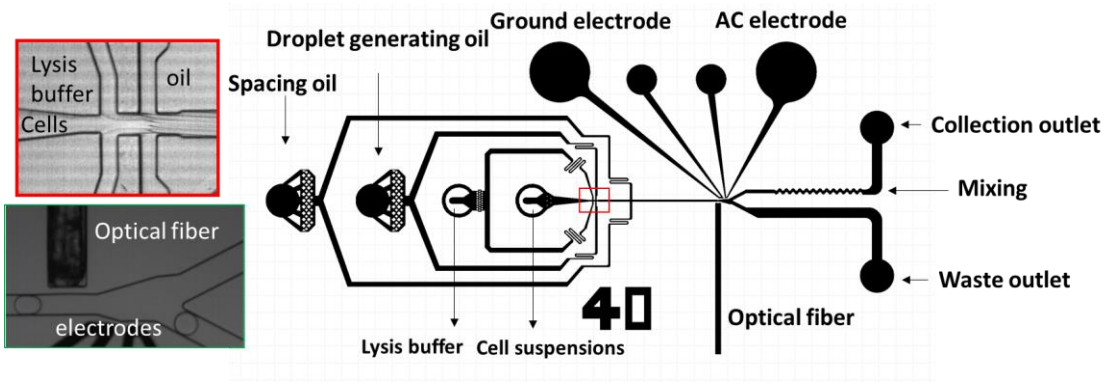

Figure 5.2 CAD layout of droplet generating/sorting devices. Droplet Generator/Sorter were used to generate 60μm-diameter droplets with single-cell lysates.

All microfluidic devices were fabricated using standard multilayer soft lithography techniques and their design has been described in chapter 3. The only exception in this experiment is that we added one more aqueous inlet into the droplet generator/sorter. Therefore, lysis buffers can co-flow with the cell suspension before droplet generation. After droplets traveling through the detection region, an additional mixing channel is used to facilitate the lysis of cells. The design of the microfluidic device for cell lysing and sorting can be found in Fig. 5.2.

5.2.2 Cells Culture and Preparation

The Jurkat, K562, and Neuro-2A cell lines were purchased from ATCC and cultured in the recommended growth medium supplemented with 10% FBS at 37 °C in a 5% CO_2 incubator.

The cells were stained with nuclei blue (Thermal Fisher) for 15 minutes before the experiment. Following the staining process, the cells were washed with phosphate buffered saline (PBS) twice and then resuspended in PBS at a population of 10^6 cells/mL with 16% OptiPrep (Sigma Aldrich, D1556). The cell suspension solution was cooled down to 4 $^{\circ}$C prior to the experiment.

5.2.3 RT-LAMP Reactions

Both the single-cell and bulk experiments used a 22.5μL RT-LAMP reactant mixture, which was composed of a 2.5μL solution of 10X primer mixture (described below), a 2.5μL solution of 10× isothermal amplification buffer 2 (New England Biolabs, NEB), a 3.5μL solution of 10 mM dNTP mixture (NEB), a 1.5μL solution of 100 mM $MgSO_4$ (NEB), a 1μL solution of Bst 3.0 DNA Polymerase (8,000 U/mL) (NEB), a 0.5μL solution of WarmStart RTx Reverse Transcriptase (15k U/mL) (NEB), a 2.5μL solution of 10× isothermal amplification buffer 2 (New England Biolabs, NEB), a 0.625μL solution of 4μM Bovine serum albumin (NEB), a 0.625μL solution of RNase inhibitor (40,000 U/mL) (NEB), a 1μL solution of 625μM Calcein (Sigma), and a 1μL solution of 12.5mM $MnCl_2$ (Sigma), a solution of 5% NP-40 (Thermo Fisher) with a desired volume. The rest of the volume of RT-LAMP reactant mixture was filled with RNase free water (Sigma). For the benchtop experiment (i.e., bulk assay), the RT-LAMP reactant mixture was mixed with a 2.5μL sample, which resulted in the final volume of 25μL. In the droplet assay, reactors, each consisting of a 1nL LAMP reactant droplet (Droplet A) fused with a 110pL single-cell droplet (Droplet B), were formed. The droplet reactor volume was 22500-fold as small as the reactor volume used in the bulk assay.

The 10X primer mixture contained solutions of 16μM forward outer primer (F3): AGAGTGATTCGCGTGGGTA, 16uM backward outer primer (B3): ACTTCATTCTTCTCCAGGGC, 4μM forward interior primer (FIP):

TCAAACTGCAGGCCAGGGTACCAGCTTGCTCGCATACAGAC, 4μM backward interior primer (BIP)TTGCTATGTCCACCACAGGGGAAGCTCCTTGGTAAACAGG C, 2μM forward loop primer (FLP): GTTGCCACCACACTGTCC, and 2μM backward loop primer (BLP): CAAGATTCTTGATACTGCAC TCTCT. These sequences are written from 5' to 3' and specific to human hydroxymethylbilane synthase mRNA[118].

5.2.4 Operation of Microfluidics device

The generation of fluid flows within the microchannels of our devices used 1mL BD syringes, syringe needles (Ga# 30, CML supply), a PTFE tubing (ID:0.012 OD:0.030 inches, Cole Parmer), and syringe pumps (KD Scientific, Legato-200). Fluorocarbon oil (HFE7500) with 2% EA-surfactant (Ran Biotechnologies) was used as the surrounding phase of water-in-oil droplets. When loading an aqueous phase flow to a device with a microbore tubing, the syringe was prefilled with oil to reduce the dead volume. As a result, the sample (e.g., cell suspension or LAMP reactant mixture) volume required for each experiment could be minimized to be as small as 10-20μl. Using the flow-focusing droplet generator (Orifice cross section: 120 x 120 μm), 1nL droplets with RT-LAMP reactants (Droplet As) were generated by injecting aqueous and oil phase flows into the microfluidic channel at 2μL/min and 7μL/min, respectively. Approximately 2,000 droplets were loaded to the merging device via the PTFE tubing from the droplet generator device and trapped into the droplet storage microwells on the merging device by means of buoyancy force. Subsequently, using another device with both co-flow droplet generation and sorting functions (Fig. 5.2), 110pL single-cell droplets (Droplet Bs) were generated using a flow of aqueous phase with a single profile of cells and the lysis buffer at 3μL/min, a sheath flow of oil at 10μL/min, and a spacing flow of oil at 20μL/min. Within the same channel, Droplet Bs were excited at a wavelength of 405nm using a laser

diode. The emission light from each droplet was collected by an optical fiber with a bandpass filter (CW520/25) and detected by a photomultiplier tube (H9306-03, Hamamatsu) connected to the optical fiber. The signal was processed by an in-house electrical circuit in real time. The circuit triggered a high-voltage AC pulse (800 Vp, 30 kHz) at the microelectrodes to generate a spatially non-uniform electric field within the microchannel of the sorter device upon detecting a bright fluorescence emission signal. Dielectrophoresis (DEP) force originating from the electric field selectively pulled fluorescence signal-emitting droplets into the collection channel. Empty (non-fluorescence signal-emitting) droplets were simply flowed into the waste channel without activating the AC pulse at the microelectrodes. Approximately 2,000 of Droplet Bs were additionally collected by the same merging devices and paired one-to-one with previously collected Droplet As. The excess droplets remaining in the flow channel were flushed out with a flow of oil phase. An AC electrical pulse (1kVp, 10kHz, 0.1sec) was applied on two parallel electrodes across the array of droplet pairs. To perform the RT-LAMP reaction within the droplets stored in the merging device, the whole device chip was sealed in a plastic bag for preventing droplet evaporation and submerged in 62°C water bath for 30min.

5.2.5 Fluorescence Imaging and Data Analysis

The imaging setup consisted of an epi-fluorescence microscope (Eclipse Ti, Nikon) equipped with an XY motorized stage, a 10X objective lens (CFI Plan, Nikon), and an electron multiplying charge-coupled device (EMCCD) camera (Evolve 512, Photometrics). Three-filter settings with bright-field, blue band (for nuclei blue, ex405/em450), and green band (for Calcein ex470/em520) channels were used to record the images. The recorded images were analyzed with a customized MATLAB code.

5.3 Result and discussion

5.3.1 Optimization of RT-LAMP assay

Loop-mediated isothermal amplification (LAMP) as an alternative DNA amplification method has been shown to have much higher amplification sensitivity than conventional poly-chain reaction (PCR)[119]. Because LAMP can be carried out at a constant temperature and does not require a thermal cycler, it is also a preferred method for microfluidic on-chip gene amplification and detection. When coupled with cell lysis and mRNA reverse transcription (RT), RT-LAMP became a sensitive and selective gene expression detection method. The principle of an RT-LAMP reaction is shown in Fig. 5.3a. In brief, in the presence of the target mRNA, ssDNA primers and reverse transcription enzyme, a synthesized complementary DNA (cDNA) contains a dumbbell-like structure at its both ends by self-annealing. To achieve high detection sensitivity and specificity, we utilized six LAMP primers targeting six regions of a specific mRNA[119]. DNA elongation and cycling amplification were initiated with this dumbbell-like precursor, which produced a great amount of cDNA products within a very short time (< 1 hour). To allow monitoring the completeness of LAMP reaction in real time, a

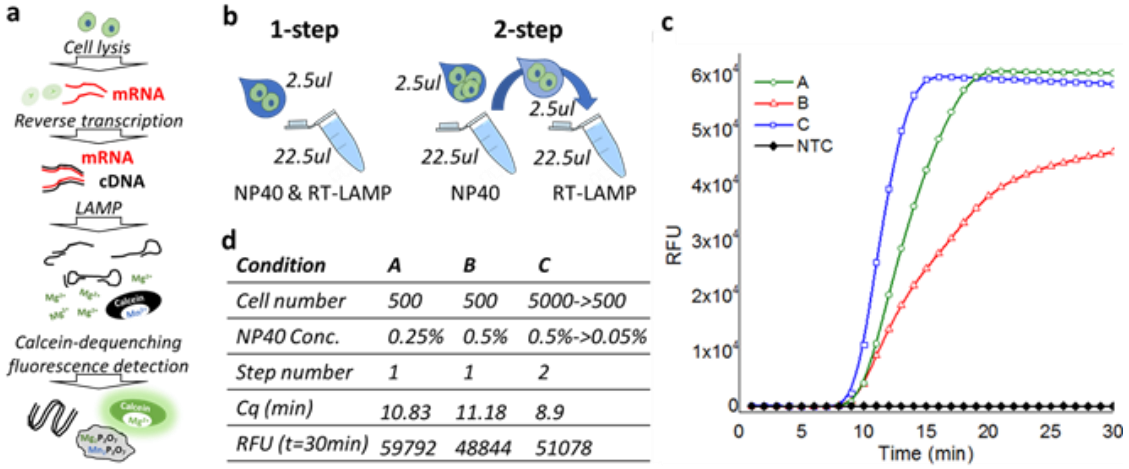

Condition	A	B	C
Cell number	500	500	5000->500
NP40 Conc.	0.25%	0.5%	0.5%->0.05%
Step number	1	1	2
Cq (min)	10.83	11.18	8.9
RFU (t=30min)	59792	48844	51078

Figure 5.3. Schematics of RT-LAMP and assay optimization in bulk solution. (a) Schematics of RT-LAMP and principle of reaction detection by Calcein fluorescence dequenching. (b) Schematics of one-step and two-step RT-LAMP reactions. (c) Representative results of real-time quantitative measurements of Calcein fluorescence under different conditions. (d) Table summarizes different assay conditions and the corresponding RT-LAMP results measured from (c). Cq is the critical time at which the reaction reaches the exponential phase, and RFU is the relative fluorescent intensity.

Calcein fluorescence dequenching method was developed[120]. The fluorescence property of the Calcein molecule is known to be sensitive to some divalent metallic ions. In our case, pyrophosphate ions were generated during the polymerization of nucleotides and reacted with Mn^{2+} ions to form $Mn_2P_2O_7$ precipitations. As a result, the concentration of Mn^{2+} ions decreased in the solution, leading to enhanced Calcein fluorescence intensity[120].

As all the droplet-manipulation devices only allow adding new reactants to, but not removing them from a droplet, an optimal scRT-LAMP assay needs to be efficient in cell lysis, reverse transcription, LAMP reaction and detection without centrifuging or washing. Since each operation step accumulates a new reactant in the droplet, the assay is potentially affected by cross-reaction between different reactants. This necessitates careful selection of reactants in our study. Specifically, we need to select a detergent that can be used to efficiently lyse the cells while not inhibiting downstream reactions. We picked Nonidet P-40, a solubilizing detergent, which has been shown to have no adverse effect on polymer chain reaction (PCR)[121]. However, its effect on reverse transcription or LAMP reaction is unknown. To save time and reduce operational variations, we optimized the scRT-LAMP protocol using bulk solution assays that mimic the in-droplet reaction conditions (Fig. 5.3b).

To determine the influence of NP-40 to the efficiency of RT-LAMP reactions, we added a 2.5μL Jurkat cell solution that contains 500 cells directly into a 22.5μL buffer that contained 0.25% or 0.5% NP-40, six LAMP primers specific to the human hydroxymethylbilane synthase (HMBS), a house-keeping gene that is essential in the heme biosynthetic pathway in all cell types[122]–[124], and one step RT-LAMP mix (WarmStart® LAMP Kit, New England Biolabs), followed by incubating and monitoring Calcein fluorescence changes in a real-time PCR machine at 62°C for 30 minutes (Fig. 5.3b, 1-step).

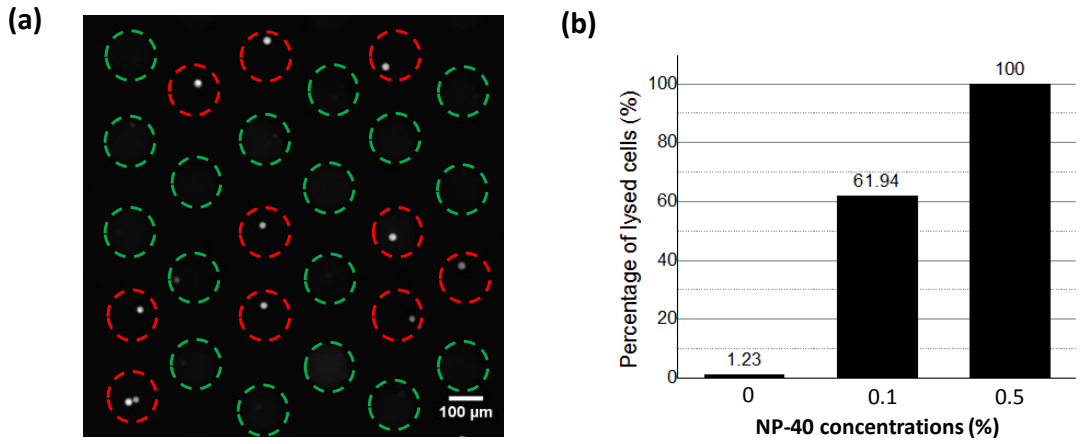

Figure 5.4. Effect of detergent concentration on cell lysing efficiency. (a) The florescence image shows that each stained Jurkat cell was encapsulated in a microdroplet with lysis buffer containing 0.1% of NP-40. The dashed circles indicate the positions of microdroplets. The cells remain fluorescent if they are not lysed in the droplets (red circles). The droplets showing dim and spatially uniform fluorescence indicate that the cells are lysed in the droplets (green circles). (b) Population (%) of droplets with lysed cells at different NP-40 concentrations (0%, 0.1%, and 0.5%). The number of droplets (cells) for each test are 500.

We found that the RT-LAMP reactions were more efficient in the buffer that contained 0.25% NP-40 than in that contained 0.5% NP-40 (Fig 2c and 2d, conditions A and B, respectively). This suggests that lower NP-40 concentration is desired to achieve higher RT-LAMP efficiency. However, lysis buffers with lower than 0.5% NP-40 may not sufficiently lyse mammalian cells, which may reduce the mRNA detection sensitivity (Fig. 5.4). To overcome this dilemma, we designed a 2-step protocol, in which a 2.5μL solution that contained 5,000 Jurkat cells was first added to a 22.5μL lysis buffer that only contained 0.5% NP-40 and then 2.5μL of the lysate solution (equivalent to 500 cell content) was added into a 22.5μL solution that contained HMBS gene-specific primers, and one-step RT-LAMP mix (Fig. 5.3b, 2-step). This allowed us to use a higher concentration of NP-40 to effectively lyse the cells while subsequently diluting the NP-40 by 10-fold to achieve an optimal RT-LAMP efficiency (Fig 5.3c -d, condition C).

5.3.2 Workflow of single-cell RT-LAMP assay using Sort N' Merge platform

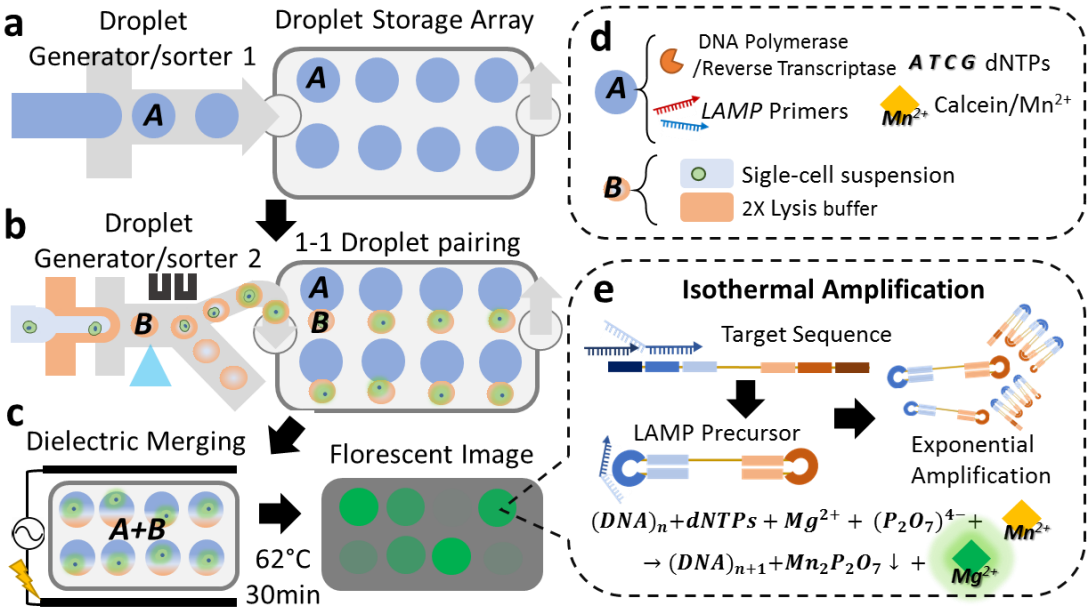

Figure 5.5. Schematics of single-cell RT-LAMP assay using Sort N' Merge platform. (a) Droplets containing RT-LAMP reactants (Droplet A) are first generated by droplet generator 1 and populate the pairing-merging wells in the storage device. (b) Droplets containing single-cell and lysis buffer (Droplet B) are then generated and sorted into the storage device and populate the pairing-merging wells. Droplet A and Droplet B are anchored and paired by buoyancy and the physical trap. (c) The paired droplets are merged by electrohydrodynamic force. RT-LAMP reaction is performed at 62°C for 30min followed by imaging-based fluorescence measurement. (d) The components of the droplets. (e) Principle of RT-LAMP reactions.

The unique advantages of our "Sort N' Merge" platform satisfy the requirements of the 2-step RT-LAMP assay by performing the lysis and the following steps separately in two types of droplets (Fig. 5.5). We first generated 125µm-diameter droplets (Droplet A) containing a mixture of total mRNA reverse transcription and HMBS gene-specific primers, RT-LAMP mix and Calcein/Mn^{2+} dye using a droplet generating device with a flow-focusing structure (Droplet Generator 1) and populated them in the pairing/merging microwell array (Droplet Storage Array) in the droplet storage device. We then generated 60µm-diameter droplets by co-flowing a nucleus-stained live Jurkat cell suspension and a lysis buffer solution in a different droplet generator/sorter device (Droplet Generator/Sorter 2). The cells were resuspended to an average density of 1 cell per 20 droplets to avoid encapsulating more than

one cell in a droplet. We applied fluorescence-activated droplet sorting (FADS) to isolate droplets that contain a single cell (Droplet B) and to selectively flow them into the collection outlet of the Droplet Generator/Sorter 2 (Fig. 5.5b). As the cell suspension and lysis buffer would not mix until they are co-encapsulated in a droplet, we positioned the fluorescence detection and dielectric sorting right after droplet separation to capture the stained cell before lysis. Droplet Bs were subsequently loaded to the storage mentioned above device, during which the cells were spontaneously lysed over time. The storage device has a two-layer structure composed of the first layer with a large flow channel and the second layer with the droplet pairing/merging microwell array. Each microwell has two-sized trapping sites each of which can fit in a 125μm-diameter droplet (Droplet A) or a 60μm-diameter droplet (Droplet B), respectively. Droplet As and Droplet Bs were populated in the microwell trapping sites sequentially by manually tilting the storage device to allow them to spread and float into the trapping sites by buoyancy. We removed uncaptured droplets from the flow channel by introducing an additional oil phase flow. Then, we applied an AC electric field across the droplet pairing/merging array to fuse each droplet pair into one merged droplet by dielectrophoresis to allow dilution of NP-40 and addition of RT-LAMP mix to the cell lysis (Fig. 5.5c). Finally, the one-step RT-LAMP reaction was carried out in the merged droplets at 62°C for 30 minutes (Fig. 5.5e).

5.3.3 Quantitative Analysis of Multi-step Droplet Assay Effectiveness

Next, we want to access the performance of our Sort N' Merge platform for high-throughput assays that involve more than two reaction steps. To do so, our platform needs to precisely co-encapsulate only one cell in a droplet with the first reactant for the first step reaction. Subsequently, each new reaction step requires a precise fusion of two droplets, one

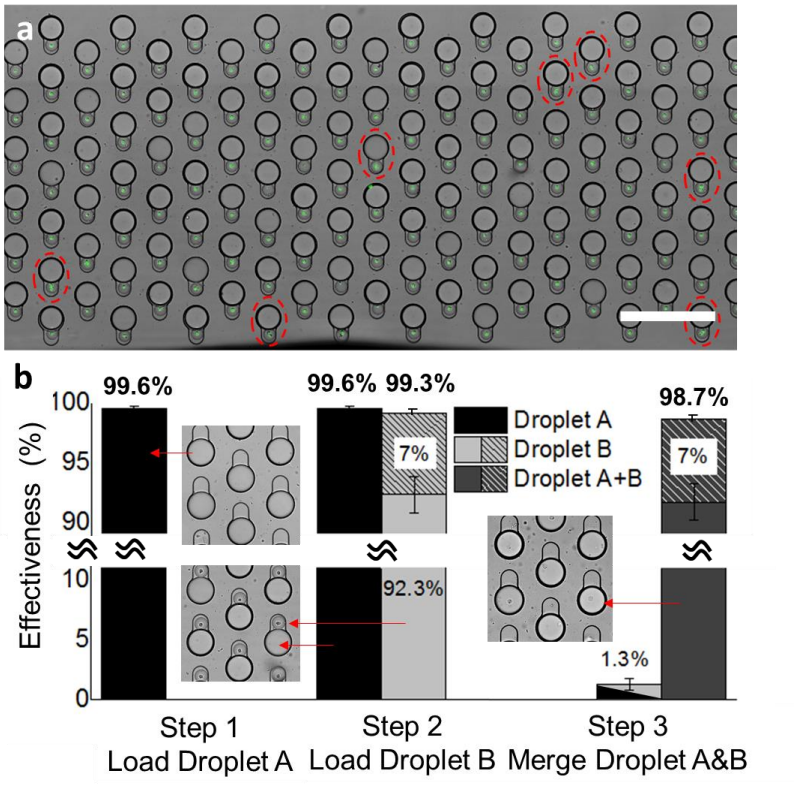

Figure 5.10. Quantification of the merging device effectiveness. (a) Image of paired droplets in droplet storage array. The dashed circles indicate there are multiple cells in single droplet Bs. (b) Effectiveness for droplet trapping, pairing, and merging steps. The slash bars indicate the percentage of droplets containing more than one cell.

of which contains the newly added reactants. During this process, there are several sources of error, including multiple cells encapsulated in the same droplet, false positives droplets generated from tissue debris, not one-to-one droplet paring, and incomplete merging of droplet pairs. One notable advantage of our setup is the ability to visually monitor the completion of each step in a multi-step droplet assay (Fig. 5.10). The effectiveness of each step can be quantified by characterizing the content of each droplet and the occupation of pairing/merging microwells from an optical image covering the entire droplet storage array (Fig. 5.10a).

Here, we quantified the effectiveness for each step of loading Droplet A, loading Droplet B, and merging Droplets A and B. Specifically, the effectiveness is defined as the fraction of microwells containing the desired droplets over all the microwells of a single

merging device after each assay step. First, we loaded the large-size Droplet As, containing primers and RT-LAMP mix to the merging device and observed that the trapping of these droplets was achieved at effectiveness of 99.6% averaged over three repeats with a standard deviation (S.D.) of 0.19% (Red in Fig. 6b). We occasionally found a small number of vacant microwells due to undesired dust or debris trapped in them.

Second, we loaded the small-size Droplet Bs to the merging device to trap and pair them with Droplet As (Green in Fig. 6b). We observed that the filling and paring process was achieved at average effectiveness of 99.3% ± 0.24% (Mean ± S.D.). The small decrease of effectiveness after the droplet pairing process came from the accumulation of errors, which result from an increased number of empty microwells after the repeated droplet trapping. Among all the droplet pairs, 7% ± 1.48% (Mean ± S.D.) of them contained multiple cells, which is slightly higher than a theoretical value of 4.9% predicted by the Poisson distribution. This is likely due to an input of too high concentration of cell suspension or due to incomplete cell dissociation yielding clusters of cells. The former error can be minimized by setting a high-intensity cutoff in the sorting step or by diluting the cell suspension to a much lower concentration. In conventional droplet merging approaches based on either co-following or additive merging, diluting the sample leads to higher reagent costs and longer processing time. In contrast, our method decouples the cell droplets and reactant droplet generation steps that only a very low amount of reactant is needed to fill the whole microwell array. This significantly saves the reagent costs even using very diluted cell suspension. The drawback of increasing the droplet sorting time with more empty droplets can be mitigated by a sorting rate as high as 30kHz.

Finally, we determined the effectiveness of the merging process, in which all the droplet pairs were simultaneously electrocoalescence (Blue in Fig. 5.10b). The average effectiveness of the merging process was 98.7% ± 0.60% (Mean ± S.D.). As such, we observed an overall 97.6% Droplet pairing-and-merging efficiency that resulted in successful cell lysis in a droplet, followed by mixing with new reactants and on-chip RT-LAMP reaction. Among these particular experiments, we observed 7.0% ± 1.48% (Mean ± S.D.) of the droplets contains more than one cell. And the unsuccessful merging events were found in 1.3% ± 0.45% (Mean ± S.D.) of the total microwells, due to missing a small Droplet B or failure of droplet merging. The failure of droplet merging was caused by the outlier Droplet Bs that are smaller than the designed size that could not form physical contact with the adjacent large Droplet As.

5.3.4 Characterization of RT-LAMP Assay in Microdroplets

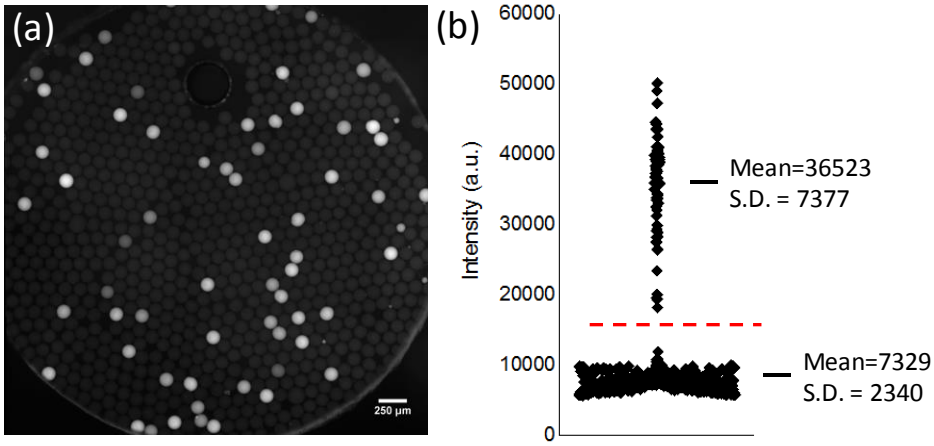

Figure 5.6. Quantification of the dynamic range of fluorescence change in our scRT-LAMP system. (a) Fluorescence image of droplets containing LAMP reactant mixtures and purified lambda DNA templates, as described in Ref [1]. The lambda DNA templates were diluted to the population of ~ 1 copy per 10 droplets. Thus, only ~10% of the droplets showed an increased fluorescence signal after incubated at 62°C for 30min. (b) Dot plot of fluorescence intensity distribution across 679 droplets, where each dot represents the fluorescence intensity of each droplet. The two clusters of droplets with and without lambda DNA template ("On" and "Off" droplets) can be clearly distinguished by the average values of fluorescence intensity of 36523 a.u. and 7329 a.u., respectively.

To estimate the dynamic range of fluorescence change in our scRT-LAMP system, we diluted lambda DNA to ~ one copy per 10 droplet as input instead of cells and quantified the fluorescence intensity fold-change after the RT-LAMP reaction (Fig. 5.6a). We could clearly distinguish two populations of droplets based on the three-sigma rule, among which the brighter ones had at least 2.5-fold (ave. ~5-fold) higher intensity than the dimmer ones (Fig. 5.6b). The ratio of two populations is about 1:10 (bright : dim) as expected. Since we expect most of the "bright" droplets (>90%) to contain only one initial template molecule, we believe that the wide-spread distribution of the signal is due to the intrinsically stochastic nature of the amplification techniques rather than a variance in the number of copies generated for the initial templates across these droplets. We measured the fluorescence intensity at the transient (exponential) phase rather than the saturation phase of the amplification to avoid the false-

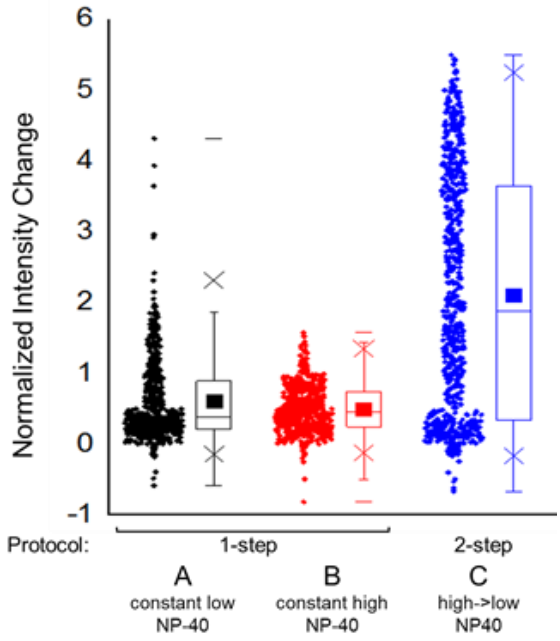

Figure 5.7 Effect of detergent concentration on droplet-based single-cell RT-LAMP efficiency. Box plot of scRT-LAMP result from three different protocols with Jurkat cells. Each dot represents the post-reaction fluorescence signal from each single cell, hence the expression level of each cell's HMBS gene. The normalized intensity change is defined as (I-I_0)/I_0, where I is the end-point intensity and I_0 is the initial intensity of each droplet. The experiment conditions are identical to those in Figure 2, except that the reaction volume is reduced from 25μL in bulk to 1.1nL in droplet. The numbers of data points for the A, B, and C tests are 607, 612, and 668, respectively.

positive signal contributed from non-specific amplification. At the transient phase, the randomness of the annealing and denaturation steps is pronounced. This would yield the variance of the amplification speed, thus introducing the large standard deviation to the signal distribution across the bright droplets. This phenomenon is also commonly found with other droplet assays performing DNA/RNA amplification elsewhere [46][89-91]. We perform the assay based on a binary approach of evaluating the signal that only determines whether or not the initial templates are successfully amplified. As such, the wide signal standard deviation does not cause any concern for the downstream analysis.

In addition, we confirmed that the 2-step detergent dilution (0.5%->0.05% NP-40) protocol also had a higher scRT-LAMP efficiency over either a constant low detergent concentration (0.25% NP-40) protocol or a constant high detergent concentration (0.5% NP-40) protocol (Fig 5.7).

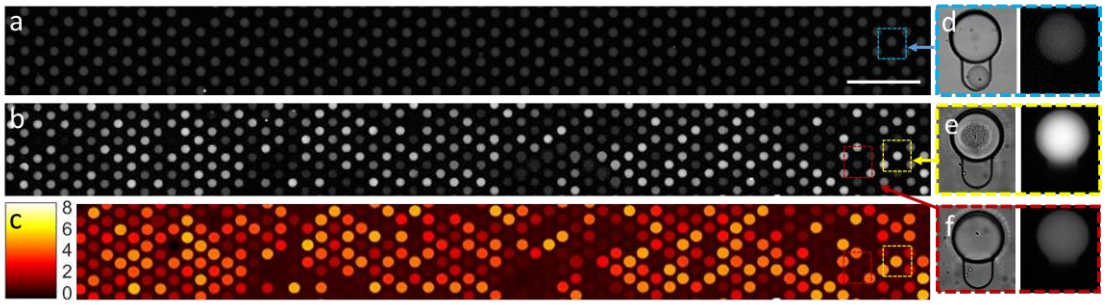

Figure 5.8. Visualization and quantification of scRT-LAMP in the Sort N' Merge storage device. Florescent images of droplets before merging (a), and after (b) merging/RT-LAMP, respectively. (c) The normalized intensity changes $(I_b - I_a)/ I_a$ before and after merging/RT-LAMP reaction. Magnified transmit light and fluorescent images show two paring/merging microwells with cell-containing droplets before merging (d) and after merging/RT-LAMP reaction (e), respectively. We found that the microwell containing a HMBS+ cell showed salt precipitation and bright Calcein fluorescence in the transmit light and fluorescence images, respectively (e), and the HMBS- cell (d) showed no salt precipitation nor fluorescence after RT-LAMP reaction (f).

Finally, we set out to quantify the relative expression level of the HMBS gene in single cells from the encapsulating droplets. Figure 5.8 shows the fluorescence images before (Fig.

5.8a, d) and after (Fig. 5.8b, e, f) RT-LAMP reaction. We found a wide range of fluorescent signal increase in each microwell, indicating the heterogenous expression levels of the HMBS gene in individual Jurkat cells (Fig. 5.8c). We also found that the fluorescence increase was always accompanied by precipitation of $Mg_2P_2O_7/Mn_2P_2O_7$ salt crystal, i.e., the LAMP reaction products, which was visible under transmitted light imaging (Fig. 5.8e).

5.3.5 Detection of HMBS gene expression pattern amount different cell types

As an essential gene in the heme synthesis pathway in all cell types, human hydroxymethylbilane synthase (HMBS) has been used as one of the quantitative real-time PCR (qRT-PCR) biomarkers in studying the pathophysiology of human diseases, including neurodegenerative diseases such as Alzheimer's disease, Parkinson's disease, and dementia with Lewy bodies[27]. We are motivated to access whether our scRT-LAMP platform can reveal

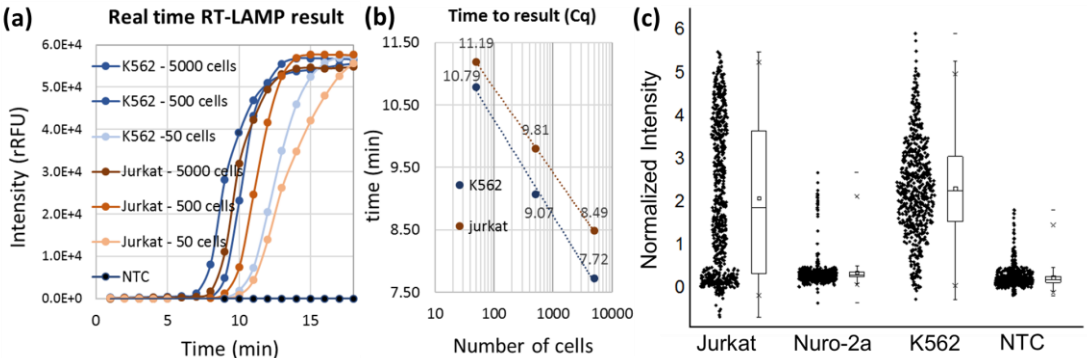

Figure 5.9. Distinct HMBS mRNA expression pattern in different cell types. (a) Real time RT-LAMP measurements of overall HMBS mRNA expression levels in different total number of cells. (b) While the maximum fluorescence intensity eventually reaches the similar level in all samples, the critical time to achieve exponential amplification is dependent on the total cell number. (c) Box plot of scRT-LAMP results obtained with Jurkat cells, Neuro-2A cells, K562 cells, and no cell control (NCC). Each dot represents the LAMP signal fold-change in each single-cell, hence the relative expression level of each cell's HMBS mRNA. The normalized intensity change is defined as $(I - I_0)/I_0$, where I is the end-point intensity and I_0 is the initial intensity of each single-cell droplet. The experiment conditions are identical to Figure 4 except the reaction volume reduce from 25μL in bulk to 1.1 nL in a droplet. The numbers of data points (i.e. single cell or empty droplets) are 668, 654, 612, and 655 for Jurkat cells, K562 cells, Neuro-2A cells, and NCC, respectively.

the HMBS expression heterogeneity between individual single cells among different cell types, which would not be able to discover by traditional qRT-PCR[125].

It has been shown that the protein expression level of HMBS in the bone marrow-derived K562 cells is higher than that in the Jurkat cells[122]. We therefore chose to access the level of HMBS mRNA in these two cell lines along with a mouse neuroblastoma derived Neuro-2A cell line (Fig. 5.9). We first used the 2-step bulk RT-LAMP protocol to compare the overall HMBS mRNA levels in 50, 500, or 5000 Jurkat or K562 cells. We found that while eventually similar fluorescence intensity has been recorded by the qPCR machine, there is a significant difference in the time required to reach the maximum fluorescent intensity (Fig. 5.9a). Plotting the critical time that reaches the exponential phase with different cell inputs indicates that K562 cells indeed have higher mRNA level than Jurkat cells (Fig. 5.9b).

To access the HMBS mRNA level in these cell lines at the single cell resolution, we next used our scRT-LAMP assay to quantify about six hundred droplet-encapsulated cells of each of these cell lines along with droplets containing only PBS buffer as a negative control in four storage devices. In our scRT-LAMP assay, both K562 cells and Jurkat cells showed a larger population (92.77% and 70.56%, respectively) that expressed HMBS mRNA than Neuro-2A cells and the no cell negative control (4.69% and 3.91%, respectively). The low level of HMBS mRNA detection in mouse Neuro-2A cells is expected since the primers were specific to human, but not to mouse HMBS gene. The higher detection rate of HMBS mRNA for K562 than Jurkat cells was also consistent with the bulk RT-LAMP result that the K562 cells show a smaller Cq value than Jurkat cells (Fig. 5.9b). Interestingly, we observed that while the mRNA level of individual K562 cells falls into a smooth normal distribution, that of the Jurkat cells can be partitioned into a large non-expressing population, similar to those of

the Neuro-2A cells and the no cell control, and the rest, a population that evenly distributed throughout all expression level. These control and new finding confirmed that our novel scRT-LAMP assay is suitable for characterizing the mRNA expression level of selected genes in individual cells of different subpopulations. We expect that it will also be suitable for cells extracted from tissue to reveal gene expression pattern that cannot be identified by canonical bulk measurements.

Chapter VI

Conclusions and Future Work

6.1 Thesis summary

This thesis has developed a new microdroplet-based platform (Sort N' Merge) for single-cell assays. We have successfully demonstrated the use of the Sort N' Merge system in a single-cell transcriptomic analysis. The accomplishments of this thesis are summarized in the following sections.

6.1.1 Sort N' Merge platform

This thesis proposes the first conceptual microfluidic system combining high throughput droplet sorting in continuous flow and precise droplet merging in a static array. The microfluidic system provides a universal platform to partition biochemistry reactions in an array of thousands of pico- or nanoliter sized droplets. The capabilities of precise control of each reactor's contents and the speedy analysis address the needs of single-cell assays. In the Sort N' Merge platform, the desired cells, engineered microbeads, and reagents are actively sorted by fluorescence-activated droplet sorting and additively merged into the same droplet.

The co-encapsulation of two or three fluorescence microbeads achieved high yields of 87.0% and 80.1%, respectively. This is a significant improvement compared to the conventional co-flow methods governed by *Poisson* statistics, in which the theoretical maximum yields are limited to 13.4% and 5.0%, respectively. In addition, our technology allows for cell sorting, multi-step reaction processing, and time-course imaging using one integrative droplet microfluidic format. This makes our platform readily available for a wide spectrum of single-cell studies. The system is also highly miniaturized compared to a conventional benchtop setup. For a typical reaction volume of 25 µL in a bulk molecular biology experiment, our droplet-based system allows thousands of experiments to be run simultaneously. The number of cells per experiment can be easily scaled up by increasing the microwell density of ~2000 pairing/merging wells/cm^2 on the storage device. It is also possible to sequentially sort droplets into multiple storage devices for massively parallel operation of the assay. Furthermore, the full on-chip processing minimizes the time and error for manual hands-on operation and could potentially be further improved by automating the entire process.

6.1.2 Single-cell mRNA-sequencing using the Sort N' Merge platform

Our Sort N' Merge platform integrates active droplet sorting and downstream one-to-one droplet pairing-merging processes to overcome the inefficiency of co-encapsulating a cell and a barcoded microbead in other droplet-based csRNAseq platforms. Our light-activated sorting device is highly efficient and generates barcoded beads containing droplets at a rate of about 600 droplets/min, and > 99% of the microwells in the merging chip are correctly filled with the droplets within several minutes. We adjusted the concentration of cells to a ratio of 1 cell: 20 droplets to avoid "cell- doublets" (two or more cells) in a droplet. As the volume of each droplet is small (~50 pL), this dilution ratio is equivalent to a concentration as high as 1

million cells/mL. With a flow rate of ~1500 droplets/sec (5 μL/min), we could complete the screening of all cells in a 50 μL sample within 10 min. Under the appropriate experiment conditions, all of the desired cells can be sorted and sequenced with no loss. The accuracy of our platform was validated by an experiment with a one-to-one mixture of human Hela and the mouse Neuro2A cell lines. The experiment showed a high single-cell encapsulation accuracy (doublet ratio < 2%) without significant dilution of the cells. The ability to work with a wide range of cell concentrations provides the flexibility of sample types and a faster sample processing time. Moreover, we integrated the cell sorting and sequencing processes, making the process specifically suitable for studying type-specific or rare cells directly extracted from primary tissues. We successfully demonstrated sorting and sequencing of a neural subpopulation from single Gal4 drive Drosophila, in which about 1,000 stem cells expressed the green fluorescent protein among 100,000 neural cells. The transcriptomic information from those specifically labeled cells is crucial to reveal the lineage progression from neural stem cells to neurons and to identify crucial molecules that emerge during these transitions. Furthermore, our platform enables a multi-step workflow that could be useful for optimizing the performance of mRNA barcoding and cDNA synthesis.

6.1.3 Single-cell mRNA detection by RT-LAMP

Using the Sort N' Merge platform, we performed an integrated droplet-based single-cell RT-LAMP assay for high-throughput selective gene detection from single cells. Enabling a fully on-chip droplet workflow that covers droplet generating, storing, paring, and merging processes, the Sort N' Merge platform significantly reduced the complexity of the hands-on inter-device operation and sample processing time. The highly sensitivity and fast speed of the sc-RT-LAMP assay permitted quantification of the expression levels of a target mRNA in

hundreds to thousands of single cells within 1 hour. This sc-RT-LAMP assay also showed high specificity, as using primers designed for human HMBS. As a result, we obtained a very low level of amplification signal from mouse Neuro-2A cells and the cell-empty control sample. This droplet-based sc-RT-LAMP assay allowed us to observe that human K562 cells have higher HMBS mRNA expression than human Jurkat cells at the population level, which may lead to higher HMBS protein expression in K562 cells than in Jurkat cells, as reported previously by bulk measurements (https://amp.pharm.mssm.edu/archs4/gene/HMBS). In addition, this sc-RT-LAMP assay revealed, for the first time, the heterogeneous HMBS mRNA expression pattern from individual cells of different types. Interestingly, the lower overall HMBS expression in Jurkat cells was due to a bi-phasic expression pattern within the population. It means that a large proportion of cells have non-detectable HMBS expression while an equal number of cells express HMBS at higher levels. On the other hand, the expression levels of HMBS mRNA in K562 cells fell into a standard normal distribution with the mean at a high expression level.

In addition to its usefulness for detecting mRNA, our assay strategy provides an optimized solution for cell lysis and mRNA amplification in the same droplet. A similar protocol could be applied to single-cell mRNA-sequencing experiment for a higher mRNA recovering yield.

6.1.4 Other potential applications using the Sort N' Merge platform

Applications of our Sort N' Merge platform are not limited to single-cell mRNA studies, as demonstrated in this thesis. Operation of our platform integrating continuous flow and stationary operations together is similar to the traditional approach using a combination of flow cytometry and pipetting of microtiter plates. This means that various canonical single-cell

assays can be easily adapted to our system, such as cytotoxicity assays, co-culture assays, and cell secretion assays. Most of the existing droplet-based single-cell assays are also compatible with our platform, which can accommodate all major droplet manipulation. Moreover, several unique features of our system provide new experimental designs. For example, integrated cell sorting would enable targeted studies of rare cells labeled according to their specific subtypes. The flexibility and precision of our system in designing and executing multi-step protocols allows for improved assay sensitivity and efficiency and will permit novel assays for multiplex measurements of the same single cell. Our system also enables time-course imaging of the droplet reactors, so the sample quality can be monitored and biochemical reactions of single cells can be quantified in a massively parallel manner at high throughput.

In addition to providing the flexibility for laboratory-level single-cell research as described above, our platform could serve as a tool highly benefiting studies carried out in a larger clinical research community. With the recent increase of biological knowledge from high-throughput single-cell analysis, we foresee that such knowledge will be eventually transferred to the clinical side for accelerating disease diagnosis and treatment. From the clinical users' perspective, it is critical to standardize and automate the assay workflow with the minimum hands-on operations for on-site applications. For example, a system enabling rapid isolation of target cancer cells from a tumor biopsy and providing the answer of their corresponded biomarkers will make the precision cancer therapy possible. Although our platform is still in a preliminary stage, we have demonstrated such important functions for the potential clinical applications. The future effort towards this goal will be discussed in the next session.

6.2 Future work

This thesis demonstrated the preliminary setup of the Sort N' Merge system and demonstrated two single-cell mRNA experiments as proof of application. Continued study of the Sort N' Merge platform for transcriptomic analysis will potentially revolutionize the method for high-throughput single-cell analysis. Future work will focus on enhancing the sensitivity of mRNA detection and barcoding. As this system permits a multi-step workflow, several new protocols can be tested and will be discussed in the next section. The future direction on the engineering side is to work on system automation and explore scalable microfluidic device fabrication for future mass production. The operation of the current system still relies on a well-trained technician with a sophisticated background in droplet microfluidics, which limits its wide dissemination in the laboratory. Our future effort will include the automation of this system for broader impacts of our work.

6.2.1 Enhance mRNA Recovery Yield from Single Cells

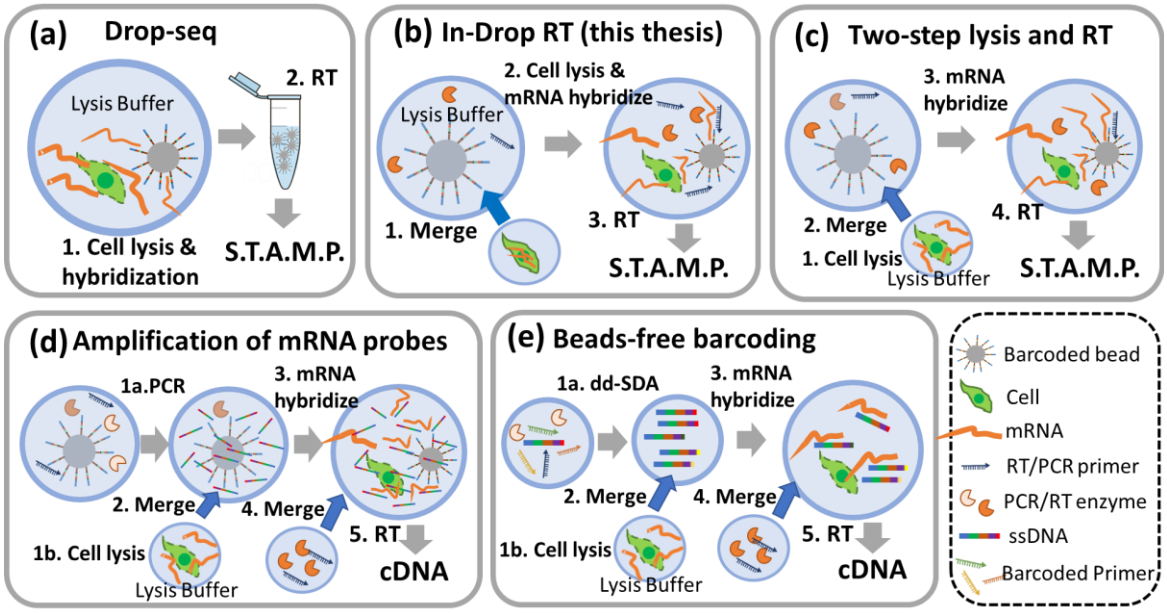

Figure 6.1 Evolution of droplet based single-cell mRNA-seq protocols from previous (a) Drop-Seq, (b) current In-Drop RT, to future work (c)–(e).

The efficiency of a molecular biology reaction is typically sensitive to assay conditions. Conventional Drop-seq retrieves mRNA with two- to three-fold lower efficiency than other methods such as 10X genomics, In-Drop, or Smart-seq [109]. We hypothesized that this is because: 1) the diffusion and binding of large mRNA molecules to the probes on the beads are inefficient; 2) the delicate mRNA molecules are lost or degraded during the off-chip elution process; and 3) a limited number of ssDNA probes are synthesized on each bead. To overcome these limitations, we developed a plan to explore the potential solution, as shown in Fig. 6.1. In this thesis, we incorporated a reverse-transcription (RT) reaction in the droplets for the sc-mRNA-seq experiment (Fig. 6.1b) as with the In-Drop method [94], but we did not observe a significant improvement in the mRNA recovery yield. Later, we found that the two-step protocol with separate lysis and RT processes provided much better RT and amplification performance for the sc-RT-LAMP experiment. This finding indicates that the use of the two-step sc-mRNA-seq protocol could potentially improve assay performance (Fig. 6.1c). To increase the number of capture probes, we have designed an in-droplet amplification step to generate a large number of freely diffusive ssDNA probes in the bead-droplet (Fig. 6.1d). Complementary probes with a random cell barcode will be synthesized on each microbead by the "split-and-pool" process similar to what has been done in Drop-seq. We will include PCR reagent and amplification primers, each of which contains random unique molecule identifiers (UMI) and a template switching oligo to on-chip amplify the barcoded probes on the sorted beads in the droplets. We anticipate that the freely diffusive ssDNA probes will hybridize with the mRNA molecules more efficiently than the previous microbead-based approach. Once we verify this idea, our ultimate goal is to remove the microbeads from Drop-seq as they increase the difficulty of the microfluidic operation. ssDNA probes are directly amplified from a single

template containing a cell barcode with primers containing random UMIs by droplet-based digital strand displacement amplification (dd-SDA). The droplets containing the amplified barcode are sorted with fluorescent dyes and merged with cell-containing droplets. This approach is expected to maximize the degrees of freedom for other molecular biology experiments, such as genetic or epigenetic assays.

6.2.2 System automation

Although droplet microfluidic technology was invented two decades ago, there are only a handful of droplets generating and detection modules available on the market, such as 10X genomics for sc-mRNA-seq and Bio-Rad Laboratories for droplet-digital-PCR. Most of the advanced designs are task-specific, so there is not enough motivation to push the technology to the industrial level. As our platform can be universally applied to various types of single-cell assays and biological samples, I believe making this system available to the broader biological community will directly facilitate the development of commercial single-cell technologies.

Robotic fluid-handling at the tens of microliters scale is already a mature technology. The difficulty of building an automated system is actually associated with fabricating a robot-compatible microfluidic chip. Conventional microfluidic devices are fabricated by soft lithography using PDMS as the channel layer and glass as the substrate layer. This approach is suitable for prototyping but not for industrial applications. Micro-embossed or injection-molded approaches may not meet the requirements of pattern resolution. Therefore, using glass and silicon compatible with semiconductor and microelectromechanical systems manufacturing remains the first choice. How to design a robust process flow to meet all optical,

electrical, and fluidic criteria of the microfluidic chip becomes the last piece of the puzzle for lab-on-a-chip technology.

Appendices

Appendix A. Fabrication of Microfluidic Devices with electrodes

A.1. Fabrication of Microfluidic Channels Mold.

1. Photoresist Patterning

1) Spin coat SU-8 2050 photoresist at 500 rpm for 10 seconds and 3200* rpm for 30 seconds.

2) Softbake at 65°C for 2* min and 95°C 5* min.

3) Expose the photoresist using MA/BA-6 Mask Aligner (Exposure intensity ~20 J/s) for 25 s*.

4) Post-exposure back at 65°C for 1* min and 95°C 6* min.

5) Developed the exposed photoresist using SU-8 developer for 5* minutes or until the unexposed SU-8 photoresist is dissolved.

6) Rinse with IPA, water, and air dye with a nitrogen gun.

7) Hard bake at 150°C for 10 min.

*These values could vary with the desired thickness of SU-8 film. The relation between film thickness and the parameters is provided in the data sheet (http://microchem.com/pdf/SU-82000DataSheet2000_5thru2015Ver4.pdf).

2. Silicon Surface Silanization

1) Plasma active the silicon mold surface (Air plasma, 60W, 200mT, 30s)

2) place silicon mold into a vacuum desiccator. Drop 100 µL of Silane

(tridecafluoro-1 ,1, 2, 2-tetrahydrooctyl)-1-trichlorosilane (United Chemical Technologies) on the glass slide and put into the desiccator for 1 hr under vacuum.

A.2. Fabrication of microfluidic droplet generator/sorter/merger.

1. Fabrication of PDMS microfluidic channel

1) Mix the Sylgard 184 base and curing agent in a weight ratio of 10:1.

2) Degas in a vacuum desiccator for about 60 min.

1) Place the silanized silicon mold in a petri dish.

3) Pour PDMS over the Silicon-SU-8 mold (Thickness 5-10 mm).

3) Degas in the desiccator for 10 min. Make sure the silicon wafer is in the horizon.

4) Cure PDMS in the oven (60 °C 4 hr- overnight).

5) Peel off PDMS from a silicon wafer.

6) Punch holes through PDMS using a Biopsy punch with a diameter of 0.075mm or 0.15mm.

7) Plasma active the PDMS surface and glass slides (Air plasma, 60W, 200mT, 30s)

8) Bond PDMS channel to the glass slide. For multi-layer channel design, perform the bonding process under the stereomicroscope.

2. Fabrication of electrodes.

1) Place low-melting metal alloy into the pre-drilled holes for the electrode channel.

2) Place PDMS chips on a hot plate for 30 sec at 120°C.

3) Manually add little pressure on the metal alloy to make sure it is in contact with the bottom of devices. Once the metal alloy is in contact with the microfluidic channel and melted, the metal electrodes will automatically be formed due to the capillary force.

4) Cool down the devices in room temperature for 3 min.

3. Prepare the embedded optical fiber.

1 Cleave the fiber

1) Pull the fiber taut and keep tension in the fiber.

2) Place a drop of water on the cleave site.

3) Cleave the fiber using a ruby scribe. Make sure it is cleaved at a perpendicular angle.

4) Inspect the end of the fiber under a microscope. The fiber end should be flat and perpendicular to the optic axis. If not, repeat the cleaving process again.

2 Polish the fiber

1) Insert the fiber end into a polishing disk.

2) Place a sheet of the 30 μm polishing film on the flat surface.

3) Gently place the polishing disc on the film with fiber end contacting the film.

4) Polish the fiber in a figure eight pattern for about 1 min.

4) Repeat above processes with 6 um, 1 um and 0.02 um polishing film to achieve the optimized result.

Appendix B. Sketch of droplet sorting for the Arduino compatible Microcontroller

```
double Threshold0 = 0.4; // Set 450 laser threshold(unit:V)
double Threshold1_upper = 1; // Set 530 laser upper threshold (unit:V)
double Threshold1_bottom = 0.5; // Set 530 laser lower threshold (unit:V)
int values0[2]={0,0};
int TH0 = round(Threshold0*67);
int TH1 = round(Threshold1_upper*67);
int TH2 = round(Threshold1_bottom*67);
int maxvalue1=0; int delaytime = 200;
const int ledPin1 =  11; const int ledPin2 =  13;
int count=0;
unsigned long TTLtime[4] ={4294967295,4294967295,4294967295,4294967295};
int sensorPin0 = A0;
int sensorPin2 = A2;
// Define various ADC prescaler
void setup() {
  Serial.begin(9600);
  pinMode(ledPin1, OUTPUT);
  pinMode(ledPin2, OUTPUT);
  pinMode(sensorPin0, INPUT);
  pinMode(sensorPin2, INPUT);
  // set up the ADC}
void loop() {
unsigned long currentMicros = micros();
if(currentMicros >= 4294966295){
```

```
TTLtime[0] =4294967295;
 TTLtime[1] =4294967295;
  TTLtime[2] =4294967295;
   TTLtime[3] =4294967295;
   delay(10);  }
if(currentMicros >= TTLtime[0]) {
  digitalWrite(ledPin1, HIGH);
  digitalWrite(ledPin2, HIGH);
  TTLtime[0]=TTLtime[1];
  TTLtime[1]=TTLtime[2];
  TTLtime[2]=TTLtime[3];
  TTLtime[3] = 4294967295;
  count--;
  delayMicroseconds(50);  }
  values0[1] = analogRead(sensorPin2);
  maxvalue1=max(values0[1],maxvalue1);
   if (values0[1] < TH2 && values0[0] >= TH2){
   if(maxvalue1 < TH1){
   int  maxvalue2=0;
    for (int i=0; i <= 19; i++){
    maxvalue2=max(analogRead(sensorPin0),maxvalue2);      }
    if ( maxvalue2 >= TH0){    //450thresholds
    TTLtime[count]=micros()+delaytime;
    count++;
    }     }
  maxvalue1=0;
  }
// print out the results
```

```
values0[0] =values0[1];
digitalWrite(ledPin1, LOW);
digitalWrite(ledPin2, LOW);
```

Bibliography

[1] A.Regev et al., “Science Forum: The Human Cell Atlas,” Elife, vol. 6, p. e27041, 2017.

[2] A.Tanay andA.Regev, “Scaling single-cell genomics from phenomenology to mechanism,” Nature, vol. 541, no. 7637, pp. 331–338, 2017.

[3] T.Woyke, D. F. R.Doud, andF.Schulz, “The trajectory of microbial single-cell sequencing,” Nat. Methods, vol. 14, no. 11, pp. 1045–1054, 2017.

[4] T. M.Bergholz, A. I.Moreno Switt, andM.Wiedmann, “Omics approaches in food safety: Fulfilling the promise?,” Trends Microbiol., vol. 22, no. 5, pp. 275–281, 2014.

[5] X.Zhang, S. L.Marjani, Z.Hu, S. M.Weissman, X.Pan, andS.Wu, “Single-Cell sequencing for precise cancer research: Progress and prospects,” Cancer Res., vol. 76, no. 6, pp. 1305–1312, 2016.

[6] J. R.Heath, A.Ribas, andP. S.Mischel, “Single-cell analysis tools for drug discovery and development.,” Nat. Rev. Drug Discov., vol. advance on, no. 3, pp. 204–216, 2015.

[7] O.Caen, H.Lu, P.Nizard, andV.Taly, “Microfluidics as a Strategic Player to Decipher Single-Cell Omics?,” Trends Biotechnol., vol. 35, no. 8, pp. 713–727, 2017.

[8] S.Simon andE.Ezan, “Ultrasensitive bioanalysis: Current status and future trends,” Bioanalysis, vol. 9, no. 9, pp. 753–764, 2017.

[9] S. M.Prakadan, A. K.Shalek, andD. A.Weitz, “Scaling by shrinking: Empowering single-cell ‘omics’ with microfluidic devices,” Nat. Rev. Genet., vol. 18, no. 6, pp. 345–361, 2017.

[10] O.Stegle, S. A.Teichmann, andJ. C.Marioni, “Computational and analytical challenges in single-cell transcriptomics.,” Nat. Rev. Genet., vol. 16, no. January 2014, pp. 133–145, 2015.

[11] R.Sender, S.Fuchs, andR.Milo, “Revised Estimates for the Number of Human and Bacteria Cells in the Body.,” PLoS Biol., vol. 14, no. 8, p. e1002533, 2016.

[12] D. L.Ellsworth, H. L.Blackburn, C. D.Shriver, S.Rabizadeh, P.Soon-Shiong, andR. E.Ellsworth, “Single-cell sequencing and tumorigenesis: improved understanding of tumor evolution and metastasis,” Clin. Transl. Med., vol. 6, no. 1, 2017.

[13] T.Baslan andJ.Hicks, “Unravelling biology and shifting paradigms in cancer with single-cell sequencing,” Nat. Rev. Cancer, vol. 17, no. 9, pp. 557–569, 2017.

[14] T.Gerber et al., “Mapping heterogeneity in patient-derived melanoma cultures by single-cell RNA-seq,” Oncotarget, vol. 8, no. 1, pp. 846–862, 2016.

[15] R.DiLoreto, K.Khush, andI.DeVlaminck, “Precision monitoring of immunotherapies in solid organ and hematopoietic stem cell transplantation,” Adv. Drug Deliv. Rev., vol. 114, pp. 272–284, 2017.

[16] P.Dalerba, R. W.Cho, andM. F.Clarke, “Cancer stem cells: models and concepts.,” Annu. Rev. Med., vol. 58, pp. 267–284, 2007.

[17] L.Solden, K.Lloyd, andK.Wrighton, “The bright side of microbial dark matter: Lessons learned from the uncultivated majority,” Curr. Opin. Microbiol., vol. 31, pp. 217–226, 2016.

[18] M.Goldsmith andD. S.Tawfik, “Directed enzyme evolution: Beyond the low-hanging fruit,” Curr. Opin. Struct. Biol., vol. 22, no. 4, pp. 406–412, 2012.

[19] L.Mazutis, J.Gilbert, W. L.Ung, D. A.Weitz, A. D.Griffiths, andJ. A.Heyman, “Single-cell analysis and sorting using droplet-based microfluidics,” Nat. Protoc., vol. 8, no. 5, pp. 870–891, 2013.

[20] D.Yalcin, Z. M.Hakguder, andH. H.Otu, “Bioinformatics approaches to single-cell analysis in developmental biology,” Mol. Hum. Reprod., vol. 22, no. 3, pp. 182–192, 2015.

[21] N.Yosef andA.Regev, “Impulse control: Temporal dynamics in gene transcription,” Cell, vol. 144, no. 6, pp. 886–896, 2011.

[22] A.Shpunt et al., “Genome-Wide Detection of Single-Nucleotide and Copy-Number Variations of a Single Human Cell,” Science (80-.)., vol. 338, no. December, pp. 1622–1627, 2012.

[23] X.Wang, “Gene mutation-based and specific therapies in precision medicine,” J. Cell. Mol. Med., vol. 20, no. 4, pp. 577–580, 2016.

[24] C.Gawad, W.Koh, andS. R.Quake, “Single-cell genome sequencing: Current state of the science,” Nat. Rev. Genet., vol. 17, no. 3, pp. 175–188, 2016.

[25] S. J.Clark, H. J.Lee, S. A.Smallwood, G.Kelsey, andW.Reik, “Single-cell epigenomics: powerful new methods for understanding gene regulation and cell identity,” Genome Biol., vol. 17, no. 1, p. 72, 2016.

[26] S. A.Smallwood et al., “Single-cell genome-wide bisulfite sequencing for assessing epigenetic heterogeneity,” Nat. Methods, vol. 11, no. 8, pp. 817–820, 2014.

[27] T.Kalisky et al., “A brief review of single-cell transcriptomic technologies,” Brief. Funct. Genomics, vol. 17, no. 1, pp. 64–76, 2018.

[28] F.Tang et al., “mRNA-Seq whole-transcriptome analysis of a single cell,” Nat. Methods, vol. 6, no. 5, pp. 377–382, 2009.

[29] Y.Ben-Ari et al., “The life of an mRNA in space and time,” J. Cell Sci., vol. 123, no. 10, pp. 1761–1774, 2010.

[30] Y.Su, Q.Shi, andW.Wei, "Single cell proteomics in biomedicine: High-dimensional data acquisition, visualization, and analysis," Proteomics, vol. 17, no. 3–4, pp. 3–4, 2017.

[31] Q.Shi et al., "Single-cell proteomic chip for profiling intracellular signaling pathways in single tumor cells," Proc. Natl. Acad. Sci., vol. 109, no. 2, pp. 419–424, 2011.

[32] S. M. S.Quadri, "Single-cell western blotting," West. Blotting Methods Protoc., vol. 11, no. 7, pp. 455–464, 2015.

[33] A.Frei et al., "Highly multiplexed simultaneous detection of RNAs and proteins in single cells," Nat. Methods, vol. 13, no. 3, pp. 269–277, 2016.

[34] P.Chen, N. T.Huang, M. T.Chung, T. T.Cornell, andK.Kurabayashi, "Label-free cytokine micro- and nano-biosensing towards personalized medicine of systemic inflammatory disorders," Adv. Drug Deliv. Rev., vol. 95, pp. 90–103, 2015.

[35] R.Zenobi, "Single-cell metabolomics: Analytical and biological perspectives," Science (80-.)., vol. 342, no. 6163, pp. 0–11, 2013.

[36] A.Gross, J.Schoendube, S.Zimmermann, M.Steeb, R.Zengerle, andP.Koltay, "Technologies for single-cell isolation," Int. J. Mol. Sci., vol. 16, no. 8, pp. 16897–16919, 2015.

[37] V.Espina, M.Heiby, M.Pierobon, andL. A.Liotta, "Laser capture microdissection technology," Expert Rev. Mol. Diagn., vol. 7, no. 5, pp. 647–657, 2007.

[38] S. C.Bendall, G. P.Nolan, M.Roederer, andP. K.Chattopadhyay, "A deep profiler's guide to cytometry," Trends Immunol., vol. 33, no. 7, pp. 323–332, 2012.

[39] D.Hümmer, F.Kurth, N.Naredi-Rainer, andP. S.Dittrich, "Single cells in confined volumes: microchambers and microdroplets," Lab Chip, vol. 16, pp. 447–458, 2015.

[40] D. C.Duffy, J. C.McDonald, O. J. A.Schueller, andG. M.Whitesides, "Rapid prototyping of microfluidic systems in poly(dimethylsiloxane)," Anal. Chem., vol. 70, no. 23, pp. 4974–4984, 1998.

[41] P. K.Chattopadhyay, T. M.Gierahn, M.Roederer, andJ. C.Love, "Single-cell technologies for monitoring immune systems," Nat Immunol, vol. 15, no. 2, pp. 128–135, 2014.

[42] G. M.Whitesides, "The origins and the future of microfluidics.," Nature, vol. 442, no. 7101, pp. 368–73, 2006.

[43] C. N.Baroud, F.Gallaire, andR.Dangla, "Dynamics of microfluidic droplets," Lab Chip, vol. 10, no. 16, p. 2032, 2010.

[44] M.Sesen, T.Alan, andA.Neild, "Droplet control technologies for microfluidic high throughput screening (μHTS)," Lab Chip, vol. 17, no. 14, pp. 2372–2394, 2017.

[45] T. S.Kaminski andP.Garstecki, "Controlled droplet microfluidic systems for multistep chemical and biological assays," Chem. Soc. Rev., vol. 46, no. 20, pp. 6210–6226, 2017.

[46] D. J.Eastburn, A.Sciambi, andA. R.Abate, "Ultrahigh-throughput mammalian single-

cell reverse-transcriptase polymerase chain reaction in microfluidic drops," Anal. Chem., vol. 85, no. 16, pp. 8016–8021, 2013.

[47] A.Rotem et al., "Single-cell ChIP-seq reveals cell subpopulations defined by chromatin state," Nat. Biotechnol., vol. 33, no. 11, pp. 1165–72, 2015.

[48] P.Shahi, S. C.Kim, J. R.Haliburton, Z. J.Gartner, andA. R.Abate, "Abseq: Ultrahigh-throughput single cell protein profiling with droplet microfluidic barcoding," Sci. Rep., vol. 7, no. February, pp. 1–12, 2017.

[49] J. J.Agresti et al., "Ultrahigh-throughput screening in drop-based microfluidics for directed evolution.," Proc. Natl. Acad. Sci. U. S. A., vol. 107, no. 9, pp. 4004–9, 2010.

[50] M. T.Chung, D.Nunez, D.Cai, andK.Kurabayashi, "Sort'N merge: A deterministic microfluidic platform for co-encapsulating distinct particles in microdroplets," in 2018 IEEE Micro Electro Mechanical Systems (MEMS), 2018, pp. 265–268.

[51] M. T.Chung, D.Núñez, D.Cai, andK.Kurabayashi, "Deterministic droplet-based co-encapsulation and pairing of microparticles: Via active sorting and downstream merging," Lab Chip, vol. 17, no. 21, pp. 3664–3671, 2017.

[52] J.-C.Baret et al., "Fluorescence-activated droplet sorting (FADS): efficient microfluidic cell sorting based on enzymatic activity.," Lab Chip, vol. 9, no. 13, pp. 1850–8, 2009.

[53] E. Z.Macosko et al., "Highly parallel genome-wide expression profiling of individual cells using nanoliter droplets," Cell, vol. 161, no. 5, pp. 1202–1214, 2015.

[54] H.Kawaguchi, "Functional polymer microspheres," Prog. Polym. Sci., vol. 25, no. 8, pp. 1171–1210, 2000.

[55] Z.Nie et al., "Emulsification in a microfluidic flow-focusing device: Effect of the viscosities of the liquids," Microfluid. Nanofluidics, vol. 5, no. 5, pp. 585–594, 2008.

[56] D. J.Collins, A.Neild, A.deMello, A.-Q.Liu, andY.Ai, "The Poisson distribution and beyond: methods for microfluidic droplet production and single cell encapsulation," Lab Chip, pp. 3439–3459, 2015.

[57] S.Hong, Q.Pan, andL. P.Lee, "Single-cell level co-culture platform for intercellular communication," Integr. Biol., vol. 4, no. 4, p. 374, 2012.

[58] T. P.Lagus andJ. F.Edd, "High-throughput co-encapsulation of self-ordered cell trains: cell pair interactions in microdroplets," RSC Adv., vol. 3, no. 43, p. 20512, 2013.

[59] H. S.Moon et al., "Inertial-ordering-assisted droplet microfluidics for high-throughput single-cell RNA-sequencing," Lab Chip, vol. 18, no. 5, pp. 775–784, 2018.

[60] E. W. M.Kemna, R. M.Schoeman, F.Wolbers, I.Vermes, D. A.Weitz, andA.Van DenBerg, "High-yield cell ordering and deterministic cell-in-droplet encapsulation using Dean flow in a curved microchannel," Lab Chip, vol. 12, no. 16, pp. 2881–2887, 2012.

[61] S.Zeng, B.Li, X.Su, J.Qin, andB.Lin, "Microvalve-actuated precise control of individual droplets in microfluidic devices," Lab Chip, vol. 9, no. 10, pp. 1340–1343, 2009.

[62] D. J.Collins, T.Alan, K.Helmerson, andA.Neild, “Surface acoustic waves for on-demand production of picoliter droplets and particle encapsulation,” Lab Chip, vol. 13, no. 16, pp. 3225–3231, 2013.

[63] A. M.Pit, M. H. G.Duits, andF.Mugele, “Droplet manipulations in two phase flow microfluidics,” Micromachines, vol. 6, no. 11, pp. 1768–1793, 2015.

[64] B.Kintses, L. D.vanVliet, S. R. A.Devenish, andF.Hollfelder, “Microfluidic droplets: New integrated workflows for biological experiments,” Curr. Opin. Chem. Biol., vol. 14, no. 5, pp. 548–555, 2010.

[65] P.Abbyad, R.Dangla, A.Alexandrou, andC. N.Baroud, “Rails and anchors: guiding and trapping droplet microreactors in two dimensions,” Lab Chip, vol. 11, no. 5, pp. 813–821, 2011.

[66] S.Lee, H.Kim, D. J.Won, J.Lee, andJ.Kim, “On-demand, parallel droplet merging method with non-contact droplet pairing in droplet-based microfluidics,” Microfluid. Nanofluidics, vol. 20, no. 1, pp. 1–9, 2016.

[67] L.Labanieh, T. N.Nguyen, W.Zhao, andD. K.Kang, “Floating droplet array: An ultrahigh-throughput device for droplet trapping, real-time analysis and recovery,” Micromachines, vol. 6, no. 10, pp. 1469–1482, 2015.

[68] A.Huebner et al., “Static microdroplet arrays: A microfluidic device for droplet trapping, incubation and release for enzymatic and cell-based assays,” Lab Chip, vol. 9, no. 5, pp. 692–698, 2009.

[69] J. H.Jung, G.Destgeer, J.Park, H.Ahmed, K.Park, andH. J.Sung, “On-Demand Droplet Capture and Release Using Microwell-Assisted Surface Acoustic Waves,” Anal. Chem., vol. 89, no. 4, pp. 2211–2215, 2017.

[70] K.Leung et al., “A programmable droplet-based microfluidic device applied to multiparameter analysis of single microbes and microbial communities,” Proc. Natl. Acad. Sci., vol. 109, no. 20, pp. 7665–7670, 2012.

[71] A. M.Pit, S.Bonestroo, D.Wijnperlé, M. H. G.Duits, andF.Mugele, “Electrode-assisted trapping and release of droplets on hydrophilic patches in a hydrophobic microchannel,” Microfluid. Nanofluidics, vol. 20, no. 9, pp. 1–12, 2016.

[72] L.Frenz, K.Blank, E.Brouzes, andA. D.Griffiths, “Reliable microfluidic on-chip incubation of droplets in delay-lines,” Lab Chip, vol. 9, no. 10, pp. 1344–1348, 2009.

[73] I.Akartuna, D. M.Aubrecht, T. E.Kodger, andD. A.Weitz, “Chemically induced coalescence in droplet-based microfluidics,” Lab Chip, vol. 15, no. 4, pp. 1140–1144, 2015.

[74] M.Lee et al., “Synchronized reinjection and coalescence of droplets in microfluidics.,” Lab Chip, vol. 14, no. 3, pp. 509–13, 2014.

[75] L.Mazutis andA. D.Griffiths, “Selective droplet coalescence using microfluidic systems,” Lab Chip, vol. 12, no. 10, p. 1800, 2012.

[76] J.Tullis, C. L.Park, andP.Abbyad, “Selective fusion of anchored droplets via changes in surfactant concentration.,” Lab Chip, vol. 14, no. 17, pp. 3285–9, 2014.

[77] K.Ahn, J.Agresti, H.Chong, M.Marquez, andD. A.Weitz, “Electrocoalescence of drops synchronized by size-dependent flow in microfluidic channels,” Appl. Phys. Lett., vol. 88, no. 26, 2006.

[78] M.Sesen, T.Alan, andA.Neild, “Microfluidic on-demand droplet merging using surface acoustic waves,” Lab Chip, vol. 14, pp. 3325–3333, 2014.

[79] A. I.Lee, Y.-C.Tan, J. S.Fisher, A. P.Lee, andV.Cristini, “Design of microfluidic channel geometries for the control of droplet volume, chemical concentration, and sorting,” Lab Chip, vol. 4, no. 4, p. 292, 2004.

[80] H. D.Xi et al., “Active droplet sorting in microfluidics: a review,” Lab Chip, vol. 17, no. 5, pp. 751–771, 2017.

[81] S.Li et al., “An On-chip, multichannel droplet sorter using standing surface acoustic waves,” Anal. Chem., vol. 85, no. 11, pp. 5468–5474, 2013.

[82] A. R.Abate, J. J.Agresti, andD. A.Weitz, “Microfluidic sorting with high-speed single-layer membrane valves,” Appl. Phys. Lett., vol. 96, no. 20, 2010.

[83] C. N.Baroud, J. P.Delville, F.Gallaire, andR.Wunenburger, “Thermocapillary valve for droplet production and sorting,” Phys. Rev. E - Stat. Nonlinear, Soft Matter Phys., vol. 75, no. 4, pp. 1–5, 2007.

[84] A.Chen et al., “On-chip magnetic separation and encapsulation of cells in droplets,” Lab Chip, vol. 13, no. 6, pp. 1172–1181, 2013.

[85] A.Sciambi andA. R.Abate, “Accurate microfluidic sorting of droplets at 30 kHz,” Lab Chip, vol. 15, no. 1, pp. 47–51, 2015.

[86] J. J.Agresti et al., “Ultrahigh-throughput screening in drop-based microfluidics for directed evolution.,” Proc. Natl. Acad. Sci. U. S. A., vol. 107, no. 9, pp. 4004–9, 2010.

[87] N.Shembekar, C.Chaipan, R.Utharala, andC. A.Merten, “Droplet-based microfluidics in drug discovery, transcriptomics and high-throughput molecular genetics,” Lab Chip, vol. 16, pp. 1314–1331, 2016.

[88] B. E.Debs, R.Utharala, I.V.Balyasnikova, A. D.Griffiths, andC. A.Merten, “Functional single-cell hybridoma screening using droplet-based microfluidics,” Proc. Natl. Acad. Sci., vol. 109, no. 29, pp. 11570–11575, 2012.

[89] S. C.Kim, I. C.Clark, P.Shahi, andA. R.Abate, “Single-Cell RT-PCR in Microfluidic Droplets with Integrated Chemical Lysis,” Anal. Chem., vol. 90, no. 2, pp. 1273–1279, 2018.

[90] D.Phan andC.Chen, “Lab on a Chip for single-cell miRNA detection with isothermal amplification †,” pp. 1914–1920, 2018.

[91] S.Guo, W. N.Lin, Y.Hu, G.Sun, D. T.Phan, andC. H.Chen, “Ultrahigh-throughput droplet microfluidic device for single-cell miRNA detection with isothermal

amplification," Lab Chip, vol. 18, no. 13, pp. 1914–1920, 2018.

[92] A.Rotem et al., "Single-cell ChIP-seq reveals cell subpopulations defined by chromatin state," Nat. Biotechnol., vol. 33, no. 11, pp. 1165–72, 2015.

[93] G. X. Y.Zheng et al., "Massively parallel digital transcriptional profiling of single cells," Nat. Commun., p. 14049, 2017.

[94] R.Zilionis et al., "Single-cell barcoding and sequencing using droplet microfluidics.," Nat. Protoc., vol. 12, no. 1, pp. 44–73, 2017.

[95] S.Sarkar, V.Motwani, P.Sabhachandani, N.Cohen, andT.Konry, "T Cell Dynamic Activation and Functional Analysis in Nanoliter Droplet Microarray.," J. Clin. Cell. Immunol., vol. 6, no. 3, 2015.

[96] S.Sarkar et al., "Dynamic analysis of human natural killer cell response at single-cell resolution in B-Cell Non-Hodgkin Lymphoma," Front. Immunol., vol. 8, no. DEC, pp. 1–13, 2017.

[97] M.Dhar, J. N.Lam, T.Walser, S. M.Dubinett, M. B.Rettig, andD.DiCarlo, "Functional profiling of circulating tumor cells with an integrated vortex capture and single-cell protease activity assay," Proc. Natl. Acad. Sci., vol. 115, no. 40, pp. 9986–9991, 2018.

[98] A. I.Segaliny et al., "Functional TCR T cell screening using single-cell droplet microfluidics," Lab Chip, vol. 18, no. 24, pp. 3733–3749, 2018.

[99] T.Konry, A.Golberg, andM.Yarmush, "Live single cell functional phenotyping in droplet nano-liter reactors.," Sci. Rep., vol. 3, p. 3179, 2013.

[100] T.Konry, M.Dominguez-Villar, C.Baecher-Allan, D. A.Hafler, andM. L.Yarmush, "Droplet-based microfluidic platforms for single T cell secretion analysis of IL-10 cytokine," Biosens. Bioelectron., vol. 26, no. 5, pp. 2707–2710, 2011.

[101] K. J.Son, A.Rahimian, D.-S.Shin, C.Siltanen, T.Patel, andA.Revzin, "Microfluidic compartments with sensing microbeads for dynamic monitoring of cytokine and exosome release from single cells," Analyst, vol. 141, no. 2, pp. 679–688, 2016.

[102] Z.Cao et al., "Droplet sorting based on the number of encapsulated particles using a solenoid valve," Lab Chip, vol. 13, no. 1, pp. 171–178, 2013.

[103] H.Hu, D.Eustace, andC. A.Merten, "Efficient cell pairing in droplets using dual-color sorting," Lab Chip, vol. 15, no. 20, pp. 3989–3993, 2015.

[104] T. P.Lagus andJ. F.Edd, "A review of the theory, methods and recent applications of high-throughput single-cell droplet microfluidics," J. Phys. D. Appl. Phys., vol. 46, no. 11, p. 114005, 2013.

[105] A. R.Abate, C.-H.Chen, J. J.Agresti, andD. A.Weitz, "Beating Poisson encapsulation statistics using close-packed ordering.," Lab Chip, vol. 9, no. 18, pp. 2628–2631, 2009.

[106] E.Fradet, C.McDougall, P.Abbyad, R.Dangla, D.McGloin, andC. N.Baroud, "Combining rails and anchors with laser forcing for selective manipulation within 2D droplet arrays," Lab Chip, vol. 11, p. 4228, 2011.

[107] C.Zhao, W.Deng, andF. H.Gage, “Mechanisms and Functional Implications of Adult Neurogenesis,” Cell, vol. 132, no. 4, pp. 645–660, 2008.

[108] K. J. T.Venken, J. H.Simpson, andH. J.Bellen, “Genetic manipulation of genes and cells in the nervous system of the fruit fly,” Neuron, vol. 72, no. 2, pp. 202–230, 2011.

[109] Christoph Ziegenhain et al., “Comparative Analysis of Single-Cell RNA Sequencing Methods: Molecular Cell,” pp. 631–643, 2017.

[110] M.Kohwi andC. Q.Doe, “Temporal fate specification and neural progenitor competence during development.,” Nat. Rev. Neurosci., vol. 14, no. 12, pp. 823–38, 2013.

[111] R.Urbach, “Molecular markers for identified neuroblasts in the developing brain of Drosophila,” Development, vol. 130, no. 16, pp. 3621–3637, 2003.

[112] O. A.Bayraktar andC. Q.Doe, “Combinatorial temporal patterning in progenitors expands neural diversity,” Nature, vol. 498, no. 7455, pp. 449–455, 2013.

[113] A.Wagner, A.Regev, andN.Yosef, “Revealing the vectors of cellular identity with single-cell genomics,” Nat. Biotechnol., vol. 34, p. 1145, Nov.2016.

[114] J. G. V.Donald Voet, Biochemistry, 4th ed. J. Wiley & Sons., 2011.

[115] M.Mollet, R.Godoy-silva, C.Berdugo, andJ. J.Chalmers, “Computer Simulations of the Energy Dissipation Rate in a Fluorescence-Activated Cell Sorter : Implications to Cells.”

[116] O. R.Rodrigues andS.Monard, “A Rapid Method to Verify Single-Cell Deposition Setup for Cell Sorters.”

[117] T. S.Kaminski andP.Garstecki, “Controlled droplet microfluidic systems for multistep chemical and biological assays,” Chem. Soc. Rev., vol. 46, no. 20, pp. 6210–6226, 2017.

[118] N. A.Tanner andT. C.Evans, “Loop-mediated isothermal amplification for detection of nucleic acids,” Curr. Protoc. Mol. Biol., no. SUPPL.105, pp. 1–14, 2013.

[119] K.Nagamine, T.Hase, andT.Notomi, “Accelerated reaction by loop-mediated isothermal ampli ® cation using loop primers,” pp. 223–229, 2002.

[120] N.Tomita, Y.Mori, H.Kanda, andT.Notomi, “Loop-mediated isothermal amplification (LAMP) of gene sequences and simple visual detection of products,” Nat. Protoc., vol. 3, no. 5, pp. 877–882, 2008.

[121] A. V. P.Le, D.Huang, T.Blick, E. W.Thompson, andA.Dobrovic, “An optimised direct lysis method for gene expression studies on low cell numbers,” Sci. Rep., vol. 5, pp. 1–10, 2015.

[122] P. D.Vargas, K.Furuyama, S.Sassa, andS.Shibahara, “Hypoxia decreases the expression of the two enzymes responsible for producing linear and cyclic tetrapyrroles in the heme biosynthetic pathway,” FEBS J., vol. 275, no. 23, pp. 5947–5959, 2008.

[123] A. S.Tsiftsoglou, A. I.Tsamadou, andL. C.Papadopoulou, “Heme as key regulator of major mammalian cellular functions: Molecular, cellular, and pharmacological aspects,” Pharmacology and Therapeutics. 2006.

[124] G.Layer, J.Reichelt, D.Jahn, andD. W.Heinz, “Structure and function of enzymes in heme biosynthesis,” Protein Sci., vol. 19, no. 6, pp. 1137–1161, 2010.

[125] D. T. R.Coulson et al., “Identification of valid reference genes for the normalization of RT qPCR gene expression data in human brain tissue,” BMC Mol. Biol., 2008.

[126] Kenneth K. Y. Ho et al., “Advanced Microfluidic Device Designed for Cyclic Compression of Single Adherent Cells,” Front. Bioeng. Biotechnol, vol . 6, 148, 2018.